CHG 9999

THÈSE DE DOCTORAT

Production à grande échelle dans *Escherichia coli* TG1 et purification de l'anticorps à domaine simple ToxA5.1 provenant du lama ayant pour cible l'entérotoxine A produite par *Clostridium difficile*

DOCTORAL THESIS

Large-scale production in *Escherichia coli* TG1 and purification of llama single domain antibody ToxA5.1 against *Clostridium difficile* toxin A

A doctoral research thesis submitted in partial fulfillment of the requirements of the doctoral program for the degree of Doctorate in Chemical Engineering

By

Albert Parisien

Supervisors

Dr. Christopher Q. Lan

Dr. Jules Thibault

Department of Chemical and Biological Engineering

University of Ottawa

May 31 2013

Résumé

Les coûts pour le système de santé associés aux problèmes causés par des souches de *Clostridium difficile* résistantes aux antibiotiques, évalués à plus d'un milliard de dollars, ne cessent d'augmenter. Les toxines excrétées par *C. difficile* sont la cause et peut-être aussi la solution à ces problèmes. En neutralisant les toxines, les effets néfastes peuvent être contrôlés. A cet effet, cette thèse présente les résultats d'études permettant la production à grande échelle en bio-fermenteurs et la purification d'un nouvel agent thérapeutique, le ToxA5.1, un anticorps à domaine simple (pSJF2H-ToxA5.1) se liant à la toxine A de *C. difficile*. Le projet a été divisé en quatre segments: 1) ToxA5.1 étant une protéine intracellulaire, une production de biomasse élevée était la première étape vers la production à grande échelle. Pour obtenir une fermentation à haute densité cellulaire (FHDC), les effets de la concentration initiale en glucose et la stratégie d'alimentation basée sur un pH-stat furent étudiés; 2) Suite à la FHDC, les effets de l'ajout d'extraits de levures, la température ainsi que la période d'induction furent étudiés; 3) Afin de récupérer la protéine recombinante, un système de lyse cellulaire sélective où les effets synergiques du Triton X-100 et de la température sur la lyse furent étudiés. Et enfin 4) La purification de ToxA5.1 à l'aide de nanoparticules de nickel synthétisées par la méthode polyol a été étudiée.

En combinant la stratégie FHDC avec une augmentation de la température d'induction et l'ajout d'extrait de levure, une concentration de 127 mg/L de ToxA5.1 a été obtenue. En utilisant la lyse synergétique à 60°C avec 1% de Triton X-100, il fut possible de récupérer 95% de ToxA5.1 initialement présent dans les cellules en plus d'augmenter la proportion de ToxA5.1 de 27% dans le lysat. De plus, ToxA5.1 purifié ne démontrait aucune perte d'activité suite au traitement thermo-chimique. Il fut déterminé que la concentration de la polyvinylpyrrolidone avait un impact sur la taille des nanoparticules lors de la synthèse avec des particules ayant des diamètres allant de 131 nm à 47 nm. Finalement, il fut possible de modéliser les interactions de liaisons du système ToxA5.1-NNP.

Abstract

Drug resistant strains of *Clostridium difficile* are a major health concern with over 3 million cases costing over 1 billion $ per year in the United-States. The diseases associated with these bacteria (CDAD) are toxin-mediated which offers a mean of treating and lessening the severity of CDAD symptoms. Toxin inactivation via antibodies therapy can drastically reduce CDAD morbidity and this project was aiming at investigating the large-scale production and recovery of a novel llama single domain antibody (pSJF2H-ToxA5.1) in recombinant *Escherichia coli* TG1 targeting *C. difficile* enterotoxin A (TcdA). In order to achieve these objectives, the project was divided into four segments: 1) ToxA5.1 being an intracellular recombinant protein, obtaining a high biomass production was the first step towards large-scale production. To achieve HCDC, effects of initial glucose concentration and pH-stat feeding strategy were studied; 2) Upon achieving HCDC, effects of parameters such as temperature, induction timing and media supplementation with complex nitrogen sources were investigated; 3) Once large-scale production of ToxA5.1 was obtained, the recombinant protein needed to be recovered and a selective cell lysis scheme where synergistic lysis effects of Triton X-100 and temperature were studied. And finally 4) Single-step purification using nickel nanoparticles (NNP) synthesized via a modified polyol method was studied.

Combining the HCDC strategy with a temperature shift and yeast extract addition at the time of induction, ToxA5.1 concentration of 127 mg/L was obtained. Synergistic and selective cell lysis using Triton X-100 and temperature was achieved where 95% of the available ToxA5.1 was recovered and still functional while ToxA5.1 fraction in the resulting lysate increased to 27% in the cell lysate. Single-step purification was achieved using the synthesized NNP which proved to be highly selective and could be used up to five times. Diameter of the NNP synthesized was controlled by using various concentration of ranging from 131 ± 80 nm to 47 ± 20 nm. Using experimental data from binding isotherm, the ToxA5.1-NNP system was modeled.

Acknowledgements

I would like first to acknowledge my supervisors, Drs. Christopher Q. Lan and Jules Thibault, for providing the opportunity to work in the field of fermentation and gene expression. Their financial support through NSERC Discovery grants and the Canada Foundation for Innovation as well as their guidance, at professional and personal levels, was really appreciated.

I would also like to acknowledge Dr. Colin Mackenzie from the NRC Institute for Biological Sciences Antibody Engineering Group for making this project possible by providing the bacterial strain. Also from the same organization, I would like to acknowledge Dr. Jamshid Tanha for his assistance and guidance and Dr. Greg Hussack who has been my primary contact and who patiently answered my many questions and performed some of the experiments reported in this thesis (ELISA and Biacore).

I would like to acknowledge lab members: Kristin Chow, Fady Al-Zarka, Aatika Ahmed, Kevin Nhan, Sallé Dembélé, Daniel O'Neil, and Christian Euler for the help they provided in experiments.

I would like to acknowledge the department staff, Louis Tremblay, Gérard Nina and Franco Ziroldo for the technical assistance as well as Francine Pétrin and Sylvie Saindon for administrative assistance.

I also would like to acknowledge the financial support of the Ontario Government through OGS scholarships, the Canadian Government through a NSERC PGSD and Excellence scholarships, and the University of Ottawa through the Excellence scholarship.

Finalement, j'aimerais exprimer ma gratitude à ma femme, Annie, pour toutes ces années de support moral ainsi qu'à mes enfants, Lauriane, Philippe et Clément pour l'inspiration dont ils ont été la source.

Table of Contents

List of Figures

List of Tables

Collaborator's Contributions

Chapter 3

Sallé Dembélé, helped with experimental procedures by preparing media, conducting experiments, sampling and monitoring OD for some of the bioreactor experiments

Jules Thibault provided experimental guidance and correction of the manuscript

Christopher Q. Lan provided experimental guidance, correction of the manuscript and corresponding author

Chapter 4

Sallé Dembélé, helped with experimental procedures by preparing media, conducting experiments, sampling and monitoring OD for some of the bioreactor experiments

Jules Thibault provided experimental guidance and correction of the manuscript

Christopher Q. Lan provided experimental guidance, correction of the manuscript and corresponding author

Chapter 5

Christian Euler helped with data analysis and helped perform experiments for the synergistic flask experiments

Kristin Chow helped perform experiments for the synergistic lysis in micro-centrifuge tubes, wrote parts of the introduction

Greg Hussack constructed the bacterial strain, performed the ELISA experiment and wrote the relevant Material and Methods section.

Jules Thibault provided experimental guidance and correction of the manuscript

Christopher Q. Lan provided experimental guidance, correction of the manuscript and corresponding author

Chapter 6

Fady Al-Zarka helped perform the binding experiments

Greg Hussack constructed the bacterial strain, performed the ELISA experiment and wrote the relevant Material and Methods section.

Elena A. Baranova provided experimental guidance and correction of the manuscript

Jules Thibault provided experimental guidance and correction of the manuscript

Christopher Q. Lan provided experimental guidance, correction of the manuscript and corresponding author

Chapter 7

Aatika Ahmed helped perform the binding experiments

Jules Thibault provided experimental guidance and correction of the manuscript

Christopher Q. Lan provided experimental guidance, correction of the manuscript and corresponding author

Chapter 8

Aatika Ahmed helped perform the binding experiments

Jules Thibault provided experimental guidance and correction of the manuscript

Christopher Q. Lan provided experimental guidance, correction of the manuscript and corresponding author

Nomenclature

Acronyms

ATP	Adenosine triphosphate
BoNT/A	*Botulinum* toxin A
cAMP	Cyclic adenosine monophosphate
CAP	Catabolite activator protein
CDAD	*Clostridium difficile* associated disease
CDI	*Clostridium difficile* infection
CDR	Complementary determining region
CMC	Critical micelle concentration
DMSO	Dimethyl sulfoxide
DNA	Deoxyribonucleic acid
DPPSH	Dual-point pH-stat high glucose concentration
DPPSL	Dual-point pH-stat low glucose concentration
EDTA	Ethylenediaminetetraacetic acid
EG	Ethylene glycol
ELISA	Enzyme-linked immunosorbent assay
emu	Electromagnetic unit
Fab	Fragment antigen-binding
FHDC	Fermentation à haute densité cellulaire
GRAS	Generally regarded as safe
HCDC	High cell density culture
His6	Hexahistidine
HRP	Horseradish peroxidase
IBS	Institute for Biological Sciences
IgG	Immunoglobulin G
IMAC	Immobilized metal ion affinity chromatography
IPTG	Isopropyl B-D- thiogalactopyranoside
ITL	Total concentration of ToxA5.1 in the initial sample from chemical lysis
LB	Lysogeny broth
LPS	Lipopolysaccharide
M9	Minimal salt media
MAA	Magnetic affinity adsorbent
mAb	Monoclonal antibodies
$NADH_2$	Reduced nicotinamide adenine dinucleotide

Ni	Nickel
NNP	Nickel nanoparticles
NRC	National Research Council Canada
OD	Optical density
OLE	Object linking and embedding
OPC	OLE for process control
PAGE	Polyacrylamide gel electrophoresis
PBS	Phosphate buffered saline
PBS-T	Phosphate buffered saline with Tween-20
PMMA	Polymethyl methacrylate
PMSF	Phenylmethylsulphonyle fluoride
PS	Polystyrene
PVP	Polyvinylpyrrolidone
rcf	Relative centrifugal force
RI	Refractive index
RNA	Ribonucleic acid
rpm	Revolution per minute
scFv	Single-chain variable fragment
sdAb	Single domain antibody
SDS	Sodium dodecyl sulfate
SEB	Staphylococcal enterotoxin B
SLS	Supernatant fluid of the broth after synergistic lysis
SPPS	Single-point pH-stat
SQUID	Superconducting quantum interference device
TcdA	*Clostridium difficile* toxin A
TcdB	*Clostridium difficile* toxin B
UBF	Unbound fraction
UV	Ultraviolet
v/v	Volume per volume
v/w	Volume per weight
VH	Human variable domain
VHH	Single domain antibody
vvm	Volume of air per volume of reactor per minute

Variables

C	Equilibrium bulk-phase protein concentration (mg/L)
C_{bm}	Concentration of ToxA5.1 in the initial binding mixture (mg/L)
C_{broth}	Concentration of ToxA5.1 in the initial broth (mg/L)
C_{ITL}	Total concentration of ToxA5.1 in the initial sample from chemical lysis (mg/L)
C_{SLS}	Concentration of ToxA5.1 in the supernatant fluid after synergistic (mg/L)
C_{UBF}	Concentration of ToxA5.1 in the unbound fraction (mg/L)
D_{avg}	Average diameter (nm)
DCW	Dry cell weight (g/L)
DO	Dissolved oxygen (% air saturation)
I	Imidazole concentration (M)
K	Dissociation constant (mg/L)
M_p	Mass of nickel nanoparticles (g)
n	Number of sample
n	Coefficient for the modified Freundlich model (unitless)
P	Product productivity (mg/L h)
q	Equilibrium loading of the magnetic adsorbent (mg/g)
q_0	Maximal binding capacity (mg/g)
q_{exp}	Equilibrium loading of ToxA5.1 adsorbed per unit amount of NNP during experiments (mg/g)
q_n	Equilibrium loading of ToxA5.1 adsorbed per unit amount of NNP (mg/g)
$q_{predicted}$	Equilibrium loading of ToxA5.1 adsorbed per unit amount of NNP predicted by a model (mg/g)
$q_{residual}$	Equilibrium loading of ToxA5.1 adsorbed after elution per unit amount of NNP (mg/g)
S_0	Initial substrate (glucose) (g)
S_{fed}	Substrate (glucose) fed to the fermentation culture (g)
S_{total}	Total mass of substrate (glucose) used for the fermentation (g)
V_{bm}	Colume of binding mixture (L)
V_{broth}	Volume of initial broth (L)
V_{eluate}	Volume of eluate (L)
V_{ITL}	Initial sample volume (L)
V_{SLS}	Volume of supernatant fluid after synergistic lysis (L)
V_{UBF}	Volume of the unbound fraction (L)
X	Biomass (g)
$Y_{P/S}$	Yield of product on glucose (mg/g S)
$Y_{P/X}$	Yield of protein on biomass(mg/g DCW)

$Y_{X/S}$	Yield of biomass on glucose (g DCW/g glucose)
μ_{max}	Maximal growth rate h^{-1}
ρ_{Ni}	Density of nickel kg/m³

Units

Å	Ångström
g	Gram
L	Litre
m	milli (10^{-3})
M	Molar
nm	Nanometer
Oe	Oersted

Greek letters

μ	micro (10^{-6})
σ	Standard deviation

Chapter 1: Introduction

The cost to healthcare systems caused by nosocomial diseases is constantly rising [1]. One of the major problems is the diseases caused by *Clostridium difficile*, which are mainly diarrhea due to *C. difficile* associated diseases (CDAD) [2, 3]. These diseases are caused by the presence of two toxins (namely A and B) excreted by *C. difficile*, which interfere with water uptake in the intestines [1, 4, 5]. *Clostridium difficile* is a sporulating anaerobic Gram-positive bacterium, which has been the leading and deadliest cause of nosocomial diarrhea colitis around the world [2, 3]. In the USA alone, it is estimated that 3 million cases per year associated with CDAD are costing over a one billion dollars in health care services [1]. In Canada, *C. difficile* has made the headlines, as can be seen in Figure 1-1 on numerous occasions in recent years for a series of infections in hospital settings. In Ontario, from 2009 to 2011, 75 *C. difficile* outbreaks were reported in 47

Figure 1-1: Headlines reporting *Clostridium difficile* outbreaks taken from rightinniagara.blogspot.com and stcatharinesstandard.ca.

hospitals where they lasted between 7 and 334 days with an average outbreak duration of 80 days. During the same period, 1253 cases were reported and, of these, 24% were fatal resulting in a death toll of over 300 patients [6].

It has been demonstrated that the symptoms of CDAD could be relieved by inactivating toxin A and B [7] using monoclonal antibodies [8] and thus preventing them from causing apoptosis of intestinal epithelial cells. However, monoclonal antibodies are expensive to produce [9, 10] as they must be expressed in mammalian cells requiring specific growth conditions, due to their complex structure [11]. An alternative to monoclonal antibodies is the use of single domain antibodies (sdAb), which are found in cartilaginous fish and in *camelidae*. These antibodies are comprised of only the heavy variable region of conventional antibodies, which is responsible for epitope recognition and binding. Even though their structure is simpler, they retain the binding affinity required to inactivate toxins [7, 12-15]. Furthermore, sdAb are composed of a short single polypeptide chain and can be expressed in prokaryotic systems such as *Escherichia coli*[16, 17], which is advantageous in many aspects including: (1) the short period of time between the moment a sequence of a desired protein is discovered and the successful expression optimization of the protein in expression systems such as *E. coli* [9, 16, 18]; (2) fermentations can be done in fairly inexpensive and readily available installations; and (3) production costs are significantly lower than those of mammalian cell culture due to simpler fermentation techniques and inexpensive fermentation medium.

A novel sdAb, ToxA5.1, has been developed by Dr. Colin Mackenzie's protein engineering group at the Institute for Biological Sciences (IBS), NRC, which can bind and neutralize *C. difficile* toxin A *in vitro* [19]. It is therefore of interest to optimize the

production and downstream processing of ToxA5.1 in order to produce rapidly and inexpensively large quantities of the desired protein. Since this antibody is to be administered orally, large amounts of ToxA5.1 will be required as animal studies are planned in the near future.

The objectives of this project, which focused on the large-scale production and recovery of ToxA5.1, were fourfold as can be seen on Figure 1-2:

1) Develop high cell density fermentation by studying the feeding strategy to obtain high productivity of *E. coli* biomass.

2) Enhance protein expression of the recombinant cells by studying the effect of temperature and media additives such as complex nitrogen sources and inducer molecule.

3) Develop an efficient and selective cell lysis process for the recovery of the target protein by studying the effect of temperature and Triton X-100 on the recovery of ToxA5.1.

4) Develop cost-effective protein purification technologies using magnetic adsorbents synthesized for this purpose.

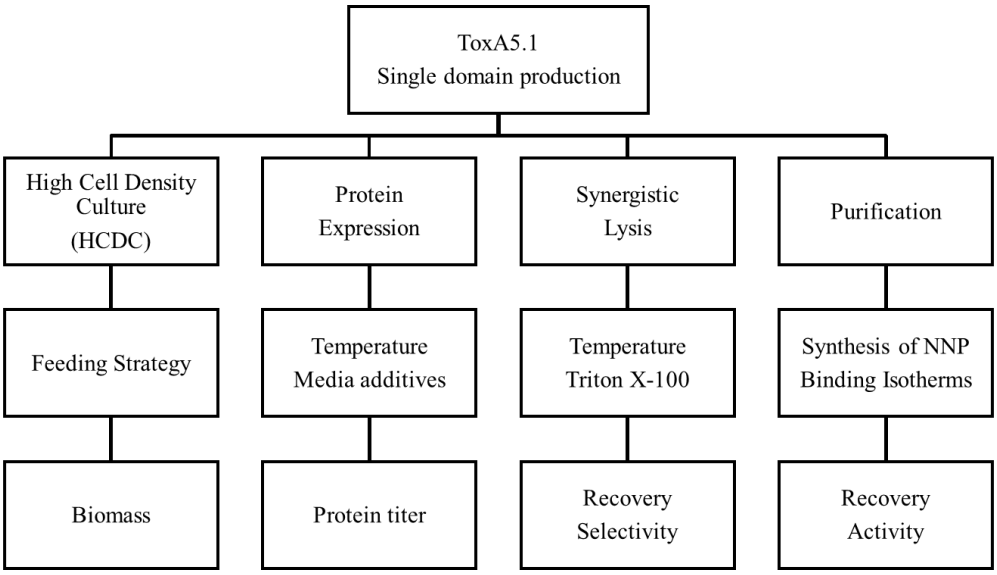

Figure 1-2: ToxA5.1 production and purification project overview. The first row shows the objectives of the project while the second row shows the parameters or strategy used to achieve the objectives and, finally, the third row shows the success indicator or the criteria used to determine success.

This thesis is comprised of nine chapters where six of these are reporting experimental results. The first chapter is an introduction to the project while the second chapter presents a literature review on the various topics of the thesis. In chapters 3 to 8, experimental results are presented and finally, conclusions and recommendations are presented in the last chapter.

ToxA5.1 being expressed as an intracellular recombinant protein, protein productivity is a function of cell productivity and protein cell content. Consequently, both high biomass productivity, which is directly related to cell density, and high protein expression level of individual cells must be achieved to obtain large protein productivity. With this in mind, the first objective was to obtain high cell density culture (HCDC) of *E. coli* TG1 ToxA5.1. Because the concentration of nutrients and carbon source required to sustain continuous bacterial growth would actually be detrimental to bacterial growth, the fermentation is carried out in two phases [20]. In the first phase, the batch phase, nutrients and carbon source concentration are sufficient to support cell growth and build biomass. Once nutrients and carbon source are depleted from the batch medium and the biomass is established, the fed-batch phase, which will sustain growth of the biomass, can be initiated. Several feeding strategies can be utilized during the fed-batch phase, some of which use direct monitoring of the carbon source concentration in the fermentation culture [21] while others use indirect indicators such as dissolved oxygen consumption or fermentation medium pH to indirectly monitor the carbon source concentration in the fermentation culture [21]. As glucose in the medium is catabolized by bacteria, the medium pH decreases due to the formation of acidic by-products. Upon glucose depletion, the acidic by-products in turn get consumed which results in an increase of the medium pH.

The pH in the medium can therefore be related to the glucose concentration and be used as an indicator of when glucose needs to be fed to the culture. Chapter 3 focuses on the use of such a strategy, called pH-stat feeding, to achieve HCDC. In addition to pH control setpoints, effects of glucose in the initial batch medium as well as the amount and the manner in which glucose was fed during the fed-batch phase of the fermentation were investigated. Using the best combinations tested, cell densities were increased from 3.6 g DCW/L in a typical batch phase to 27 g DCW/L after the pH-stat feeding strategy.

The ultimate goal of this project was to produce large amounts of functional ToxA5.1. Therefore, the next logical step after achieving HCDC was to optimize the protein expression of the recombinant strain under HCDC conditions. Organisms used for recombinant protein expression often possess a mechanism, which can be turned on at a desired time, to initiate expression. This mechanism is usually under the control of an inducer, a chemical substance that is added to the fermentation medium when induction conditions are favorable. For the expression of a recombinant gene, supplemental nutrients can also be added to the fermentation broth especially when a defined medium is used. These supplemental nutrients, often in the form of yeast extract, greatly enhance protein expression [22] by providing peptides and free amino acid, vitamins, minerals and growth factors. Temperature also influences both cell growth and recombinant protein expression in bacterial strains [23]. Lower temperatures can have a negative effect on the expression of certain genes and it was demonstrated that expression of the OmpA gene, which is present in the *E. coli* TG1 ToxA5.1 expression system, is less efficient at a temperature lower than 28°C when compared to temperature of 37°C [24]. In Chapter 4, gene expression was studied by building on the information obtained for HCDC in the

previous chapter to achieve high biomass prior to induction. It was observed that adding inducer only to a large biomass did not guarantee the success of recombinant gene expression. Other parameters were confirmed to be essential for ToxA5.1 expression. Increasing the induction temperature from 28°C to 37°C was critical as well as supplementation of a complex nutrient source in the form of yeast extract. Under the best conditions tested it was possible to achieve a ToxA5.1 concentration of 127 mg/L and a protein cell content of 11 mg /g dry cell weight of *E. coli*.

The third and fourth objectives of this project were to develop advanced downstream processing strategies for cost-effective purification of ToxA5.1. Upon expression, ToxA5.1 is exported from the cytoplasm where it is synthesized to the periplasmic space. This enables recovery of the target protein with selective lysis, i.e., selectively removing the outer membrane of the bacterial cell without causing total cell lysis. To this effect, Triton X-100, which is a surfactant that cannot induce cell lysis on its own [25], can however enhance leakage from periplasmic space once the outer membrane integrity becomes disrupted either by another chemical [26] or by mechanical action [27]. Since temperature has been known to disrupt membrane integrity and cause protein leakage [28], by combining thermolysis and Triton X-100, it was hypothesized that a synergistic effect would lead to a selective cell disruption method that could enable ToxA5.1 recovery. In Chapter 5, a synergistic and selective cell lysis was tested in which Triton X-100 and temperature were combined to recover the target recombinant protein from the periplasmic space of *E. coli* TG1-ToxA5.1. Using the conditions tested, it was possible to recover over 95% of the protein present in the bacteria while increasing the

ratio of the target recombinant protein to the total native proteins from 10% after total lysis to 27% after synergistic lysis. Furthermore, it was demonstrated that ToxA5.1 purified after synergistic lysis at 50 or 70ºC for 15 min with 1% w/v Triton X-100 concentration maintained its binding capability towards toxin A and had a similar activity to that of ToxA5.1 purified using IMAC column after chemical lysis.

Once the proteins can be accessed i.e., have been extracted from the bacteria, purification can be performed. It was originally planned on using a commercial nickel based magnetic adsorbent for the purification of ToxA5.1 since the recombinant protein bears a tag specifically designed to bind nickel in a purification scheme. After discussing the subject with a member of the department, Dr. Elena A. Baranova, it was decided to synthesize our own magnetic adsorbent using a simple and low cost method. Nickel nanoparticles were thus synthesized using a modified polyol method and proved to be an efficient, selective and reusable magnetic adsorbent for the purification of hexahistidine (His6-tagged) recombinant protein. Therefore, Chapter 6 focuses on the synthesis and the characterization of the nickel nanoparticles. It was reported that the nickel nanoparticles synthesized using a modified polyol method had an average diameter of 68 nm, were exhibiting magnetic behavior, were able to selectively purify the target protein and, furthermore, could be reused following a regeneration washing step for up to four purifications without significant losses in binding capacity.

When synthesizing nanoparticles using a modified polyol method, polyvinylpyrrolidone (PVP), a capping agent, can be used in different ratios with respect to the amount of nickel precursor. To test the effect of various nickel to PVP mass ratios on the morphology and purification ability of the synthesized nanoparticles, several

syntheses were performed. Chapter 7 highlights the findings from these syntheses. The average diameter of the nanoparticles decreased as the Ni:PVP mass ratio decreased from 1:0 to 1:5. Average diameter for the 1:0 ratio was of 131 ± 80 nm while an average diameter of 47 ± 20 nm was obtained for the 1:5 Ni:PVP mass ratio. All of the synthesized nanoparticles could efficiently and selectively bind the His6-taggedrecombinant protein and could be reused up to four following a regenerative washing step.

As the previous chapter demonstrated, the synthesized nanoparticles could bind His6-tagged recombinant proteins and, therefore, the next logical question was how much can these NNP bind. Consequently, the last contribution to this thesis was to measure the binding capacity of the novel synthesized material. Chapter 8 reports on binding experiments that were performed using clarified cell lysate and buffer containing various concentrations of the chemical used to elute the His6-tagged protein from the nanoparticles. It was found that when nickel nanoparticles were used to purify a His6-tagged recombinant protein from clarified bacterial lysate, 13.26 mg of ToxA5.1 could bind to 1 g of nickel nanoparticles. It was also possible to derive modified Langmuir and Freundlich models to predict the binding of ToxA5.1 to the NNP.

In summary, this project was proposing to study the production in *E. coli* TG1 of a novel therapeutic protein, ToxA5.1 single domain antibody, to neutralize a toxin of one of the deadliest nosocomial infection agent afflicting hospitals. This was achieved through high cell density cultivation and gene expression optimization investigations. Recovery of fully functional ToxA5.1 was achieved using synergistic lysis as a selective

cell disruption technology combining Triton X-100 and temperature while the synthesis of a novel adsorbent material enabled the purification of ToxA5.1. In the end, it was possible to produce 12 g/L of *E. coli* TG1 biomass that was able to accumulate the recombinant ToxA5.1 sdAb at a concentration of 127 mg/L. The activity of ToxA5.1 purified using the nickel nanoparticles after synergistic lysis at 60°C with 1% Triton X-100 was tested against a ToxA5.1 control at NRC-IBS facilities. ToxA5.1 purified under the previous conditions showed no significant difference with the standard ToxA5.1 used in a binding assay against *C. difficile* toxin A. Therefore, it was possible to produce large quantities of active ToxA5.1 and the next step will be to produce sufficient ToxA5.1 for animal studies.

1.1 References

1. Oldfield III, E.C. *Clostridium difficile*-associated diarrhea: Risk factors, diagnostic methods, and treatment. *Reviews in Gastroenterological Disorders* **4**, 186-195 (2004).
2. Bobak, D.A. The molecular pathogenesis of *Clostridium difficile*-associated disease. *Current Infectious Disease Reports* **10**, 111-115 (2008).
3. Kelly, C.P., Pothoulakis, C. and Lamont, J.T. *Clostridium difficile* colitis. *New England Journal of Medicine* **330**, 257-262 (1994).
4. Tonna, I. and Welsby, P.D. Pathogenesis and treatment of *Clostridium difficile* infection. *Postgraduate Medical Journal* **81**, 367-369 (2005).
5. Voth, D.E. and Ballard, J.D. *Clostridium difficile* toxins: Mechanism of action and role in disease. *Clinical Microbiology Reviews* **18**, 247-263 (2005).
6. Whelan, M. and Raju, S., *Clostridium difficile* outbreaks in hospitals: 2009 to 2011. Vol. 2013 (Public Health Ontario, 2012) url: http://www.oahpp.ca/resources/documents/presentations/2012may28-29/2.0%20-%20Epi%20Data/CDI%20Outbreak%20presentation%202012.pdf. Last access May 28 2013.
7. Weiss, K. Toxin-binding treatment for *Clostridium difficile*: a review including reports of studies with tolevamer. *International Journal of Antimicrobial Agents* **33**, 4-7 (2009).

8. Salcedo, J., Keates, S., Pothoulakis, C., Warny, M., Castagliuolo, I., LaMont, J.T. and Kelly, C.P. Intravenous immunoglobulin therapy for severe *Clostridium difficile* colitis. *Gut* **41**, 366-370 (1997).

9. Gasser, B. and Mattanovich, D. Antibody production with yeasts and filamentous fungi: On the road to large scale? *Biotechnology Letters* **29**, 201-212 (2007).

10. Muyldermans, S. Single domain camel antibodies: Current status. *Reviews in Molecular Biotechnology* **74**, 277-302 (2001).

11. Plückthun, A. Biotechnological aspects of antibody production in *E. coli*. *Acta Biotechnologica* **11**, 449-456 (1991).

12. Cortez-Retamozo, V., Backmann, N., Senter, P.D., Wernery, U., De Baetselier, P., Muyldermans, S. and Revets, H. Efficient cancer therapy with a nanobody-based conjugate. *Cancer Research* **64**, 2853-2857 (2004).

13. Hmila, I., Abdallah R, B.A.B., Saerens, D., Benlasfar, Z., Conrath, K., Ayeb, M.E., Muyldermans, S. and Bouhaouala-Zahar, B. VHH, bivalent domains and chimeric Heavy chain-only antibodies with high neutralizing efficacy for scorpion toxin AahI'. *Molecular Immunology* **45**, 3847-3856 (2008).

14. Krüger, C., Hultberg, A., Marcotte, H., Hermans, P., Bezemer, S., Frenken, L.G.J. and Hammarström, L. Therapeutic effect of llama derived VHH fragments against Streptococcus mutans on the development of dental caries. *Applied Microbiology and Biotechnology* **72**, 732-737 (2006).

15. Liu, J.L., Anderson, G.P. and Goldman, E.R. Isolation of anti-toxin single domain antibodies from a semi-synthetic spiny dogfish shark display library. *BMC Biotechnology* **7** (2007).

16. Arbabi-Ghahroudi, M., Tanha, J. and MacKenzie, R. Prokaryotic expression of antibodies. *Cancer and Metastasis Reviews* **24**, 501-519 (2005).

17. Fernandez, L.A. Prokaryotic expression of antibodies and affibodies. *Current Opinion in Biotechnology* **15**, 364-373 (2004).

18. Plückthun, A. Antibody engineering: Advances from the use of *Escherichia coli* expression systems. *Nature Biotechnology* **9**, 545-551 (1991).

19. Hussack, G., Arbabi-Ghahroudi, M., Van Faassen, H., Songer, J.G., Ng, K.K.S., MacKenzie, R. and Tanha, J. Neutralization of *Clostridium difficile* toxin A with single-domain antibodies targeting the cell receptor binding domain. *Journal of Biological Chemistry* **286**, 8961-8976 (2011).

20. Shiloach, J. and Fass, R. Growing *E. coli* to high cell density - A historical perspective on method development. *Biotechnology Advances* **23**, 345-357 (2005).

21. Riesenberg, D. and Guthke, R. High-cell-density cultivation of microorganisms. *Applied Microbiology and Biotechnology* **51**, 422-430 (1999).

22. Nancib, N., Branlant, C. and Boudrant, J. Metabolic roles of peptone and yeast extract for the culture of a recombinant strain of *Escherichia coli*. *Journal of Industrial Microbiology* **8**, 165-169 (1991).

23. Donovan, R.S., Robinson, C.W. and Click, B.R. Review: Optimizing inducer and culture conditions for expression of foreign proteins under the control of the lac promoter. *Journal of Industrial Microbiology* **16**, 145-154 (1996).

24. Afonyushkin, T., Moll, I., Bläsi, U. and Kaberdin, V.R. Temperature-dependent stability and translation of *Escherichia coli* ompA mRNA. *Biochemical and Biophysical Research Communications* **311**, 604-609 (2003).

25. Tsuchido, T., Katsui, N. and Takeuchi, A. Destruction of the outer membrane permeability barrier of *Escherichia coli* by heat treatment. *Applied and Environmental Microbiology* **50**, 298-303 (1985).

26. Naglak, T.J. and Wang, H.Y. Recovery of a foreign protein from the periplasm of *Escherichia coli* by chemical permeabilization. *Enzyme and Microbial Technology* **12**, 603-611 (1990).

27. Anand, H., Balasundaram, B., Pandit, A.B. and Harrison, S.T.L. The effect of chemical pretreatment combined with mechanical disruption on the extent of disruption and release of intracellular protein from *E. coli*. *Biochemical Engineering Journal* **35**, 166-173 (2007).

28. Ren, X., Yu, D., Yu, L., Gao, G., Han, S. and Feng, Y. A new study of cell disruption to release recombinant thermostable enzyme from *Escherichia coli* by thermolysis. *Journal of Biotechnology* **129**, 668-673 (2007).

Chapter 2: Literature review

2.1 *Clostridium difficile* and *Clostridium difficile* associated diseases

The pathogenicity of *C. difficile* is associated with the production of enterotoxin A (TcdA) and cytotoxin B (TcdB) [1-6]. Once the toxins are excreted in the intestines by *C. difficile*, they are taken up by the target cells, i.e. intestinal epithelial cells, via surface receptor-mediated endocytosis and gain access to the cytosol [6-9]. Inside the cytosol, TcdA and TcdB start to modulate host cell physiology by interfering with protein responsible for the production of the actin skeleton, cell junctions and by interfering with cell signalization [6]. This action results in epithelial cell apoptosis which prevents water uptake and leads to severe diarrhea.

It has been demonstrated that the severity and the duration of CDAD is linked to the amount of toxin present [10] and that large quantities of anti-TcdA IgG are sufficient to prevent CDAD resurgence in patients [11, 12]. In order to prevent CDAD, immunoglobulin-directed therapies were investigated and several of them were reported to have protective effects in murine models [11, 13-19]. By binding to the toxin, antibodies can prevent the toxin from binding to its intended receptor on the epithelial cell. Since it has been reported that TcdA can be neutralized by monoclonal antibodies, the use of a novel type of antibodies, single domain antibodies that are antibodies found in *camelidae* and cartilaginous fish [20], could also be used as toxin inactivator as reported in some papers [21, 22]. The ability of sdAb to bind with high specificity can also be used against toxins to prevent them from binding to their intended receptors hence to neutralize toxins. This strategy has been used successfully in murine models to prevent tooth caries [23] or to inactivate the toxin of

venom bites [24]. This strategy was also used against tetanus toxin with good results [25]. Several other sdAb have been reported to bind toxins; Goldman *et al.* [26] reported ricin toxin binding, Liu *et al.* [21] reported sdAb binding to three toxins: staphylococcal enterotoxin B (SEB), ricin, and *botulinum* toxin A (BoNT/A) complex toxoid while Shuntao *et al*. [22] reported sdAb binding and inactivating ricin toxin.

2.2 Monoclonal antibodies and single domain antibodies

In order to satisfy the demand for antibodies, large-scale production must be carried out in a cost effective manner. Production of large quantities of mAb is hindered because scale-up of processes is complex and facilities are costly to build and operate [27-29]. Single domain antibodies do not require extensive folding or glycosylation in order to be functional, making the production of this kind of antibodies using recombinant bacteria and yeast possible, which can significantly reduce the costs associated with their production [30].

Prokaryotic cells, mainly *E. coli*, have several advantages when it comes to protein expression [31]. The first one is the short period of time between the moment a sequence of a desired protein becomes known and the final expression optimization of this protein in *E. coli* [29, 32, 33]. This is greatly due to the extensive molecular biology information available on *E. coli*, which makes cloning, transformation and selection of a recombinant strain an efficient process. Furthermore, fermentation can be done in fairly inexpensive and readily available installations, which reduces capital costs. Operation costs are also significantly lower than that of mammalian cell culture since fermentation techniques are simple and medium is inexpensive. Another advantage of the *E. coli*

system is that there is no possibility for virus contamination. However, a major drawback is the possibility of endotoxin contamination [34] and, therefore, efficient protein purification must be performed. Even in that case, extra care must be taken as some immunogenic response-triggering agent such as lipopolysaccharide can be tightly bound to purified protein. In order to circumvent endotoxin problem, sdAb could be produced in bacteria that are GRAS (generally regarded as safe) such as lactic acid producing bacteria[35]. This could even serve as a delivery system, with the production of sdAb directly in the gut where antibodies would be needed to fight parasitic or bacterial infections.

Early clinical tests using sdAb have shown very promising results. It is therefore very important to develop optimized protocols for the cost-effective, large-scale production of this new therapeutic agent [36].

As mentioned previously, very few papers considered sdAb production in *E. coli* but it was possible to find information on antibody fragment production (Fab and dimeric miniantibodies), which have similarities to sdAb in terms of structures and molecular size. Horn *et al.* [37] reported an optimized production of scFv (single chain variable domain fragments) using an *E. coli* strain of about 4 g/L in a fed-batch culture grown for 33 h at a cell density of 145 g/L on glucose mineral salt medium. Of these, 80% were functionally assembled [37]. This number seems surprisingly high when compared to other results obtained by Corsideo and Wang [38], where optimized expression conditions for the production of a Fab yielded only 16 mg/L (shake flasks in LB medium).

Regarding sdAb production, Rahbarizadeh *et al.* [39] produced up to 42 mg/L in batch culture using LB media (8 h induction time at 37°C) under optimized conditions.

This study shows that production of sdAb can vary greatly. Other papers reported higher sdAb production even though they were not aimed at optimizing the production but merely producing sdAb for further biochemistry experiments. Tanha *et al.* [40] reported a sdAb production of 80 mg/L and in other papers, quantities of sdAb produced varied from 10 to 100 mg/L [24, 26, 39, 41, 42] in unoptimized similar flask conditions. As mentioned in Harmsen and De Haard [43], sdAb varying only by a few amino acids can have significantly different expression levels.

2.3 High cell density culture

2.3.1 Cell growth

Developments in biochemical engineering that occurred since the early 90's have led to high cell density culture (HCDC) when bacterial cells, especially *E. coli*, are grown in fed-batch mode. Several authors reported cell densities of 86, 110 and even 134 g/L on a dry cell weight basis (DCW) [44] but the exact cell density for a culture to be designated as a HCDC is not agreed upon as an *E. coli* culture of 17.6 g/L is considered a HCDC [45]. Being able to achieve high cell densities significantly reduces capital investments as well as operation costs because HCDC leads to very high volumetric productivity (g of desired protein unit volume^{-1} time^{-1}) [44, 46]. HCDC are carried out in a two-stage fermentation. The first phase is a batch phase where all nutrients, including carbon sources, required for maximum cell growth are present and the second stage consists of a fed-batch where the carbon source and other macro nutrients are fed to the culture enabling control over bacterial cell growth rates.

One of the problems with batch fermentation is that substrate inhibition can occur when the concentration of a substrate is above a critical level. For instance, it was

reported that for *E. coli*, substrates became inhibitory if they were present at the following respective levels: glucose > 50 g L^{-1}, ammonia > 3 g L^{-1}, boron > 44 mg L^{-1}, cobalt > 0.5 mg L^{-1}, copper > 4.2 mg L^{-1}, iron > 1.15 g L^{-1}, magnesium > 8.7 g L^{-1} , molybdenum, >0.8 g L^{-1}, phosphorus > 10 g L^{-1} and zinc > 38 mg L^{-1}[47]. Furthermore, if the initial concentrations are too high, osmotic pressure increases in the medium, thereby leading to detrimental conditions for the cultures [44]. It is also a significant concern that some substrates may precipitate at high initial concentration [44] which makes them unavailable for cell growth.

Nutrients are required in large quantities if high cell densities are to be expected but the problem of inhibition and precipitation must be dealt with. To overcome this situation, fed-batch fermentation is commonly used. In addition, fed-batch fermentation enables the control of bacterial growth rate by the means of controlling the rate of feeding. This is crucial to achieve HCDC since high growth rates in *E. coli* are associated with acetate production. Acetate concentrations of 2-10 g/L have been reported to inhibit cell growth and protein expression [48-52] and concentration as low as 0.5 g/L can have detrimental effects on cell growth [53]. One of the primary reasons for acetate production is the presence of high concentration of glucose [53-57]. It has been reported that *E. coli* metabolism favours the maximization of ATP production [58] and this is why when excess glucose is present in the medium, acetate formation is favoured as a secondary pathway for ATP production since it produces the second largest pool of ATP and $NADH_2$ [56]. This leads to a high specific growth rate (above 0.35 h^{-1} [57]) which has been shown to stimulate acetate production. This phenomenon led to the introduction of the critical growth rate concept. Critical growth rate is the highest growth rate at which a cell can be grown

without producing acetate. Several strategies have been employed to control growth rates either by controlling the rate of glucose consumption by limiting its feeding or by the addition of chemical, such as methyl alpha-glucoside, altering the consumption of glucose [59, 60].

Different feeding strategies can be used to control growth rate and supplying adequate amounts of nutrients. Several types of these strategies exist and they are either performed without feedback control (e.g., constant, step-wise or exponential feeding) or based on direct or indirect feedback control. When for instance, glucose is the primary substrate to be fed, direct feedback control relies on on-line glucose analyzer while indirect feedback control depends on monitoring one of the more-easily measured indicators to infer glucose consumption, which include dissolved oxygen (DO), carbon dioxide evolution, medium pH and cell concentration [46].

Using feeding strategies without feedback control requires thorough knowledge and an accurate model of a system to deliver appropriate glucose feeding rate. Indirect feedback strategy may require complex equipment such as off-gas analyzer to relate the rate of oxygen consumption and the rate of CO_2 evolution to bacterial growth rate. Other devices, which are already present in fermentation setup, such as DO probe or pH electrode, can also be utilized for controlling glucose feeding rates [46]. When glucose is depleted from the culture medium, cell metabolism slows down. If no other source of carbon is available, decrease in metabolism causes DO level to increase [46]. In a DO-stat controlled system, glucose feed is adjusted to keep the DO at a certain level [46]. The absence of glucose in the medium forces cells to start consuming metabolic by-products, which are mainly acidic by-products such as propionic, acetic and lactic acids [61] and

excreting ammonium ions resulting in pH increase [62]. This variation in pH can be utilized to devise a feeding strategy such that whenever pH rises above a certain preset value, glucose is fed in the fermentation culture. This strategy, referred to as pH-stat [62], uses glucose catabolism to control medium pH.

An important factor needing control in fermentation cultures is the dissolved oxygen level in the medium. In HCDC, if oxygen supply is not well controlled, anoxic or lower level of oxygen could occur, which may adversely affect cell growth [63]. It has been well documented that dissolved oxygen concentration greatly impacts the ability of cells to grow and express protein [64-66]. A typical value for DO concentration is 20% of saturation. The critical DO concentration of HCDC can vary from 10% air saturation at 36°C at the beginning of the culture to 30% once HCDC is achieved [67].

2.3.2 Protein expression at HCDC

Factors affecting cell growth may also have a profound effect on the recombinant protein expression. Other factors ought to be investigated for optimal protein production and these can be separated into two types. The first one being the operating conditions such as pH, temperature, feeding strategy or timing of induction and the second type is related to the composition of fermentation medium such as type of medium used (complex or defined), carbon source used or medium additives used.

Recombinant protein expression, most of the time, needs to be induced. At a judicious moment, a change in the environment, more commonly the addition of an inducer molecule, frees the target genes from repression and starts the protein expression phase.

Since recombinant protein expression can produce a large metabolic stress on a cell [68], being able to control the moment of induction is critical. If the cells are induced too early, the biomass concentration will be low since the induction creates a metabolic burden in which most of the cell's energy is diverted towards protein expression, which would be detrimental to biomass production. When the product is intracellular, as is the case with ToxA5.1, a premature induction results in a lower volumetric productivity rate (g protein L^{-1} culture h^{-1}) due to the lower biomass concentration. If the product is growth-associated, a later induction phase is not recommended since cells are growing less actively which reduces the specific productivity (g protein / g DCW h). Timing of the induction is also important as the plasmid-bearing organism fraction tends to decrease with fermentation time even if selective pressure, in the form of antibiotics, is applied [69].

As important as the timing of induction, the concentration of inducer is also critical. As mentioned earlier, recombinant genes are repressed by certain types of molecule and in the case of the lac operon, which is the operon controlling protein expression in our bacteria, the inducer must displace the repressor molecule. In the case of the lac operon, glucose metabolites are preventing formation of the CAP-cAMP complex needed for DNA transcription. The inducer molecule must displace this complex to allow RNA polymerase to initiate transcription of the recombinant genes [70]. Since the inducer concentrations in the range of 0.02 mM to 5 mM have been reported to induce gene expression, further investigation is required to determine appropriate concentration for a given system[38].

Other additives to the fermentation media can increase the specific productivity and, amongst these, yeast extract is one of the most studied. Yeast extract has been

reported by multiple sources to enhance specific productivity of recombinant proteins expressed by different *E. coli* strains [71]. Since the exact composition of yeast extract is unknown, it is possible that molecules that can serve as inducers are present.

2.4 Cell disruption technologies

When recombinant protein expression is intracellular, a method is needed to release efficiently these proteins. This is accomplished through cell lysis which can be generally categorized into two types: chemical or physico-mechanical.

As the name implies, chemical lysis uses a chemical to lyse the cell by penetrating, destabilizing or disintegrating the cell wall barriers [72]. Organic solvents such as dimethyl sulfoxide (DMSO) or methanol can also be used to modify the integrity of the cell wall [73]. Detergents, either ionic such as sodium dodecyl sulfate (SDS) or non-ionic such as Tween, which are considered to be gentler, can also be used to initiate cell lysis by solubilizing the phospholipid bilayer membranes [74]. Enzymes such as lysozyme are sometime used to lyse *E. coli* cells but are generally considered too costly for industrial-scale use. Alkali can be used to raise the pH to around 13, which can also cause cell lysis [73] but this strategy is not practical at large-scale. All these methods can be used at laboratory-scale but are not considered for large-scale cell lysis since the addition of a chemical agent, especially enzymes, is costly and usually necessitates the removal of this agent in the downstream processing [73, 75].

For large-scale processes, mechanical lysis methods are usually preferred. These methods rely on two principles, either concussion or liquid shearing. Ball milling, in which cells are broken under shearing forces of grinding caused by small abrasive particles such as glass beads or sand, is one of the most frequently used concussion

device for large-scale cell lysis [73, 75]. This process generates heat and must therefore be cooled, typically with jackets to keep temperature below 25°C thus minimizing protein degradation due to high temperature.

Homogenizers are shear-based mechanical devices for cell disruption, which rely mainly on shear generated when the cell slurry is pumped at high pressure through an orifice to break up the cells. Several mechanisms participate in cell lysis in a homogenizer: 1) high shear caused by passage through the orifice, 2) sudden pressure drop when cells exit the orifice and 3) high velocity collisions of cells onto an impact plate.

2.4.1 Complete cell lysis

Conventionally, the aforementioned chemical and mechanical disruption methods lead to complete breach of cells, releasing not only the heterogeneous recombinant protein of interest but also the total cell content including native proteins, DNA, RNA, lipids, sugars, and other materials. While complete cell lysis is simple to achieve, cellular materials released in the process are contaminants that significantly complicate protein purification. These materials, especially nucleic acids polymers, also increase liquid viscosity which impedes subsequent chromatography steps used for protein purification [73, 75, 76]. Complications associated with complete cell lysis are even more problematic when high cell density techniques are used to enhance protein productivity. Mechanical cell lysis may also result in micronization of cellular debris, which may further impair the protein recovery process [73, 75, 76]. As a countermeasure, the concept of selective cell disruption, applicable to recombinant microbes whose recombinant proteins

are exported to the periplasmic space, i.e., the space between the cytoplasmic membrane and the cell wall.

2.4.2 Partial cell disruption

When recombinant proteins are exported to the periplasmic space, only the cell wall needs to be completely or partially disrupted to extract proteins. One of the major advantages of this approach, although difficult to achieve, is that the cytoplasmic membrane remains intact and only the cell wall is partially disrupted. As a result, cytoplasmic content is not released into the supernatant fluid. Consequently, fewer native proteins will be present in the supernatant fluid, thus, significantly simplifying recovery and purification of the target protein.

Several strategies have been investigated to selectively lyse cells. Most of these techniques use chemicals such as glycine, Triton X-100 or guanidine to remove or destabilize the outer membrane of bacteria [77-80], therefore enhancing protein leakage from the periplasmic space. However, as previously mentioned, the addition of chemical agents might increase the recovery costs and also cause problems in downstream processing. Heat treatment can also be used as a selective cell lysis strategy. When the cells are exposed to heat, release from the outer membrane of lipopolysaccharide (LPS), which are responsible for controlling membrane permeability, enables periplasmic proteins leakage in the medium [81]. Furthermore, release of LPS also enables diffusion across the outer membrane of molecules that were previously excluded. Using heat to enable leakage of periplasmic protein is only applicable to thermostable proteins because treating cells at a temperature above 40°C, which is required for thermolysis [82], might be problematic if the target protein is heat sensitive [82, 83]. The thermostability of ToxA5.1

has been demonstrated by circular dichroism experiments performed at IBS in which 90% of ToxA5.1 was still properly folded at a temperature of 70°C. Degradation of 50% of ToxA5.1 was observed at 73°C and unfolding of more than 90% of ToxA5.1 was observed at a temperature of 85°C. Given the fact that most indigenous proteins are not stable and will be denatured at thermolysis temperature, this approach could also serve as a preliminary step for protein purification. The denatured contaminant proteins could be subsequently removed as precipitates with other cell debris.

It was also demonstrated that the addition of some surfactants, when carefully controlled, could increase the efficiency and selectivity of periplasmic leakage. Of these surfactants, Triton X-100 [80, 84-86], glycine [78, 79, 84, 87] and guanidine hydrochloride [80, 88], which are relatively inexpensive and are not protein based, have been investigated in different scenarios but no mention of these treatments coupled with thermolysis was found in the literature.

2.5 Protein recovery and purification using magnetic affinity adsorbents (MAA)

Purification and recovery of recombinant proteins, after cell disruption, can be achieved using techniques ranging from gel chromatography, ion exchange chromatography and affinity chromatography to electrophoresis, precipitation and membrane separation [89, 90]. A versatile affinity chromatography approach for recombinant protein recovery is immobilized metal ion affinity chromatography (IMAC), which provides a high recovery and selectivity of the target protein. Nevertheless, IMAC cannot be used to efficiently separate proteins from samples containing high particulate loadings

such as crude cell lysate. While not a problem at laboratory scale as clear samples can be obtained by centrifugation, it becomes an important concern at larger scale.

A possible solution to this problem would be the use of magnetic affinity adsorbents (MAA). As will be discussed in more detail later, these particles retain the selectivity and recovery qualities of IMAC but can be applied to high-load samples since adsorbents can be recovered conveniently using a magnetic field rather than filtration. An overview of magnetic separation principles and applications as well as research areas, such as adsorbents, is discussed in the following paragraphs.

2.6 Magnetic affinity adsorbents

The principle behind magnetic separation is simple. Magnetic core particles are covered by a functional group which acts as an affinity ligand. One of the most widely used affinity ligands is nickel, which interacts with the polyhistidine tag that is fused to the recombinant target protein. Typically, a magnetic affinity adsorbent is comprised of an inorganic magnetic core particle covered by a polymer matrix with polystyrene (PS) or poly(methyl methacrylate) (PMMA) being historically most frequently used matrices for magnetic microparticles [91]. Several essential features are expected from inorganic magnetic core materials: (i) good response to the applied external magnetic field – the better the response, the lower the necessary intensity of the applied field and the better the process dynamics, (ii) very low remanence since the lower the remanence, the better the particle dispersibility after switching off the external magnetic field which allows for a fast sorption and desorption steps. Zero remanence causes no magnetic interactions between the particles (aggregation) after the removal of external field, (iii) small size (diameter); most of the separation/transport processes are heterogeneous, i.e., the smaller

the particles the higher the surface available for potential interactions, (iv) good chemical stability at different pH and redox conditions, (v) reasonable price, and (vi) easy production [91, 92]. Regarding prices, adsorbent with simple surface modifications can sell for 400 Euros per gram while more complex bioaffinity modifications such as grafting of protein A can sell for several thousand Euros per gram [92].

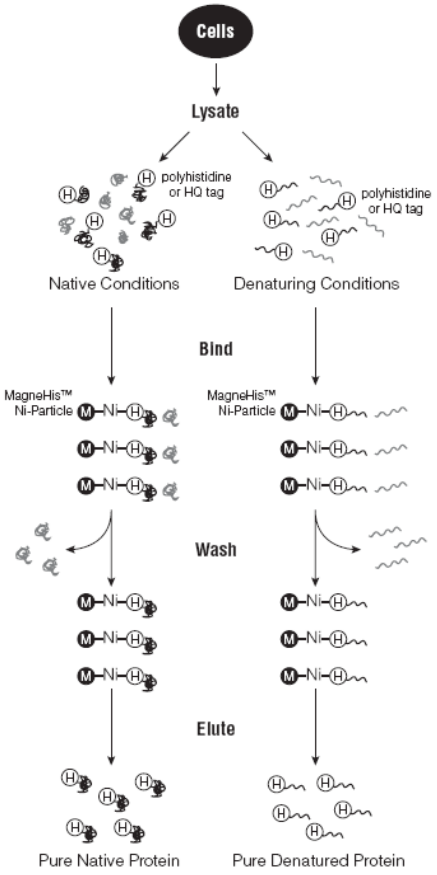

Figure 2-1 Magnetic separation of histidine-tagged protein (taken from Magne-His® user manual, Promega, WI).

As shown in Figure 2-1, recovery and purification of His6-tagged recombinant proteins using magnetic affinity adsorbents typically involves the following steps:

1) Cell lysis to expose intracellular protein

2) Application of magnetic beads slurry to capture recombinant proteins
3) Washing of magnetic beads to remove native and partially bound proteins
4) Elution of tightly bounded protein by imidazole displacement

The use of magnetic materials in practice depends on their properties, including magnetization, morphology, shape, size, and polydispersity. In terms of geometry, the bead shape is essential for practical applications if the best possible hydrodynamic flow properties are required. It offers important practical advantages of easy handling both in batch and continuous separation processes. Irregularly shaped particles are much more susceptible to mechanical attrition and breakdown than spherical ones which pose a problem when re-suspension of the adsorbent is required. As for particle shape, a narrow size distribution is advantageous because particles possess uniform physical and chemical properties and do not aggregate in liquids as easily. Larger particles have the disadvantage of a small specific surface area available for the attachment of functional groups or immobilization of bio-molecules (including enzymes) which yield a lower binding capability. This is the reason why microspheres (micrometer-size and smaller) are required, because they ensure a sufficiently high specific surface area available for the immobilization of reactive groups and other biologically active compounds. Furthermore, small size results in higher binding capacity and faster adsorption kinetics. However, too small a particle may cease to be magnetically responsive [92].

The evaluation of the ability of different magnetic adsorbents for the recovery of a variety of recombinant proteins has been carried out by many researchers. The adsorption usually follows a Langmuir-type binding equilibrium. Using the following formula, the maximum binding capacity of an adsorbent expressed in mg of bounded protein per gram

of adsorbent as well as the dissociation constant which is an indicator of how stable the complex is expressed as g/L can be determined.

$$q = q_0 \frac{C}{K + C} \qquad (2\text{-}1)$$

Where

q Equilibrium loading of the magnetic adsorbent (mg/g)

C Equilibrium bulk-phase protein concentration (mg/L)

K Dissociation constant (mg/L)

q_0 Maximum binding capacity of the adsorbent (mg/g)

It is clear that larger binding capacities are desirable since more proteins are recovered per gram of adsorbent while smaller values of K indicate a more stable complex. Franzeb *et al.* [92] looked at over 30 scientific papers of protein purification using magnetic adsorbents and extracted isotherm data. Unfortunately, several of these publications were theses for which it was difficult to retrieve useful data and validation was impossible. The parameter q_0 is the most important parameter as it provides the maximal adsorption capacity and within the papers that have been examined, its values ranged from 8 to 800 mg/g [92]. It is interesting to note that with mono component systems, i.e. with no other protein present, q_0 ranged from 42 to 800 mg/g while in feedstock systems (whey or *E. coli* lysate) q_0 only ranged from 8 to 180 mg/g. This is clearly due to the presence of multiple proteins interfering either by steric hindrance or by competing for available binding sites. As for K values, they ranged from 0.001 to 0.43 g/L for mono component systems and from 0.00077 to 0.047 g/L for feedstock systems. The initial slope of the binding isotherm (q_0/K) gives a clear indication of the sorbent suitability for a particular protein. In mono component systems, this ratio ranges from 0.58 to 99 L/g while for feedstock type systems this value ranges from 2.5 to 13. For all papers

considered by Franzeb *et al.* [92], 24 papers were from mono component systems while only seven were from feedstock systems. This is mainly due to the fact that few studies have been done with feedstock and furthermore, the values of q_0 and K were harder to extract from the published data [92]. It is clear from the reported data that feedstock systems exhibited lower q_0 than mono component systems. Furthermore, since systems are somewhat unique due to the type of feedstock and target protein, values extracted from these types of systems cannot be transposed to other systems. Mono component systems can be used for screening a type of adsorbent but if separation is planned for feedstock use, further testing is required to obtain representative binding kinetics. Adsorbent particle size also impacts on q_0, with nanoparticles showing the largest loading of 800 mg/g [93]. Micrometer size adsorbent can however support a loading that is larger than expected based on size when compared to nanometer size particles. Rather than the size of the magnetic particle, surface area available for monolayer binding of protein seems to be a better estimation of adsorbent maximal capacity [94].

2.7 Nickel nanoparticle synthesis

The polyol process in which metal salt precursors are reduced in a polyalcohol solvent has been used to produce a variety of elemental metal nanoparticles which have applications in many fields such as in magnetic resonance imaging (MRI), catalysis or solar cells [95]. Synthesis of metallic nanoparticles such as cobalt, copper, or nickel using polyol and modified method has been well studied and there magnetic characteristics are well known [95-102]. Several factors have been known to impact on the morphology and characteristics of nickel nanoparticles. Of these, the type of solvent used or more precisely the length of the solvent chain directly impact the nucleation and growth

steps [95]. It is also known that pH can have an impact on morphology and size [2-6-7] where high pH results in smaller particles diameters. Polyvinylpyrrolidone concentration has also been shown to help control particles size and morphology [96, 98-100].

2.8 References

1. Blondeau, J.M. What have we learned about antimicrobial use and the risks for *Clostridium difficile*-associated diarrhoea? *Journal of Antimicrobial Chemotherapy* **63**, 238-242 (2009).

2. Bobak, D.A. The molecular pathogenesis of *Clostridium difficile*-associated disease. *Current Infectious Disease Reports* **10**, 111-115 (2008).

3. Burakoff, R., Zhao, L., Celifarco, A.J., Rose, K.L., Donovan, V., Pothoulakis, C. and Percy, W.H. Effects of purified *Clostridium difficile* toxin A on rabbit distal colon. *Gastroenterology* **109**, 348-354 (1995).

4. Kelly, C.P., Pothoulakis, C. and Lamont, J.T. *Clostridium difficile* colitis. *New England Journal of Medicine* **330**, 257-262 (1994).

5. Lee, J.Y., Kim, H., Cha, M.Y., Park, H.G., Kim, Y.J., Kim, I.Y. and Kim, J.M. *Clostridium difficile* toxin A promotes dendritic cell maturation and chemokine CXCL2 expression through p38, IKK, and the NF-κB signaling pathway. *Journal of Molecular Medicine* **87**, 169-180 (2009).

6. Voth, D.E. and Ballard, J.D. *Clostridium difficile* toxins: Mechanism of action and role in disease. *Clinical Microbiology Reviews* **18**, 247-263 (2005).

7. Florin, I. and Thelestam, M. Internalization of *Clostridium difficile* cytotoxin into cultured human lung fibroblasts. *BBA - Molecular Cell Research* **763**, 383-392 (1983).

8. Henriques, B., Florin, I. and Thelestam, M. Cellular internalisation of *Clostridium difficile* toxin A. *Microbial Pathogenesis* **2**, 455-463 (1987).

9. Mitchell, M.J., Laughon, B.E. and Lin, S. Biochemical studies on the effect of *Clostridium difficile* toxin B on actin in vivo and in vitro. *Infection and Immunity* **55**, 1610-1615 (1987).

10. Burdon, D.W., George, R.H. and Mogg, G.A.G. Faecal toxin and severity of antibiotic-associated pseudomembranous colitis. *Journal of Clinical Pathology* **34**, 548-551 (1981).

11. Corthier, G., Muller, M.C., Wilkins, T.D., Lyerly, D. and L'Hardion, R. Protection against experimental pseudomembranous colitis in gnotobiotic mice by use of monoclonal antibodies against *Clostridium difficile* toxin A. *Infection and Immunity* **59**, 1192-1195 (1991).

12. Kyne, L., Warny, M., Qamar, A. and Kelly, C.P. Association between antibody response to toxin A and protection against recurrent *Clostridium difficile* diarrhoea. *Lancet* **357**, 189-193 (2001).

13. Babcock, G.J., Broering, T.J., Hernandez, H.J., Mandell, R.B., Donahue, K., Boatright, N., Stack, A.M., Lowy, I., Graziano, R., Molrine, D., Ambrosino, D.M. and Thomas Jr, W.D. Human monoclonal antibodies directed against toxins A and B prevent *Clostridium difficile*-induced mortality in hamsters. *Infection and Immunity* **74**, 6339-6347 (2006).

14. Casadevall, A., Dadachova, E. and Pirofski, L.A. Passive antibody therapy for infectious diseases. *Nature Reviews Microbiology* **2**, 695-703 (2004).

15. Lyerly, D.M., Bostwick, E.F., Binion, S.B. and Wilkins, T.D. Passive immunization of hamsters against disease caused by *Clostridium difficile* by use of bovine immunoglobulin G concentrate. *Infection and Immunity* **59**, 2215-2218 (1991).

16. Taylor, C.P., Tummala, S., Molrine, D., Davidson, L., Farrell, R.J., Lembo, A., Hibberd, P.L., Lowy, I. and Kelly, C.P. Open-label, dose escalation phase I study in healthy volunteers to evaluate the safety and pharmacokinetics of a human monoclonal antibody to *Clostridium difficile* toxin A. *Vaccine* **26**, 3404-3409 (2008).

17. Salcedo, J., Keates, S., Pothoulakis, C., Warny, M., Castagliuolo, I., LaMont, J.T. and Kelly, C.P. Intravenous immunoglobulin therapy for severe *Clostridium difficile* colitis. *Gut* **41**, 366-370 (1997).

18. Sougioultzis, S., Kyne, L., Drudy, D., Keates, S., Maroo, S., Pothoulakis, C., Giannasca, P.J., Lee, C.K., Warny, M., Monath, T.P. and Kelly, C.P. *Clostridium difficile* toxoid vaccine in recurrent *C. difficile*-associated diarrhea. *Gastroenterology* **128**, 764-770 (2005).

19. Wilcox, M.H. Descriptive study of intravenous immunoglobulin for the treatment of recurrent *Clostridium difficile* diarrhoea. *Journal of Antimicrobial Chemotherapy* **53**, 882-884 (2004).

20. Hamers-Casterman, C., Atarhouch, T., Muyldermans, S., Robinson, G., Hamers, C., Songa, E.B., Bendahman, N. and Hamers, R. Naturally occurring antibodies devoid of light chains. *Nature* **363**, 446-448 (1993).

21. Liu, J.L., Anderson, G.P. and Goldman, E.R. Isolation of anti-toxin single domain antibodies from a semi-synthetic spiny dogfish shark display library. *BMC Biotechnology* **7** (2007).

22. Shuntao, W., Jiannan, F., Jianwei, G., Leiming, G., Yan, L., Yingxun, S., Weisong, Q., Meiru, H., Gencheng, H. and Beifen, S. A novel designed single domain antibody on 3-D structure of ricin A chain remarkably blocked ricin-induced cytotoxicity. *Molecular Immunology* **43**, 1912-1919 (2006).

23. Krüger, C., Hultberg, A., Marcotte, H., Hermans, P., Bezemer, S., Frenken, L.G.J. and Hammarström, L. Therapeutic effect of llama derived VHH fragments against Streptococcus mutans on the development of dental caries. *Applied Microbiology and Biotechnology* **72**, 732-737 (2006).

24. Stewart, C.S., MacKenzie, C.R. and Christopher Hall, J. Isolation, characterization and pentamerization of α-cobrotoxin specific single-domain antibodies from a naïve phage display library: Preliminary findings for antivenom development. *Toxicon* **49**, 699-709 (2007).

25. Arbabi Ghahroudi, M., Desmyter, A., Wyns, L., Hamers, R. and Muyldermans, S. Selection and identification of single domain antibody fragments from camel heavy-chain antibodies. *FEBS Letters* **414**, 521-526 (1997).

26. Goldman, E.R., Andersen, G.P., Liu, J.L., Delehanty, J.B., Sherwood, L.J., Osborn, L.E., Cummins, L.B. and Hayhurst, A. Facile generation of heat-stable antiviral and antitoxin single domain antibodies from a semisynthetic llama library. *Analytical Chemistry* **78**, 8245-8255 (2006).

27. Holliger, P. and Hudson, P.J. Engineered antibody fragments and the rise of single domains. *Nature Biotechnology* **23**, 1126-1136 (2005).

28. Gibbs, W.W. Nanobodies. *Scientific American* **293**, 78-83 (2005).

29. Arbabi-Ghahroudi, M., Tanha, J. and MacKenzie, R. Prokaryotic expression of antibodies. *Cancer and Metastasis Reviews* **24**, 501-519 (2005).

30. Plückthun, A. Biotechnological aspects of antibody production in *E. coli*. *Acta Biotechnologica* **11**, 449-456 (1991).

31. Fernandez, L.A. Prokaryotic expression of antibodies and affibodies. *Current Opinion in Biotechnology* **15**, 364-373 (2004).

32. Gasser, B. and Mattanovich, D. Antibody production with yeasts and filamentous fungi: On the road to large scale? *Biotechnology Letters* **29**, 201-212 (2007).

33. Plückthun, A. Antibody engineering: Advances from the use of *Escherichia coli* expression systems. *Nature Biotechnology* **9**, 545-551 (1991).

34. Wakelin, S.J., Sabroe, I., Gregory, C.D., Poxton, I.R., Forsythe, J.L.R., Garden, O.J. and Howie, S.E.M. "Dirty little secrets"-Endotoxin contamination of recombinant proteins. *Immunology Letters* **106**, 1-7 (2006).

35. Yeh, C.M., Yeh, C.K., Hsu, X.Y., Luo, Q.M. and Lin, M.Y. Extracellular expression of a functional recombinant Ganoderma lucidium immunomodulatory protein by *Bacillus subtilis* and *Lactococcus lactis*. *Applied and Environmental Microbiology* **74**, 1039-1049 (2008).

36. Surawicz, C.M., Brandt, L.J., Binion, D.G., Ananthakrishnan, A.N., Curry, S.R., Gilligan, P.H., McFarland, L.V., Mellow, M. and Zuckerbraun, B.S. Guidelines for diagnosis, treatment, and prevention of *Clostridium difficile* infections. *American Journal of Gastroenterology* **108**, 478-498 (2013).

37. Horn, U., Strittmatter, W., Krebber, A., Knüpfer, U., Kujau, M., Wenderoth, R., Müller, K., Matzku, S., Plückthun, A. and Riesenberg, D. High volumetric yields of functional dimeric miniantibodies in *Escherichia coli* , using an optimized expression vector and high-cell-density fermentation under non-limited growth conditions. *Applied Microbiology and Biotechnology* **46**, 524-532 (1996).

38. Corisdeo, S. and Wang, B. Functional expression and display of an antibody Fab fragment in *Escherichia coli* : Study of vector designs and culture conditions. *Protein Expression and Purification* **34**, 270-279 (2004).

39. Rahbarizadeh, F., Rasaee, M.J., Forouzandeh-Moghadam, M. and Allameh, A.A. High expression and purification of the recombinant camelid anti-MUC1 single domain antibodies in *Escherichia coli* . *Protein Expression and Purification* **44**, 32-38 (2005).

40. Tanha, J., Dubuc, G., Hirama, T., Narang, S.A. and MacKenzie, C.R. Selection by phage display of llama conventional VH fragments with heavy chain antibody VHH properties. *Journal of Immunological Methods* **263**, 97-109 (2002).

41. Alvarez-Rueda, N., Behar, G., Ferre, V., Pugnière, M., Roquet, F., Gastinel, L., Jacquot, C., Aubry, J., Baty, D., Barbet, J. and Birkle, S. Generation of llama single-domain antibodies against methotrexate, a prototypical hapten. *Molecular Immunology* **44**, 1691-1701 (2007).

42. Omidfar, K., Rasaee, M.J., Modjtahedi, H., Forouzandeh, M., Taghikhani, M. and Golmakani, N. Production of a novel camel single-domain antibody specific for the type III mutant *Tumor Biology* **25**, 296-305 (2004).

43. Harmsen, M.M. and De Haard, H.J. Properties, production, and applications of camelid single-domain antibody fragments. *Applied Microbiology and Biotechnology* **77**, 13-22 (2007).

44. Shiloach, J. and Fass, R. Growing *E. coli* to high cell density - A historical perspective on method development. *Biotechnology Advances* **23**, 345-357 (2005).

45. Son, Y.J., Bae, J.Y., Chong, S.H., Lee, H.S., Mo, S.H., Kim, T.Y. and Choe, H. Expression, high cell density culture and purification of recombinant EC-SOD in *Escherichia coli* . *Applied Biochemistry and Biotechnology*, 1-14 (2010).

46. Lee, S.Y. High cell-density culture of *Escherichia coli*. *Trends in Biotechnology* **14**, 98-105 (1996).

47. Riesenberg, D. High-cell-density cultivation of *Escherichia coli*. *Current Opinion in Biotechnology* **2**, 380-384 (1991).

48. Hempfling, W.P. and Mainzer, S.E. Effects of varying the carbon source limiting growth on yield and maintenance characteristics of *Escherichia coli* in continuous culture. *Journal of Bacteriology* **123**, 1076-1087 (1975).

49. Phue, J.N., Noronha, S.B., Hattacharyya, R., Wolfe, A.J. and Shiloach, J. Glucose metabolism at high density growth of *E. coli* B and *E. coli* K: Differences in metabolic pathways are responsible for efficient glucose utilization in *E. coli* B as determined by microarrays and Northern blot analyses. *Biotechnology and Bioengineering* **90**, 805-820 (2005).

50. Sung, K.L. and Keasling, J.D. Effect of glucose or glycerol as the sole carbon source on gene expression from the Salmonella prpBCDE promoter in *Escherichia coli* . *Biotechnology Progress* **22**, 1547-1551 (2006).

51. El-Mansi, E.M.T. and Holms, W.H. Control of carbon flux to acetate excretion during growth of *Escherichia coli* in batch and continuous cultures. *Journal of General Microbiology* **135**, 2875-2883 (1989).

52. Sun, W.J., Lee, C., George, H.A., Powell, A.L., Dahlgren, M.E., Greasham, R. and Park, C.H. Acetate inhibition on growth of recombinant *E. coli* and expression of fusion protein TGFα-PE40. *Biotechnology Letters* **15**, 809-814 (1993).

53. Nakano, K., Rischke, M., Sato, S. and Märkl, H. Influence of acetic acid on the growth of *Escherichia coli* K12 during high-cell-density cultivation in a dialysis reactor. *Applied Microbiology and Biotechnology* **48**, 597-601 (1997).

54. De Mey, M., De Maeseneire, S., Soetaert, W. and Vandamme, E. Minimizing acetate formation in *E. coli* fermentations. *Journal of Industrial Microbiology and Biotechnology* **34**, 689-700 (2007).

55. Eiteman, M.A. and Altman, E. Overcoming acetate in *Escherichia coli* recombinant protein fermentations. *Trends in Biotechnology* **24**, 530-536 (2006).

56. Han, K., Lim, H.C. and Hong, J. Acetic acid formation in *Escherichia coli* fermentation. *Biotechnology and Bioengineering* **39**, 663-671 (1992).

57. Meyer, H.P., Leist, C. and Fiechter, A. Acetate formation in continuous culture of *Escherichia coli* K12 D1 on defined and complex media. *Journal of Biotechnology* **1**, 355-358 (1984).

58. Majewski, R.A. and Domach, M.M. Simple constrained-optimization view of acetate overflow in *E. coli*. *Biotechnology and Bioengineering* **35**, 732-738 (1990).

59. Chou, C.H., Bennett, G.N. and San, K.Y. Effect of modulated glucose uptake on high-level recombinant protein production in a dense *Escherichia coli* culture. *Biotechnology Progress* **10**, 644-647 (1994).

60. Chou, C.H., Bennett, G.N. and San, K.Y. Effect of modified glucose uptake using genetic engineering techniques on high-level recombinant protein production in *Escherichia coli* dense cultures. *Biotechnology and Bioengineering* **44**, 952-960 (1994).

61. Kim, B.S., Lee, S.C., Lee, S.Y., Chang, Y.K. and Chang, H.N. High cell density fed-batch cultivation of *Escherichia coli* using exponential feeding combined with pH-stat. *Bioprocess and Biosystems Engineering* **26**, 147-150 (2004).

62. Suzuki, T., Yamane, T. and Shimizu, S. Phenomenological background and some preliminary trials of automated substrate supply in pH-stat modal fed-batch culture using a setpoint of high limit. *Journal of Fermentation and Bioengineering* **69**, 292-297 (1990).

63. Fyferling, M., Uribelarrea, J.L., Goma, G. and Molina-Jouve, C. Oxygen transfer in intensive microbial culture. *Bioprocess and Biosystems Engineering* **31**, 595-604 (2008).

64. Castan, A., Näsman, A. and Enfors, S.O. Oxygen enriched air supply in *Escherichia coli* processes: Production of biomass and recombinant human growth hormone. *Enzyme and Microbial Technology* **30**, 847-854 (2002).

65. Çalik, P., Yilgör, P., Ayhan, P. and Demir, A.S. Oxygen transfer effects on recombinant benzaldehyde lyase production. *Chemical Engineering Science* **59**, 5075-5083 (2004).

66. Belo, I. and Mota, M. Batch and fed-batch cultures of *E. coli* TB1 at different oxygen transfer rates: Effect of stirring and oxygen partial pressures on cell growth and cytochrome b5 production. *Bioprocess Engineering* **18**, 451-455 (1998).

67. Cutayar, J.M. and Poillon, D. High cell density culture of *E. coli* in a fed-batch system with dissolved oxygen as substrate feed indicator. *Biotechnology Letters* **11**, 155-160 (1989).

68. Bentley, W.E., Mirjalili, N., Andersen, D.C., Davis, R.H. and Kompal a, D.S. Plasmid-encoded protein: The principal factor in the 'metabolic burden' associated with recombinant bacteria. *Biotechnology and Bioengineering* **35**, 668-681 (1990).

69. Yildir, C., Önsan, Z.I. and Kirdar, B. Optimization of starting time and period of induction and inducer concentration in the production of the restriction enzyme EcoRI from recombinant *Escherichia coli* 294. *Turkish Journal of Chemistry* **22**, 221-226 (1998).

70. Griffiths, A.J.F., Miller, J.H., T.Suzuki, D., Lewontin, R.C. and Gelbart., W.M. An Introduction to genetic analysis. (W.H. Freeman, New York; 2000).

71. Nancib, N., Branlant, C. and Boudrant, J. Metabolic roles of peptone and yeast extract for the culture of a recombinant strain of *Escherichia coli*. *Journal of Industrial Microbiology* **8**, 165-169 (1991).

72. Hopkins, T.R. Physical and chemical cell disruption for the recovery of intracellular proteins *Bioprocess technology* **12**, 57-83 (1991).

73. Majors, R.E. Sample preparation for large-scale protein purification *LC-GC Europe* **19**, 82-92 (2006).

74. Helenius, A. and Simons, K. Solubilization of membranes by detergents. *Biochimica et Biophysica Acta* **415**, 29-79 (1975).

75. Harrison, S.T.L. Bacterial cell disruption: A key unit operation in the recovery of intracellular products. *Biotechnology Advances* **9**, 217-240 (1991).

76. Balasundaram, B., Harrison, S. and Bracewell, D.G. Advances in product release strategies and impact on bioprocess design. *Trends in Biotechnology* **27**, 477-485 (2009).

77. Allen, J.R., Patkar, A.Y., Frank, T.C., Donate, F.A., Yuk, C.C., Shields, J.E. and Gustafson, M.E. Use of glycol ethers for selective release of periplasmic proteins from Gram-negative bacteria. *Biotechnology Progress* **23**, 1163-1170 (2007).

78. Hammes, W., Schleifer, K.H. and Kandler, O. Mode of action of glycine on the biosynthesis of peptidoglycan. *Journal of Bacteriology* **116**, 1029-1053 (1973).

79. Kaderbhai, N., Karim, A., Hankey, W., Jenkins, G., Venning, J. and Kaderbhai, M.A. Glycine-induced extracellular secretion of a recombinant cytochrome expressed in *Escherichia coli*. *Biotechnology and Applied Biochemistry* **25**, 53-61 (1997).

80. Naglak, T.J. and Wang, H.Y. Recovery of a foreign protein from the periplasm of *Escherichia coli* by chemical permeabilization. *Enzyme and Microbial Technology* **12**, 603-611 (1990).

81. Tsuchido, T., Katsui, N. and Takeuchi, A. Destruction of the outer membrane permeability barrier of *Escherichia coli* by heat treatment. *Applied and Environmental Microbiology* **50**, 298-303 (1985).

82. Ren, X., Yu, D., Han, S. and Feng, Y. Thermolysis of recombinant *Escherichia coli* for recovering a thermostable enzyme. *Biochemical Engineering Journal* **33**, 94-98 (2007).

83. Ren, X., Yu, D., Yu, L., Gao, G., Han, S. and Feng, Y. A new study of cell disruption to release recombinant thermostable enzyme from *Escherichia coli* by thermolysis. *Journal of Biotechnology* **129**, 668-673 (2007).

84. Yang, J., Moyana, T., Mackenzie, S., Xia, Q. and Xiang, J. One hundred seventy-fold increase in excretion of an FV fragment-tumor necrosis factor alpha fusion protein (sFV/TNF-α) from *Escherichia coli* caused by the synergistic effects of glycine and Triton X-100. *Applied and Environmental Microbiology* **64**, 2869-2874 (1998).

85. Choi, J.I. and Lee, S.Y. Efficient and economical recovery of poly(3-hydroxybutyrate) from recombinant *Escherichia coli* by simple digestion with chemicals. *Biotechnology and Bioengineering* **62**, 546-553 (1999).

86. Mörbe, J.L. and Riesenberg, D. Release of miniantibodies from *E. coli* cells into the supernatant at low and high cell densities. *Microbiological Research* **152**, 385-394 (1997).

87. Jang, K.H., Seo, J.W., Song, K.B., Kim, C.H. and Rhee, S.K. Extracellular secretion of levansucrase from *Zymomonas mobilis* in *Escherichia coli*. *Bioprocess Engineering* **21**, 453-458 (1999).

88. Anand, H., Balasundaram, B., Pandit, A.B. and Harrison, S.T.L. The effect of chemical pretreatment combined with mechanical disruption on the extent of disruption and release of intracellular protein from *E. coli*. *Biochemical Engineering Journal* **35**, 166-173 (2007).

89. Langer, E. and Ranck, J. Capacity bottleneck squeezed by downstream processes. *BioProcess Int* **4**, 14-18 (2006).

90. Low, D., O'Leary, R. and Pujar, N.S. Future of antibody purification. *Journal of Chromatography B: Analytical Technologies in the Biomedical and Life Sciences* **848**, 48-63 (2007).

91. Horák, D., Babič, M., Macková, H. and Beneš, M.J. Preparation and properties of magnetic nano- and microsized particles for biological and environmental separations. *Journal of Separation Science* **30**, 1751-1772 (2007).

92. Franzreb, M., Siemann-Herzberg, M., Hobley, T.J. and Thomas, O.R.T. Protein purification using magnetic adsorbent particles. *Applied Microbiology and Biotechnology* **70**, 505-516 (2006).

93. Bucak, S., Jones, D.A., Laibinis, P.E. and Hatton, T.A. Protein separations using colloidal magnetic nanoparticles. *Biotechnology Progress* **19**, 477-484 (2003).

94. O'Brien, S.M., Sloane, R.P., Thomas, O.R.T. and Dunnill, P. Characterisation of non-porous magnetic chelator supports and their use to recover polyhistidine-tailed T4 lysozyme from a crude *E. coli* extract. *Journal of Biotechnology* **54**, 53-67 (1997).

95. Carroll, K.J., Reveles, J.U., Shultz, M.D., Khanna, S.N. and Carpenter, E.E. Preparation of elemental Cu and Ni nanoparticles by the polyol method: An experimental and theoretical approach. *Journal of Physical Chemistry C* **115**, 2656-2664 (2011).

96. Ai, F., Yao, A., Huang, W., Wang, D. and Zhang, X. Synthesis of PVP-protected NiPd nanoalloys by modified polyol process and their magnetic properties. *Physica E: Low-Dimensional Systems and Nanostructures* **42**, 1281-1286 (2010).

97. Bai, L., Fan, J., Cao, Y., Yuan, F., Zuo, A. and Tang, Q. Shape-controlled synthesis of Ni particles via polyol reduction. *Journal of Crystal Growth* **311**, 2474-2479 (2009).

98. Couto, G.G., Klein, J.J., Schreiner, W.H., Mosca, D.H., de Oliveira, A.J.A. and Zarbin, A.J.G. Nickel nanoparticles obtained by a modified polyol process: Synthesis, characterization, and magnetic properties. *Journal of Colloid and Interface Science* **311**, 461-468 (2007).

99. Li, P., Guan, J., Zhang, Q. and Zhao, W. Preparation and characterization of monodisperse nickel nanoparticles by polyol process. *Journal Wuhan University of Technology, Materials Science Edition* **20**, 35-37 (2005).

100. Okram, G.S., Soni, A. and Prasad, R. The pH-controlled particle size tuning of nanocrystalline ni in polyol synthesis method without additional cappant. *Advanced Science Letters* **4**, 132-135 (2011).

101. Omrani, A.D., Bousnina, M.A., Smiri, L.S., Taibi, M., Leone, P., Schoenstein, F. and Jouini, N. Elaboration of nickel nanoparticles by modified polyol process and their spark plasma sintering, characterization and magnetic properties of the nanoparticles and the dense nano-structured material. *Materials Chemistry and Physics* **123**, 821-828 (2010).

102. Saravanan, P., Jose, T.A., Thomas, P.J. and Kulkarni, G.U. Submicron particles of Co, Ni and Co-Ni alloys. *Bulletin of Materials Science* **24**, 515-521 (2001).

Chapter 3: High cell density culture of recombinant *Escherichia coli* expressing ToxA5.1 using dual-point pH-stat fed-batch fermentation

Albert Parisien, Sallé Dembélé, Jules Thibault and Christopher Q. Lan*

Chemical and Biological Engineering Department, University of Ottawa, Ottawa, ON, Canada K1N 6N5

Corresponding author: Christopher Q. Lan, Christopher.Lan@uottawa.ca

3.1 Abstract

A novel fed-batch strategy, dual-point pH-stat (DPPS), was developed for high cell density culture (HCDC) of recombinant *Escherichia coli* TG1 expressing ToxA5.1, a single domain antibody neutralizing *Clostridium difficile* toxin A. A final biomass of 26.6 g DCW/L was achieved using the DPPS fed-batch. This strategy does not require sophisticated instrumentation and proved to be a simple and yet efficient way of achieving HCDC.

Keywords: *E. coli*, Fed-batch, Fermentation, pH-stat

3.2 Introduction

Drug resistant strains of *Clostridium difficile* are a major health concern in hospital settings [1]. *C. difficile* associated diseases (CDAD) are toxin-mediated, which can be treated by means of lessening the severity of symptoms via toxin inactivation using antibodies [2] to drastically reduce CDAD morbidity. A novel llama single domain antibody (pSJF2H-ToxA5.1) was expressed in recombinant *Escherichia coli* TG1 targeting *C. difficile* enterotoxin A (TcdA) and shown to have toxin neutralizing activities [3]. Furthermore, a novel purification method was developed in a previous study [4] to selectively recover ToxA5.1. It is therefore of great interest to develop optimized processes for its cost-effective production at large scale and obtaining high cell density culture is the first step towards this goal.

Developments in biochemical engineering since the early 90's have led to high cell density culture (HCDC) when cells such as bacteria, yeast or fungi are grown in fed-batch mode. Several researchers reported cell densities for *E. coli* ranging from 17.6 to 134 g/L on a dry cell weight basis (DCW) [5, 6]. Being able to achieve high cell density significantly reduces capital investments as well as operation costs because HCDC leads to high volumetric productivity (g of product unit volume^{-1} time^{-1}) [5, 7].

One of the major problems with batch fermentation is that substrate inhibition can occur when the concentration of a substrate is above a critical level. For instance, it was reported that for *E. coli*, substrates and nutrients become inhibitory if they are present at the following respective levels: glucose > 50 g/L, NH_4OH > 3 g/L, boron > 44 mg/L, cobalt > 0.5 mg/L, copper > 4.2 mg/L, iron > 1.15 g/L, magnesium > 8.7 g/L, molybdenum >0.8 g/L, phosphorus > 10 g/L and zinc > 38 mg/L [8]. Possible mechanisms

of substrate inhibition include: 1) osmotic pressure increase in the medium when the initial concentrations are too high, thereby leading to detrimental conditions for the cultures [5], 2) It is also a significant concern that some substrates may precipitate at high initial concentration [5] which makes them unavailable for cell growth, and 3) many bacterial strains can produce inhibitory products such as acidic metabolic by-products when a specific substrate concentration such as glucose is too high [9].

Nutrients are required in large quantities if high cell densities are to be achieved but the problem of substrate inhibition and precipitation due to low solubility must be dealt with. Furthermore, the fast growth of some microbial strains is associated with production of large quantities of inhibitory metabolites. For instance, when *E. coli* is cultivated in high glucose concentration medium, it may overproduce acetic acid as a byproduct of glucose catabolism in association with fast cell growth [10]. It is therefore necessary to control the cell growth of these strains below a given specific growth rate, known as the critical growth rate [11-15]. To this end, fed-batch fermentation is commonly used. Fed-batch fermentation is a two-phase process with the first phase being a batch phase where all nutrients required for cell growth are present in non-inhibitory concentrations and the second phase consisted in the feeding of limiting nutrients in a controlled manner to avoid substrate inhibition while supplying sufficient nutrients for HCDC. These limiting nutrients are typically the carbon source (e.g., sugars) and other macronutrients.

Different feeding control strategies have been developed for HCDC in the last few decades. These strategies are implemented either with or without feedback control. Feeding with feedback control can be further classified into two groups: direct or indirect

feedback control. Direct feedback control relies on the *in situ* measurement of the concentration of the substrate of primary concern (e.g., on-line glucose analyzer for glucose feeding) while indirect feedback control can be achieved by monitoring one of the more easily measured indicators to infer the key substrate consumption. For instance, when glucose is the key substrate, indirect feedback control indicators such as dissolved oxygen (DO), carbon dioxide evolution, medium pH and cell concentration are commonly used [7]. Feeding without feedback control strategies include intermittent feeding, constant rate feeding, linear feeding, stepwise feeding, and exponential feeding. Some of these strategies such as intermittent feeding, constant rate feeding, linear feeding, and stepwise feeding do not offer good control over the key substrate in the culture and are suitable for a very limited number of processes. On the other hand, more precise strategies, such as exponential feeding, require a thorough knowledge and an accurate model of the system to deliver the appropriate control for HCDC.

One of the most promising indirect feedback control feeding strategies is the use of a pH probe for the feedback control of glucose feeding, which is called pH-stat feeding. It is advantageous since pH probes are sensitive, reliable, easy to use and readily available in standard fermentation setup [7]. The strategy of pH-stat relies on the pH change of culture, which is closely associated with glucose catabolism, for feeding control. When glucose is exhausted from the medium, the pH of the culture rises because the cells are forced to consume the acidic by-products of glucose catabolism. This change in pH can be utilized to devise a feeding strategy such that whenever the pH rises above a certain preset value, glucose is fed to the fermentation culture [16]. For instance, an on-

demand pH-stat glucose feeding strategy was reported to achieve a biomass concentration of *E. coli* of 15 g DCW /L [17].

The potential of fed-batch fermentation is better demonstrated by studies involving more sophisticated strategies. For instance, coupling the pH-stat strategy with fuzzy control or with an exponential feeding strategy with monitoring of the biomass to compute the proper amount of feeding solution to be added at a particular feeding point were reported to lead to a biomass level of 61 g DCW/L [18] or 72 g DCW/L [19], respectively. Furthermore, it was reported by Korz *et al*. [20] that *E. coli* TG1 wild-type could be cultivated to reach a HCDC of 128 g DCW/L using an exponential feeding strategy. These strategies, however, require either complex control systems or process-specific mathematic models or both to succeed. It is therefore of great interest to develop simplistic, robust and efficient feeding control strategies.

In this research, we demonstrated that a simple dual-point pH-stat feeding strategy could enable HCDC of *E. coli* by providing indirect feedback control over feeding of solution containing glucose and other macronutrients.

3.3 Materials and Methods

3.3.1 Bacterial strain and plasmid

DNA encoding ToxA5.1, a llama single domain antibody with specificity for *C. difficile* toxin A [3], was cloned into the expression vector pSJF2H [21] via BbsI and BamHI (New England Biolabs, Mississauga, ON) restriction sites. Protein expression was performed in TG1 *E. coli* cells purchased from Invitrogen (Carlsbad, CA). The empty vector strain consisted of TG1 *E. coli* cells bearing an empty expression vector pSJF2H (no DNA insert). Recombinant strains were grown in 20 g/L LB Lennox medium (Fisher

Scientific, Pittsburgh, PA) and screened for the best sdAb producer when applicable. The best expressing recombinant colony was seeded in 50 mL of defined medium [20] containing 10 g/L of glucose and 100 µg/mL of ampicillin in a 250 mL Erlenmeyer flask at 30°C for 18 h in an orbital shaker at 200 rpm. The culture, to which 15% sterile glycerol was added, was then aliquoted as 1.5 mL in 2 mL micro-centrifuge tubes, kept in a freezer (Thermo Electron Corp. Asheville, NC) at -80°C, and served as primary inoculum for the bioreactors.

3.3.2 Media and feeding solution

3.3.2.1 Medium composition

Batch medium and feeding solution used in this study are identical to those reported by Korz et al. [20] except that the glucose concentration was 7 g/L or varied as specified in the text. Defined medium consisted in glucose 7 g/L, KH_2PO_4 13.3 g/L, $(NH_4)_2HPO_4$ 4 g/L, $MgSO_4$ 1.2 g/L, citric acid 1.7 g/L, trace metal solution consisted in EDTA 8.4 mg/L, $CoCl_2 \bullet 6\ H_2O$ 2.5 mg/L, $MnCl_2 \bullet 4\ H_2O$ 15 mg/L, $CuCl_2 \bullet 2\ H_2O$ 1.5 mg/L, H_3BO_3 3 mg/L, $Na_2MoO_4 \bullet 2\ H_2O$ 2.5 mg/L, $Zn(CH_3COO)_2 \bullet 2\ H_2O$ 13 mg/L, Fe (III) citrate 100 mg/L, thiamine HCl 4.5 mg/L, and ampicillin 100 mg/L. Fed-batch feeding solution contained glucose 600 g/L, $MgSO_4$ 20 g/L, trace metal solution consisted in EDTA 13 mg/L, $CoCl_2 \bullet 6\ H_2O$ 4 mg/L, $MnCl_2 \bullet 4\ H_2O$ 23.5 mg/L, $CuCl_2 \bullet 2\ H_2O$ 2.5 mg/L, H_3BO_3 5 mg/L, $Na_2MoO_4 \bullet 2\ H_2O$ 4 mg/L, $Zn(CH_3COO)_2 \bullet 2\ H_2O$ 16 mg/L, and Fe (III) citrate 40 mg/L.

The ammonium hydroxide solution used for pH control contained 25% v/v of NH_4OH (Fisher Scientific).

3.3.2.2 Inoculum preparation

Four 500 mL Erlenmeyer flasks each containing 100 mL of defined medium were inoculated with 1 mL culture preserved in a -80^{o}C freezer, which was thawed at room temperature before transfer. The seeded flasks were then incubated at 30°C for 12 h in an orbital shaker at 200 rpm. The inoculum medium was the aforementioned defined medium containing 10 g/L of glucose and 100 μg/mL of ampicillin. The culture was transferred to two sterile 200 mL centrifuge bottles and centrifuged at 2 550 rcf for 20 min at 20°C using a Hermle Labortechnik GmbH centrifuge (Wehingen, Germany). The supernatant fluid was discarded and both pellets were then re-suspended with 25 mL of defined medium and mixed together, for a total of 50 mL at 8-fold concentration. This concentrated mixture served as inoculum for the bioreactors where a sufficient amount was added to each bioreactor to obtain approximately an initial OD_{600} of 0.15.

3.3.3 Fermentations

Fermentations were performed in New-Brunswick Scientific (Edison, NJ) BioFlo110 3-L bioreactors with a working volume of 1.5 L. Batch phase was carried out in 1.5 L of defined medium containing 100 μg/mL of ampicillin. Temperature (28°C) and agitation with two 6-blades Rushton impeller on a shaft (300 rpm) were kept constant via the control module of the bioreactors. During the batch phase, the culture pH was controlled by the addition of 25% v/v NH_4OH solution (Fisher Scientific) when the pH dropped to a value lower than the setpoint, i.e., pH 6.6. The lower limit of the dissolved oxygen (DO) was set at 20% air saturation and a constant airflow of 1 vvm was sparged into the fermentation medium. When the oxygen demand could not be satisfied with the air supply, pure oxygen (Linde Canada, Ottawa, ON) was used to increase the oxygen

mole fraction of the inlet gas stream via the BioFlo110 gas mix module while the inlet gas flow rate remained constant at 1 vvm. The bioreactors were inoculated as described in the previous section.

3.3.4 Feeding strategies

3.3.4.1 Single-point pH-stat (SPPS) Fed-batch

When the single-point pH-stat strategy (SPPS) was employed, the addition of the feeding solution was controlled by the acid pump of the built-in pH control loop of the bioreactor. Instead of feeding an acid solution to lower the pH, the feeding solution containing 600 g/L of glucose and other macronutrients was added to the fermentation broth and the organic acids such as acetic acid produced as by-products of glucose metabolism would result in a decrease of pH. This was done via the bioreactor controller and did not require any particular equipment. When pH decreased below the setpoint of 6.8, NH_4OH (25% v/v) was added to raise the pH.

3.3.4.2 Dual-point pH-stat (DPPS) control strategy

This strategy was implemented using the bioreactor pH control loop coupled with a LabVIEW interface and OPC (Object Linking and Embedding (OLE) for Process Control) functions to prevent the pH from falling below the lower setpoint or from rising above the upper setpoint. When pH decreased below the lower setpoint, which was set to 6.6 in this investigation, NH_4OH (25% v/v) was added to the medium via the pH control loop. When the pH rose to above the upper setpoint, i.e., pH 6.8, an injection of 25 ml of feeding solution containing 600 g/L glucose was added, corresponding to addition of 15 g glucose or elevating the glucose concentration of the culture by 10 g glucose/L. To avoid excessive sugar addition, a LabVIEW subroutine prevented the injection of a second

feeding solution pulse for 5 min which was sufficient time to allow pH to decrease below 6.8shortly after addition of glucose.

3.3.5 Analysis of glucose and acetate

The concentrations of glucose and acetate were determined using an Agilent 1200 HPLC unit (Agilent Technologies, Foster City, CA) with a Shodex S-1011 column (Showa Denko K.K., Kawasaki, Japan) and a Shodex SG-1011 guard column. Samples of 50 μL were loaded and the mobile phase (5 mM, H_2SO_4) was run at 0.6 mL/min. Glucose was quantified using a refractive index (RI) detector while acetate was quantified using a UV detector (λ= 210 nm).

3.4 Results

3.4.1 Batch fermentation at high initial glucose concentration

It was reported by Korz *et al*. [20] that *E. coli* TG1 wild-type could be grown to reach a HCDC of 128 g DCW/L with an initial glucose concentration of 25 g/L using an exponential feeding strategy. However, our attempt to repeat these experiments failed with cell growth being completely inhibited in the batch phase, i.e., before the fed-batch phase was started. The glucose, biomass, and acetate profiles of a typical batch phase are shown in Figure 3-1.

As shown in Figure 3-1, up to approximately 11.5 h in the batch phase, 11.57 g/L of glucose was consumed to produce 1.78 g/L DWC of biomass for a yield of 0.15 g DCW/g glucose. During that period, the acetate concentration reached 2 g/L. However, further depletion of the remaining 16 g/L of glucose from 11.5 to 29 h in the batch phase only led to a biomass increase of 0.82 g/L DCW with a biomass yield of 0.05 g DCW/g

glucose, which is only 1/3 of that in the earlier stage (i.e., from time 0 to 11.5 h). In the same period, acetate concentration increased from 2.0 g/L at 11.5 h to 9.16 g/L at 29 h.

At the end of the fermentation, a final biomass concentration of 2.94 g DCW/L was obtained, resulting in an overall yield of biomass on glucose ($Y_{X/S}$) of 0.1 g DCW/g glucose Table 3-1. It is worth noting that, after 4h of fermentation, the acetate level became detectable in the culture and increased quickly thereafter until the end of the batch phase with a final concentration of 9.16 g/L.

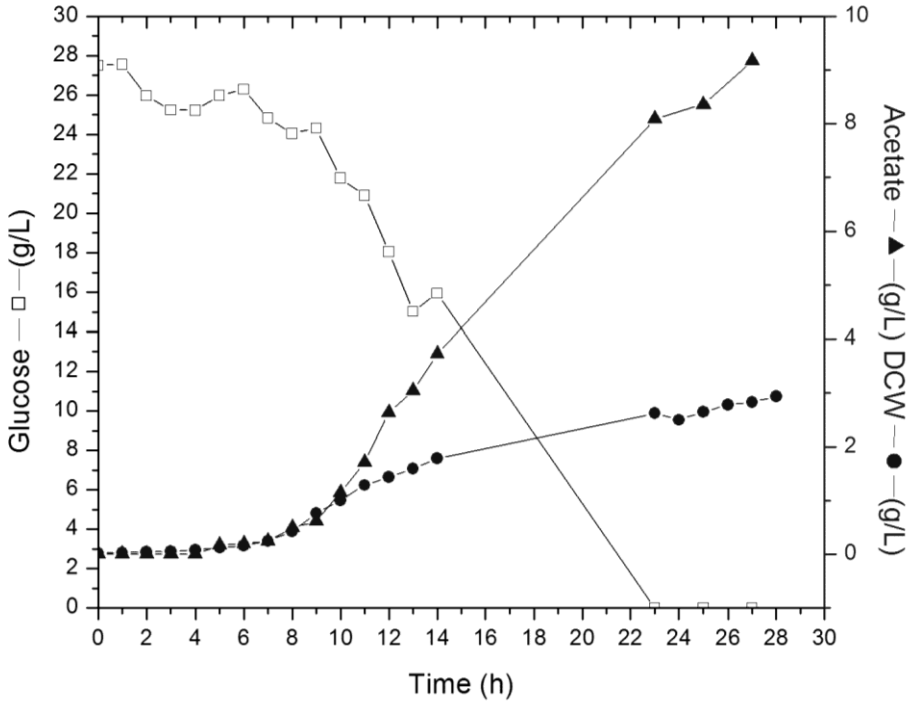

Figure 3-1: Batch growth of *E. coli* TG1 bearing the plasmid for the expression of ToxA5.1 single domain antibody against *C. difficile* toxin A. Cells were grown in defined medium containing initially 27 g/L of glucose at 28°C.

Table 3-1: Parameters and kinetic coefficients for the different pH-stat experiments: SSPS (single-point pH-sat), DPPSL (Dual-point pH-stat low glucose pulse), and DPPSH (Dual-point pH-stat high glucose pulse).

	Batch				Fed-batch			Overall			
	S_0	μ_{max}	X	$Y_{X/S}$	S_{fed}	X	$Y_{X/S}$	S_{total}	X	$Y_{X/S}$	NH_3
	g/L	h^{-1}	g/L	g X/g S	g	g/L	g X/g S	g	g/L	g X/g S	g
Batch	27	2.12	2.94	0.10	---	---	---	---	---	---	---
SPPS	7	0.66	0.48	0.018	---	---	---	---	---	---	---
DPPSL	7	1.41	1.82	0.26	5	0.61	0.12	12	2.43	0.20	1.0
DPPSH	7	2.06	1.97	0.28	318	26.6	0.16*	325	26.6	0.17	30.5

* $Y_{X/S}$ was calculated using glucose added up to the point where the biomass stopped increasing

3.4.2 Effect of genetic modification on cell growth

The strain of *E. coli* used in our attempts to achieve HCDC using Korz's [20] approach was a genetically engineered strain bearing the pSJF2H-ToxA5.1 plasmid and the genetic modification could have been responsible for the failure to initiate the fed-batch phase [22]. To test this hypothesis, experiments were performed comparing growth characteristics of *E. coli* TG1 wild-type, *E. coli* TG1 transformed with an empty pSJF2H vector and *E. coli* TG1 recombinant with pSJF2H vector containing the ToxA5.1 gene.

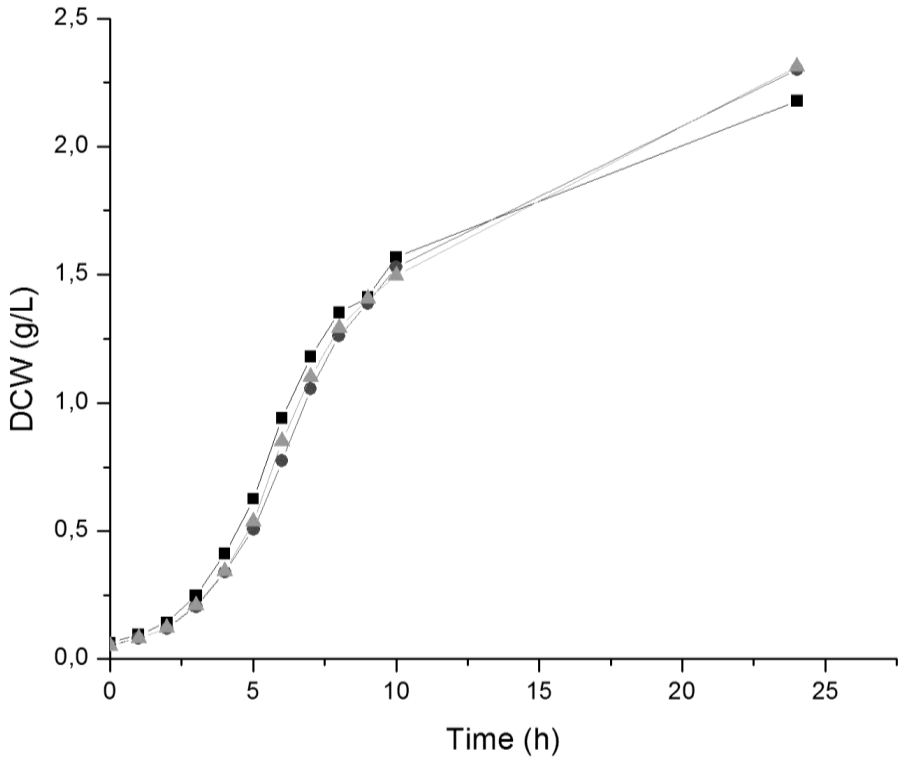

Figure 3-2: Growth curves of TG1 strains in defined medium (glucose 25 g/L) at 28 °C. *E. coli* TG1 wild-type (–■–), *E. coli* TG1 transformed with an empty pSJF2H vector (–▲–) and *E. coli* TG1 recombinant with pSJF2H vector containing the ToxA5.1 gene (–●–). Points represent a triplicate average and standard deviations are not shown for clarity. The average standard deviation observed was 0.024 g DCW/L for wild-type, 0.025 g/L for recombinants containing empty vectors and 0.015 g/L for recombinant *E. coli* TG1.

As shown in Figure 3-2, the genetic modification did not yield a significant difference in either the biomass concentration profiles or the final biomass between the wild-type *E. coli* TG1 (2.18 g/L DCW), *E. coli* TG1 transformed with an empty vector (2.31 g/L DCW) and *E. coli* TG1 recombinant with vector containing the ToxA5.1 gene 2.31 g/L DCW). It was concluded that the genetic modification was not the cause for the low biomass during the batch phase.

3.4.3 Single point pH-stat (SPPS)

In single point pH-stat (SPPS), the culture pH was controlled at a single setpoint of 6.8 (Figure 3-3A) by adding NH_4OH solution (25% v/v) to raise the pH and the feeding solution, containing 600 g/L of glucose as specified in Materials and Methods section, to lower the pH. The profiles of key parameters of a typical fed-batch fermentation using SPPS are shown in Figure 3-3. Figure 3-3A indicates that the culture pH was well controlled at the setpoint of 6.8 throughout the entire course of the fermentation. Figure 3-3B shows the outputs of the NH_4OH pump and the feeding solution pump, which were controlled by the built-in pH control loop of the bioreactor. When the output value was positive, it indicates the NH_4OH pump was activated with NH_4OH solution added. The percentage value represents the actual flowrate in comparison to the total flowrate when the pump is fully operating. When the value was negative, it indicates that the feeding solution pump was operating at the specified percentage of the full capacity of the pump.

As shown in Figure 3-3B, only NH_4OH solution was added for approximately the first 18 h of fermentation. Then the feeding solution pump was activated, marking the end of the batch phase and the beginning of the fed-batch phase. During the fed-batch phase, both NH_4OH and feeding solution (containing 600 g/L glucose) were added in an alternating manner to maintain the pH at the setpoint of 6.8 (Figure 3-3A). The alternating cycles between the NH_4OH solution and the feeding solution, however, did not correspond to the depletion of glucose nor acidic metabolites in the culture as intended by this control strategy. A total of 30.44 g NH_4OH were added during the entire period of fermentation. Furthermore, 5.0 mL of feeding solution, corresponding to 3.6 g

of glucose were added in the fed-batch phase. Nonetheless, as shown in Figure 3-3C, cell growth stopped shortly after the fed-batch phase started. It is interesting to observe as indicated by Figure 3-3D that the DO value was decreasing until approximately 30 h of fermentation, at which point it started oscillating around the set value of 20% air saturation. This indicates that the metabolism of *E. coli* was active throughout the entire course of 48 h of fermentation, even though no cell growth was observed after 27 h of fermentation, shortly after the fed-batch phase started at around 20 h. Figure 3-3C also shows that the glucose was quickly consumed in the batch phase with the growth of biomass kept at a low level. On the other hand, a quick accumulation of acetate was observed in the period of 10-15 h and its concentration was less than 15 g/L. However, the acetate concentration increased to a high concentration of 21.8 g/L at 48 h while the glucose concentration was zero throughout the fed-batch phase, indicating that the glucose added into the culture was mainly directed to the production of acetic acid, which was probably the major cause of the cessation of cell growth in the fed-batch phase. As summarized in Table 3-1, the biomass concentration only reached 0.48 g DCW/L over a period of 48 h. During the batch phase, a μ_{max} of 0.66 h^{-1} and a biomass/glucose yield ($Y_{X/S}$) of 0.018 g X/g S prevailed.

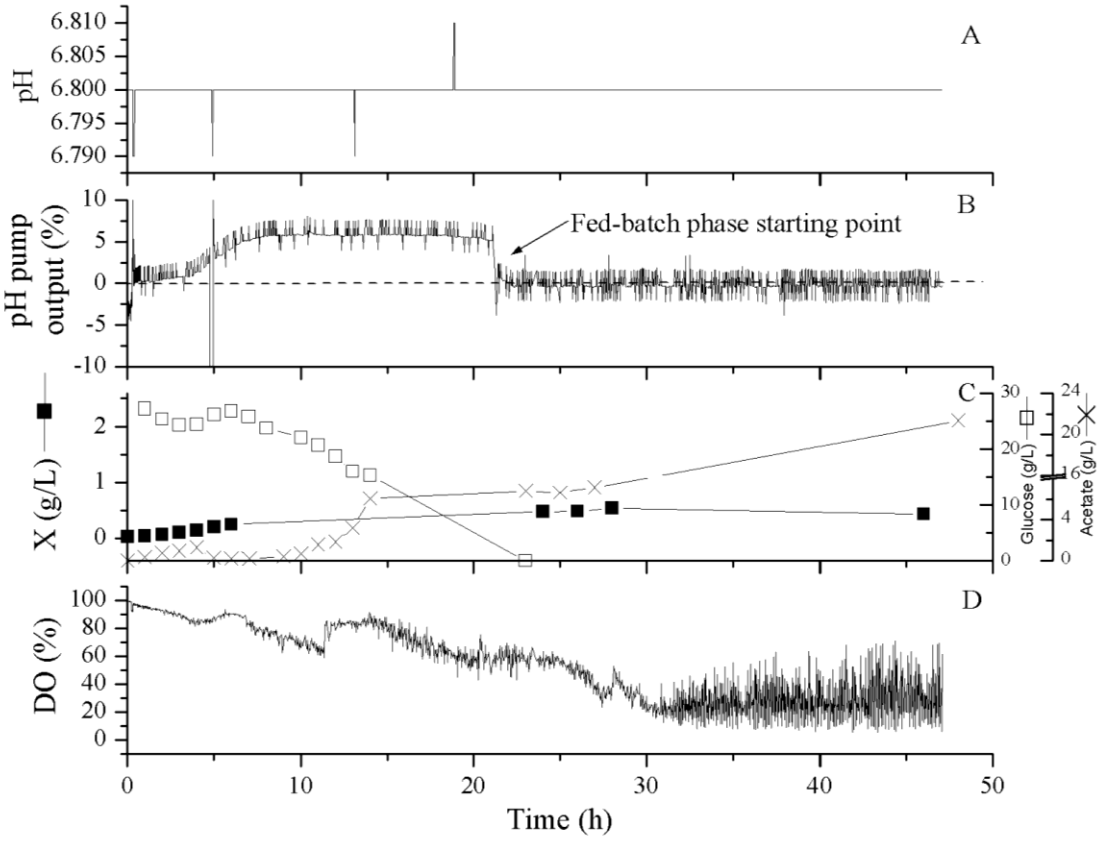

Figure 3-3: Single-point pH-stat control strategy (SPPS): (A) pH value, (B) output of the pH control module, (C) Biomass profile, and (D) Dissolved oxygen percentage saturation. The axis for acetate is broken into two sections to allow clear depiction of data in the range of 0-5 g/L and 18-22 g/L.

3.4.4 Dual point pH-stat (DPPS)

3.4.4.1 Low glucose feeding dosage (DPPSL)

The SPPS feeding strategy led to shortcut cycles, which are feeding cycles that did not correspond directly to the depletion of either glucose or acidic metabolites as desired and, consequently, failed to prevent acetate from accumulating beyond inhibitive concentration. As a result, HCDC was not achievable. To overcome the shortcut cycles, a dual-point pH-stat feeding strategy was devised and tested. In this strategy, the pH was controlled in a range between two setpoints: 6.6 to 6.8. When culture pH decreased due to the production of organic acids such as acetate during glucose metabolism by *E. coli*,

NH_4OH was added to prevent the pH from decreasing below the lower setpoint (pH 6.6). On the other hand, when the pH increased to the upper setpoint (pH 6.8) due to the consumption of acidic metabolites such as acetate upon the depletion of glucose in the culture, the feeding solution pump was activated for 3 seconds, adding 0.2 mL of the feeding solution, which corresponded to a glucose dosage of 0.12 g. The pH, biomass, and DO profiles of a typical fermentation employing this strategy are presented in Figure 3-4.

As shown in Figure 3-4A, the culture pH started at the upper setpoint of pH 6.8 and decreased gradually to the lower setpoint of pH 6.6 in approximately 7 h after inoculation. The NH_4OH pump was activated at that point to prevent pH from falling below pH 6.6. At approximately 9 h into the fermentation, pH started to increase continuously without the addition of NH_4OH solution, indicating that the glucose had been depleted from the culture and the bacteria were consuming acidic metabolites such as acetate accumulated in the early stage of fermentation for growth. At about 12 h, the injection of the feeding solution started. As shown in Figure 3-4A, these injections only resulted in slight pH decreases that never reached the lower setpoint of pH 6.6, and therefore were not sufficient to activate the NH_4OH pump. The biomass curve seen on Figure 3-4B shows that the culture was rapidly growing during the batch phase where a μ_{max} of 1.41 h^{-1} (Table 3-1) and a biomass/glucose yield ($Y_{X/S}$) of 0.26 g X/g S were estimated. Even though more than 40 feeding solution injections were made during the fed-batch phase, this strategy yielded a final biomass of only 2.43 g DCW/L (Figure 3-4B) and an overall $Y_{X/S}$ of 0.20 g X/g S. The dissolved oxygen profile during the fermentation, as shown in Figure 3-4C, indicates that the cellular metabolism was

active for 13 h, which is evidenced by the decreasing DO or its control to the setpoint of 20%. Then, the metabolic activities slowly decreased, which is signified by a decrease in the oxygen demand as revealed by the gradual increase of DO to approach 100%.

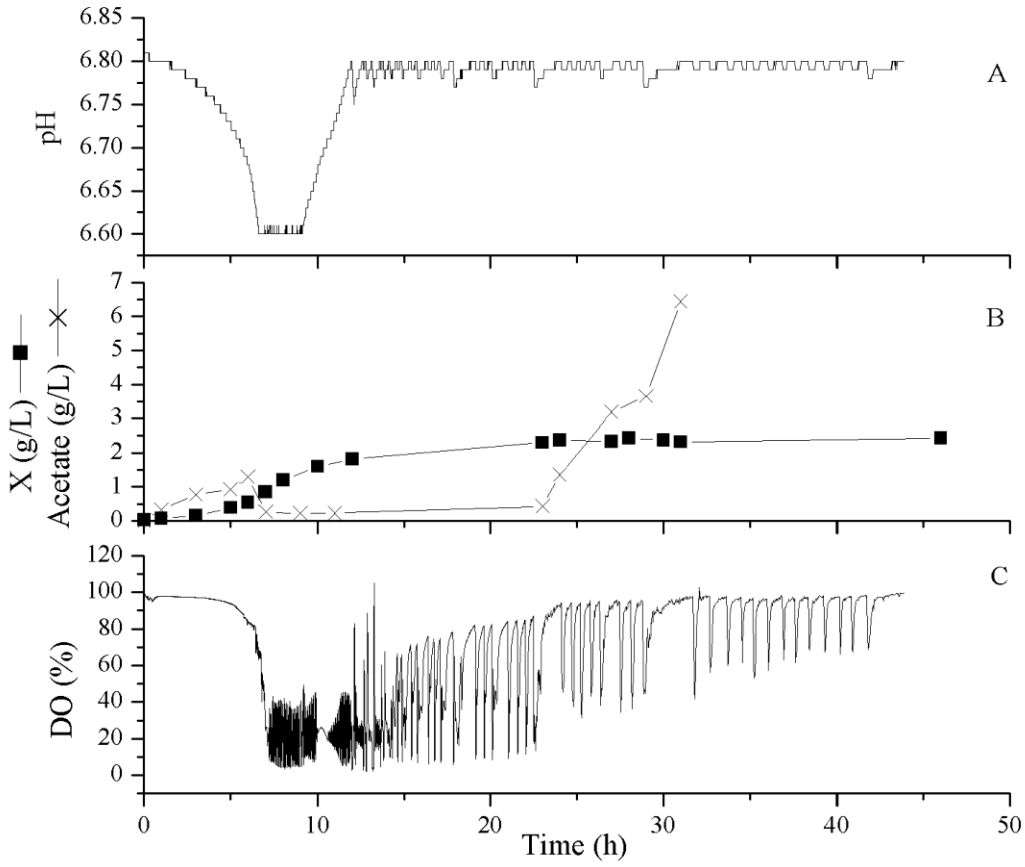

Figure 3-4: DPPSL control strategy using glucose dosage of 0.12 g glucose per injection: (A) pH value, (B) Biomass profile, and (C) Dissolved oxygen percentage saturation. The initial glucose concentration was 10 g/L.

3.4.4.2 High glucose dosages (10 g/L) (DPPSH)

The DPPSL strategy was able to prevent the excess addition of NH_4OH due to the shortcut feeding loops, leading to a biomass concentration of 2.43 g DCW/L that is higher than that obtained with SPPS (0.48 g/L). However, the resulting biomass

concentration was still far from what is expected for HCDC. It was hypothesized that the glucose dosage of each injection was too small to allow the accumulation of sufficient amount of acetic acid and other acidic metabolites to reduce the culture pH to the lower setpoint, pH 6.6. As a result, no NH_4OH was added to the culture during the entire course of fermentation and nitrogen starvation probably led to the early cessation of cell growth. To overcome this problem, an increased glucose dosage of 15 g per injection, which corresponded to an addition of 10 g/L of glucose to the culture with every injection, was implemented. The profiles of key parameters of a typical fermentation employing such a strategy are shown in Figure 3-5.

As shown in Figure 3-5A, the culture pH decreased gradually from the upper setpoint of pH of 6.8 at the beginning of the fermentation to a pH of 6.6 at approximately 9.5 h and was maintained at this value by the addition of NH_4OH solution until approximately 11 h, indicating that acidic metabolites were accumulating during this period. Then, the pH started to increase quickly first and then at a lower rate until reaching pH 6.7 at 14 h, indicating that the acidic metabolites accumulated in the earlier stage were consumed during this period of time. The pH was then stabilized at 6.7, a value too low to trigger the addition of glucose. As a result, the cell metabolism was inactive during this period, which is confirmed by the plateau in the pH profile (Figure 3-5A), biomass profile (Figure 3-5B), and the DO profile (Figure 3-5C) during this period. At 22 h of fermentation, an injection of 15 g glucose, which corresponds to 10 g/L, was added in to the culture manually. As shown by the pH, biomass, and DO profiles, the metabolism of cells was activated immediately after the addition and pH

started to decrease, biomass started to increase, and DO dropped to 20% air saturation, which was the setpoint for the DO control.

As shown in Figure 3-5A, an automatic and well-paced cyclic pattern of pH oscillation between pH 6.6 and pH 6.8 was established with the glucose feeding solution added at pH 6.8 and NH_4OH solution added at pH 6.6. It is worth noting that the frequency of pH oscillation increased with time (Figure 3-5A), apparently due to the increased rate of consumption of glucose or acidic metabolites owing to the fast-increasing biomass concentration (Figure 3-5B) during this period of time, which increased from 1.77 g DCW/L after the first manual injection to 20.2 g DCW/L at the end of the fermentation. Upon the initiation of the fed-batch phase, the characteristic cycles were observed and the biomass increased to a final concentration of 20.2 g DCW/L at 32 h at which time the fermentation stopped (Figure 3-5B). The decrease in activity in the later stage of the culture, also confirmed by the increasing trend of the DO percentage saturation profile, resulted in a very low biomass increase.

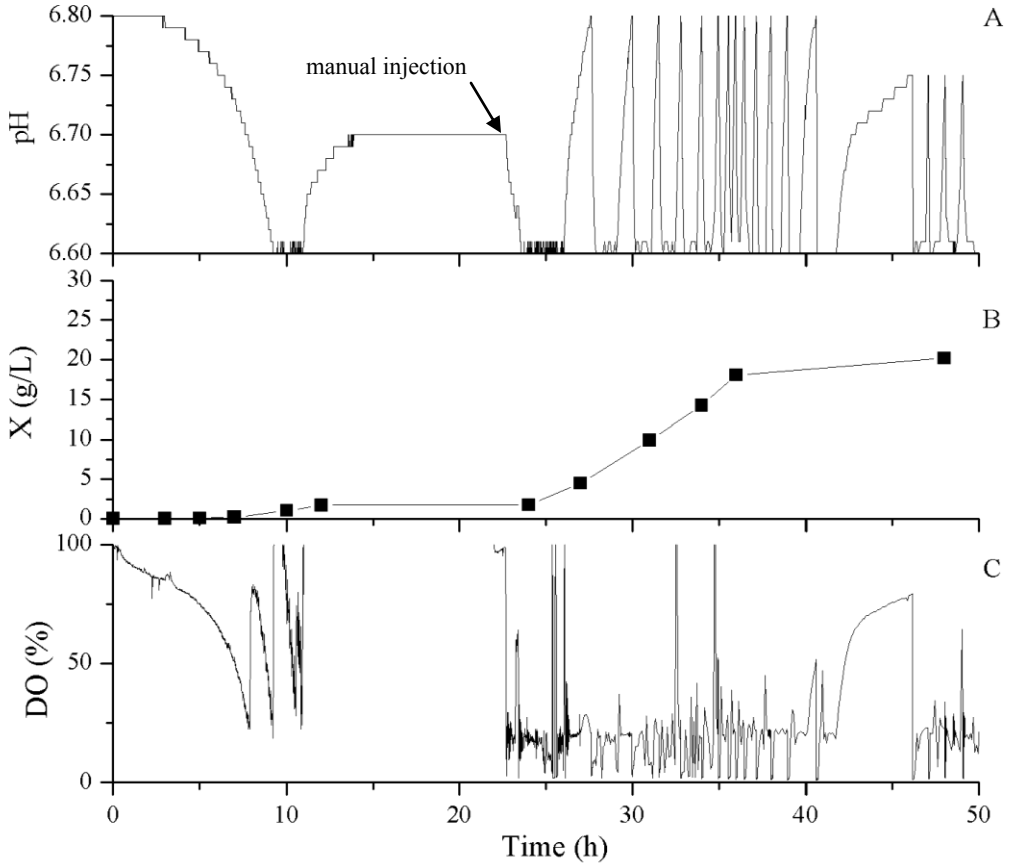

Figure 3-5: DPPSH control strategy using 7 g/L initial glucose concentration and 15 g per injection (10 g/L glucose) feeding dosage: A, pH; B, biomass; and C, dissolved oxygen (% air saturation).

Figure 3-6 depicts the profiles of pH (Figure 3-6A), biomass concentration (Figure 3-6B), and DO (Figure 3-6C) of another batch of DPPSH fermentation, which was identical with the batch shown in Figure 3-5 but had an initial glucose concentration of 10 g/L. As shown in Figure 3-6A, culture pH started at the upper setpoint of 6.8 and decreased to the lower setpoint of 6.6 at around 6 h, at which point pH was stabilized due to the addition of NH_4OH. Oscillation of pH, which corresponds to the alternating loops of glucose addition and NH_4OH addition, was established and maintained during the period of approximately 22 to 32 h, during which the cells were growing quickly (Figure 3-6B) and DO was maintained at the setpoint of 20% air saturation (Figure 3-6C).

Unlike the previous batch, no manual injection of glucose feed was necessary. The highest biomass concentration obtained was 26.6 g/L and the biomass increased to 18.3 g DCW/L in about 9 h after the fed-batch phase started. It is worth mentioning that the pH and DO profiles of this batch were less regular compared to that presented in Figure 3-5, probably due to fluctuation of culture properties in the proximity of pH and DO probes or minor instability of the control system.

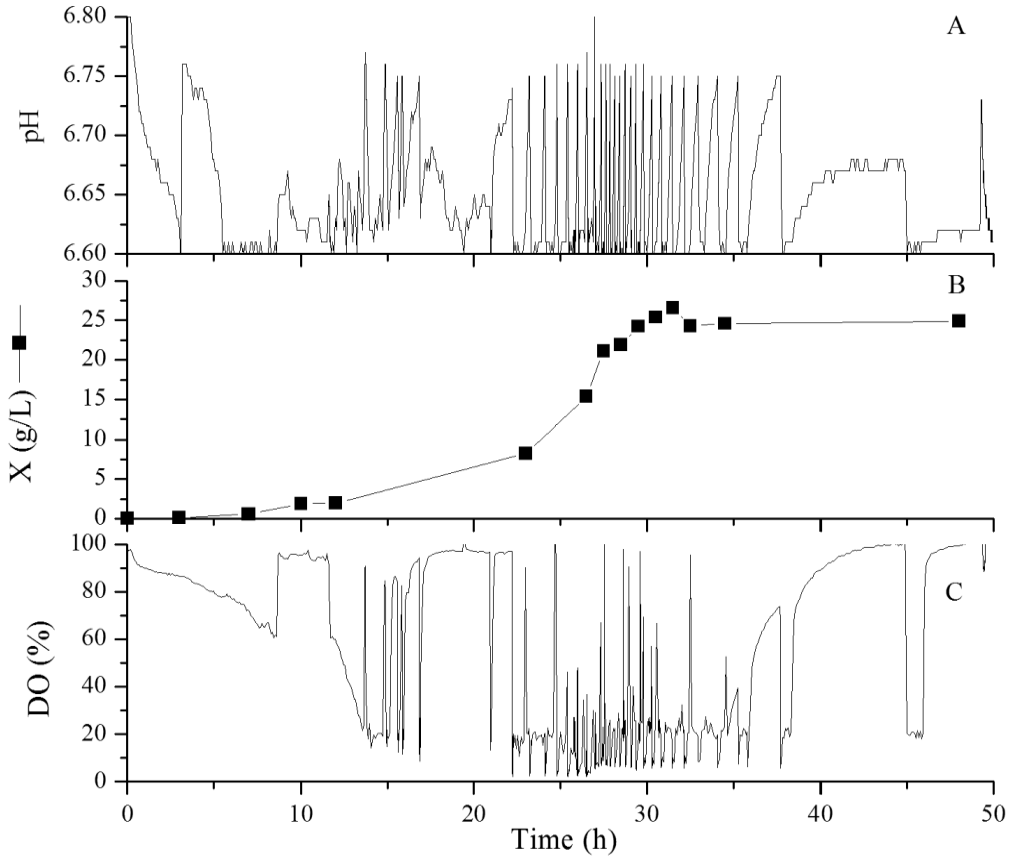

Figure 3-6. DPPSH control strategy using initial glucose concentration of 10 g/L and a feeding dosage of 10 g/L glucose: A, pH; B, Biomass; and C, dissolved oxygen (% air saturation).

3.5 Discussion

3.5.1 Effect of initial glucose concentration on HCDC

Our attempt to repeat the results of Korz *et al*. [20] with *E. coli* TG1 wild-type using an exponential feeding strategy with an initial glucose concentration of 25 g/L, which was reported to be able to reach a HCDC of 128 g DCW/L, was not successful. The failure was hypothetically attributed to the quick accumulation of high concentration of acetate in the culture, which reached 9.16 g/L, owing to the high initial glucose concentration of 27 g/L. This was compatible with the results of other researchers showing that acetate at that level could lead to complete inhibition of *E. coli* growth [23, 24]. The slow cell growth obtained in these experiments also confirms the observation of other researchers to the effect that acetate at a level of 2.0 g/L or above may inhibit growth of *E. coli* [11-15]. Consequently, the biomass concentration obtained in the SPPS experiments was extremely low.

On the other hand, it was observed that when a pH range of 6.6-6.8 was employed with the DPPS fed-batch at an initial glucose concentration of 7 g/L, manual injection of the first injection of glucose was required since consumption of the acidic metabolites produced before glucose depletion was not sufficient to raise the culture pH to the upper setpoint of 6.8. Furthermore, it was observed that an initial glucose concentration of 10 g/L was able to trigger the injection of the glucose solution automatically. These results highlights the importance of determining the initial glucose concentration at a level that is low enough to avoid inhibition of cell growth and, at the same time, high enough to match with the pre-set pH control range.

3.5.2 The shortcut feeding loop with SPPS

The pH-stat feeding strategy relies on the change of culture pH that is closely related to cellular metabolism. When glucose is present, metabolic by-products, which are mainly acids such as propionic, acetic and lactic acids [25], are produced and neutralized by the addition of basic solutions such as NH_4OH to maintain the culture pH at the desired setpoint. Then, when glucose is depleted, the cells are forced to consume the ammonium salts of the acidic metabolites, resulting in a pH increase [16] that triggers the addition of glucose to start another feeding cycle when sufficient amount of such salts are consumed to push culture pH to be above the upper setpoint, i.e., pH 6.8.

As shown in Figure 3-3, however, the SPPS feeding strategy cannot directly couple the addition of glucose and NH_4OH solutions with the total depletion of either glucose or acidic metabolites, creating shortcut loops. As shown in Figure 3-3B, the ammonium solution was added continuously in the batch fermentation phase (up to approximately 18 h after inoculation). In the fed-batch phase, alternating feeding of glucose and NH_4OH was observed. It is clear, however, that the alternating cycle was not responding to the depletion of glucose or of acidic metabolites but rather a loop responding to the slight pH changes caused by the addition of either NH_4OH or feeding solutions. Briefly, large quantities of acidic metabolites such as acetic acid were produced from glucose catabolism during the batch phase, which were neutralized by the addition of NH_4OH to keep the culture pH at the setpoint of pH 6.8. The continuous addition of NH_4OH to the culture is evidenced by the fact that the pH pump output value was maintained in the positive range as shown in Figure 3-3B. At the end of the batch phase, glucose was depleted and the cells were forced to assimilate carbonic metabolites for cell

growth and maintenance. The consumption of a small quantity of these acidic metabolites would cause a small increase of pH and, therefore, trigger the addition of glucose. Since glucose is a more favourable carbon source than acidic metabolites such as acetate, cells will assimilate glucose and produce more acidic metabolites to trigger the addition of another dose of NH_4OH and, therefore, start another shortcut feeding loop.

Apparently, the shortcut feeding loop cannot guarantee depletion of acidic metabolites before triggering the addition of a new injection of glucose. As a result, acidic metabolites such as acetate would accumulate with time and eventually reach a level that is inhibitive to cell growth. This explanation was confirmed by the accumulation of approximately 21.8 g acetate/L at 48 h of fermentation in the SPPS fed-batch fermentation (Figure 3-3). The early cessation of cell growth and low biomass concentration were clearly a result of the failure of this strategy to avoid accumulation of high level of acetate.

3.6 Effects of glucose feeding dosage in dual-point pH control

The dual-point pH-stat (DPPS) feeding strategy was devised to overcome the shortcut feeding cycle observed in SPPS. Two different glucose-feeding dosages were tested. Figure 3-4A shows that when a small glucose feeding dosage of 0.12 g of glucose per injection was used, the pH would oscillate near the upper setpoint of pH 6.8 once it has reached that level due to the consumption of acidic metabolites upon depletion of glucose at the end of batch phase. This is because the glucose dosage per injection was too small to induce the production of acidic metabolites necessary to lower the pH down to the lower setpoint of pH 6.6 after each injection. As a result, ammonia was never added to the culture and cells experienced nitrogen starvation, which caused the cessation

of cell growth. To remedy this problem, fermentations with glucose dosages of 15 g of glucose per injection, which would lead to a glucose concentration in the culture of at least 10 g/L, were carried out. As shown in Figure 3-5 and Figure 3-6, a dosage of 15 g/L glucose per injection (10 g/L) was sufficient to obtain HCDC with cell densities of 22 g/L and 26.6 g/L, respectively.

Using the pH-stat with a pulse strategy to control biomass, it is not necessary to make calculations to modify the feeding flow rate as is done in exponential feeding or to manually change the amount of glucose fed when using a step-wise feeding strategy. As biomass increases the time between the feeding periods is shortened and the more frequent feeding can sustain exponential growth. As biomass increases, feeding tends to become less frequent indicating a lack of possible macronutrient that is not present in the feeding solution. It is hypothesized that this nutrient is phosphorus as it is not present in the feeding solution and required for cell to grow. This decrease in activity is also corroborated by the dissolved oxygen profile slowly rising over time. The plateau observed in the biomass profile also suggests that a critical component is missing from the fermentation medium.

3.7 Conclusion

By using a dual setpoint pH-stat control strategy and pulse glucose feeding, a recombinant *E. coli* TG1 strain expressing the single domain antibody ToxA5.1 was grown to 26.6 g DCW/L. Initial glucose concentration in the medium should be high enough to support growth without resulting in the over-production of acetate. It was found that 10 g/L of glucose in the initial medium resulted in growth conditions that enabled fed-batch feeding to proceed when a pH range of pH 6.6-6.8 was used.

Furthermore, it was concluded that the glucose dose used per injection should be sufficiently large to allow the acidic metabolites produced during glucose catabolism to lower the culture pH to the lower setpoint (i.e., pH 6.6) to trigger the addition of NH_4OH, which served as the additional nitrogen source for cells growth in HCDC. Cell density of 26.6 g DCW/L was achieved with the current conditions.

3.8 Acknowledgements

Financial support from the Natural Science and Engineering Council of Canada (NSERC) and The Canada Foundation of Innovation (CFI) is gratefully acknowledged.

3.9 References

1. Cohen, S.H., Gerding, D.N., Johnson, S., Kelly, C.P., Loo, V.G., McDonald, L.C., Pepin, J. and Wilcox, M.H. Clinical practice guidelines for *Clostridium difficile* infection in adults: 2010 update by the Society for Healthcare Epidemiology of America (SHEA) and the Infectious Diseases Society of America (IDSA). *Infection Control and Hospital Epidemiology* **31**, 431-455 (2010).

2. Hussack, G. and Tanha, J. Toxin-specific antibodies for the treatment of *Clostridium difficile*: Current status and future perspectives. *Toxins* **2**, 998-1018 (2010).

3. Hussack, G., Arbabi-Ghahroudi, M., Van Faassen, H., Songer, J.G., Ng, K.K.S., MacKenzie, R. and Tanha, J. Neutralization of *Clostridium difficile* toxin A with single-domain antibodies targeting the cell receptor binding domain. *Journal of Biological Chemistry* **286**, 8961-8976 (2011).

4. Parisien, A., Al-Zarka, F., Hussack, G., Baranova, E.A., Thibault, J. and Qingdao Lan, C. Nickel nanoparticles synthesized by a modified polyol method for the purification of histidine-tagged single-domain antibody ToxA5.1. *Journal of Materials Research* **27**, 2884-2890 (2012).

5. Shiloach, J. and Fass, R. Growing *E. coli* to high cell density - A historical perspective on method development. *Biotechnology Advances* **23**, 345-357 (2005).

6. Son, Y.J., Bae, J.Y., Chong, S.H., Lee, H.S., Mo, S.H., Kim, T.Y. and Choe, H. Expression, high cell density culture and purification of recombinant EC-SOD in *Escherichia coli*. *Applied Biochemistry and Biotechnology*, 1-14 (2010).

7. Lee, S.Y. High cell-density culture of *Escherichia coli*. *Trends in Biotechnology* **14**, 98-105 (1996).

8. Riesenberg, D. High-cell-density cultivation of *Escherichia coli*. *Current Opinion in Biotechnology* **2**, 380-384 (1991).

9. Han, K., Lim, H.C. and Hong, J. Acetic acid formation in *Escherichia coli* fermentation. *Biotechnology and Bioengineering* **39**, 663-671 (1992).

10. De Mey, M., De Maeseneire, S., Soetaert, W. and Vandamme, E. Minimizing acetate formation in *E. coli* fermentations. *Journal of Industrial Microbiology and Biotechnology* **34**, 689-700 (2007).

11. Hempfling, W.P. and Mainzer, S.E. Effects of varying the carbon source limiting growth on yield and maintenance characteristics of *Escherichia coli* in continuous culture. *Journal of Bacteriology* **123**, 1076-1087 (1975).

12. Phue, J.N., Noronha, S.B., Hattacharyya, R., Wolfe, A.J. and Shiloach, J. Glucose metabolism at high density growth of *E. coli* B and *E. coli* K: Differences in metabolic pathways are responsible for efficient glucose utilization in *E. coli* B as determined by microarrays and Northern blot analyses. *Biotechnology and Bioengineering* **90**, 805-820 (2005).

13. Sung, K.L. and Keasling, J.D. Effect of glucose or glycerol as the sole carbon source on gene expression from the Salmonella prpBCDE promoter in *Escherichia coli*. *Biotechnology Progress* **22**, 1547-1551 (2006).

14. El-Mansi, E.M.T. and Holms, W.H. Control of carbon flux to acetate excretion during growth of *Escherichia coli* in batch and continuous cultures. *Journal of General Microbiology* **135**, 2875-2883 (1989).

15. Sun, W.J., Lee, C., George, H.A., Powell, A.L., Dahlgren, M.E., Greasham, R. and Park, C.H. Acetate inhibition on growth of recombinant *E. coli* and expression of fusion protein TGFα-PE40. *Biotechnology Letters* **15**, 809-814 (1993).

16. Suzuki, T., Yamane, T. and Shimizu, S. Phenomenological background and some preliminary trials of automated substrate supply in pH-stat modal fed-batch culture using a setpoint of high limit. *Journal of Fermentation and Bioengineering* **69**, 292-297 (1990).

17. Wang, C.K., Duan, K.J., Yeh, K.W. and Chen, W.C. Production of a fusion protein of sweet potato sporamin from recombinant *E. coli* XL1 Blue by fed-batch fermentations. *Biotechnology Letters* **23**, 475-479 (2001).

18. Liu, Y., Liu, L., Chen, J., Li, J., Du, G. and Chen, J. Effects of carbon sources and feeding strategies on heparosan production by *Escherichia coli* K5. *Bioprocess and Biosystems Engineering* **35**, 1209-1218 (2012).

19. Jin, S., Ye, K. and Shimizu, K. Efficient fuzzy control strategies for the application of pH-stat to fed-batch cultivation of genetically engineered *Escherichia coli*. *Journal of Chemical Technology and Biotechnology* **61**, 273-281 (1994).

20. Korz, D.J., Rinas, U., Hellmuth, K., Sanders, E.A. and Deckwer, W.D. Simple fed-batch technique for high cell density cultivation of *Escherichia coli*. *Journal of Biotechnology* **39**, 59-65 (1995).

21. Arbabi-Ghahroudi, M., Mackenzie, R. and Tanha, J. Selection of Non-aggregating V(H) Binders from Synthetic V (H) Phage-Display Libraries. *Methods Mol Biol* **525**, 1-30 (2009).

22. Seo, J.H. and Bailey, J.E. Effects of recombinant plasmid content on growth properties and cloned gene product formation in *Escherichia coli*. *Biotechnology and Bioengineering* **27**, 1668-1674 (1985).

23. Fass, R., Clem, T.R. and Shiloach, J. Use of a novel air separation system in a fed-batch fermentative culture of *Escherichia coli*. *Applied and Environmental Microbiology* **55**, 1305-1307 (1989).

24. Jae Gu, P., Joon Shick, R. and Lebeault, J.M. Physiological constraints in increasing biomass concentration of *Escherichia coli* B in fed-batch culture. *Biotechnology Letters* **9**, 89-94 (1987).

25. Kim, B.S., Lee, S.C., Lee, S.Y., Chang, Y.K. and Chang, H.N. High cell density fed-batch cultivation of *Escherichia coli* using exponential feeding combined with pH-stat. *Bioprocess and Biosystems Engineering* **26**, 147-150 (2004).

Chapter 4: Large-scale expression of a single domain antibody targeting *Clostridium difficile* toxin A in *Escherichia coli* TG1 using pH-stat control

Albert Parisien, Sallé Dembélé, Jules Thibault and Christopher Q. Lan*

Chemical and Biological Engineering Department, University of Ottawa, Ottawa, ON, Canada K1N 6N5

Corresponding author: Christopher Q. Lan, Christopher.Lan@uottawa.ca

4.1 Abstract

Escherichia coli TG1 expressing a single domain antibody against *Clostridium difficile* toxin A (TcdA), ToxA5.1, was grown in defined media using a dual-point pH control strategy to control the feed rate during the fed-batch portion of the fermentation. Using this dual-point pH-stat strategy, a final biomass concentration of 12.26 g DCW/L was achieved. Success of the fed-batch process was dependent on the appropriate glucose concentration in both the initial medium and the feeding solution. Higher initial glucose concentration resulted in higher acetate production for which ammonia was added in concentration inhibiting cell growth while lower initial glucose concentration did not provide enough acetate to trigger the feeding loop controlled by pH set-point. In defined media under growth phase conditions, the target protein was not expressed even with an increase in temperature and presence of inducer molecule. Expression of the target protein required an increase in the fermentation temperature from 28ºC to 37ºC, a supplement of yeast extract of 54 g/L in the feed solution and addition of inducer molecule. Under these conditions, protein expression levels were up to 127 mg ToxA5.1 /g DCW.

Keywords: *E. coli*, recombinant protein, expression, Fed-batch, pH-stat

4.2 Introduction

Clostridium difficile is a Gram-positive sporulating bacterium that generally spreads by fecal-oral route and causes, especially in persons undergoing antibiotic treatment, symptoms from light diarrhea to fatal pseudomembranous colitis [1], which are known as *C. difficile* infections (CDI). The number of CDI cases have constantly increased since 2000 [2] and it is projected that 450 000 to 750 000 [3] annual cases could be diagnosed in the US [3]. Moreover, a hypervirulent strain (BI/NAP1/027) was responsible for a series of outbreaks in Québec, Canada [4]. This hypervirulent strain has been reported worldwide including the US, Asia, UK and some European countries [5, 6]. CDIs are causing multiple problems in hospital settings and, amongst these, increased healthcare costs, which are estimated at over 3.2 billion $/year for the USA alone in 2007 [2], resulting from longer stay and higher rate of readmission. Emerging therapies against *C. difficile* have been reviewed [7] and toxin neutralization using monoclonal antibodies shows promising results [8]. Some single domain antibodies (sdAb) [9] have also shown *C. difficile* toxin neutralization abilities [8, 10]. One such sdAb is ToxA5.1, which has proven to be effective at recognizing conformational epitopes and neutralizing the cytopathic effects of toxin A on fibroblast cells in an in vitro assay [10]. Because of their pH stability [11] and proteolytic degradation resistance [12], sdAbs are good candidates for oral therapy and, therefore, large quantities of sdAbs would be required. As opposed to monoclonal antibodies, sdAb do not require extensive refolding or glycosylation to be fully functional and, therefore, can be expressed at high levels in prokaryotic cells such as *E. coli*.

When expressing recombinant protein for lab-scale applications such as protein characterization, small volumes of culture are sufficient to satisfy these applications. However, when high volumetric productivity is required as it is the case when expressing recombinant protein for commercial applications, a large volume of high biomass concentration is preferable. Commercial protein production relies on high cell density cultures which significantly reduce capital investments as well as operation costs [13, 14]. Protein expression factors affecting cell growth also have a profound effect on recombinant protein expression. Other factors ought to be investigated for optimal protein production and these can be separated into two types: the operating conditions such as pH, temperature, feeding strategy and timing of induction; and the composition of the fermentation medium (complex or defined), carbon source, medium additives, and inducer molecule used.

Recombinant protein expression, in most cases, needs to be induced. At a judicious moment, a change in the environment, commonly the addition of an inducer molecule, frees the target gene(s) from repression and starts the protein expression phase.

Since recombinant protein expression can produce a large metabolic stress on a cell [15], being able to control the moment of induction is critical. If the cells are induced too early, the biomass concentration will be low since the induction creates a metabolic burden in which most of the cell's energy is diverted towards protein expression, which would be detrimental to biomass production. When the product is intracellular as is the case with ToxA5.1, premature induction results in a lower volumetric productivity rate (g protein/L culture h) due to the lower biomass concentration. If the product is growth-associated, a later induction phase is not recommended since cells are growing less

actively, which reduces specific productivity (g protein / DCW h). Timing of the induction is also important as the plasmid-bearing organism fraction tends to decrease with fermentation time even if selective pressure, in the form of antibiotics, is applied [16].

Other additives to the fermentation medium can increase specific productivity and, amongst these, yeast extract is one of the most studied. Yeast extract has been reported by multiple sources to enhance specific productivity of recombinant proteins expressed by different *E. coli* strains [17]. Since the exact composition of yeast extract is unknown, it is possible that molecules acting as inducer are present.

In this study, we have investigated the effects of temperature on *E. coli* TG1 growth and ToxA5.1 expression, a single domain antibody that neutralizes *Clostridium difficile* enterotoxin A [10], as well as the effects of yeast extract, timing of induction and inducer concentration in order to optimize ToxA5.1 expression in a bioreactor.

4.3 Materials and Methods

4.3.1 Bacterial strain and plasmid

DNA encoding ToxA5.1 gene, a llama single domain antibody with specificity for *C. difficile* toxin A [10], was cloned into the expression vector pSJF2H [18] via BbsI and BamHI (New England Biolabs, Mississauga, ON) restriction sites. Protein expression was performed in TG1 *E. coli* cells purchased from Invitrogen (Carlsbad, CA). Recombinant strains were grown in 20 g/L lysogeny broth (LB Lennox) medium (Fisher Scientific, Pittsburgh, PA) and screened for the best sdAb producer. The best expressing recombinant strain was seeded in 50 mL of defined medium [19] containing 10 g/L of glucose and 100 µg/mL of ampicillin in a 250 mL Erlenmeyer flask at 30°C for 18 h in an orbital shaker at 200 rpm. The culture, to which 15% sterile glycerol was added, was then

aliquoted as 1.5 mL in 2 mL micro-centrifuge tubes and kept at -80°C and served as inoculum for the bioreactors.

4.3.2 Medium preparation

Batch medium and feeding solution used in this study are identical to those reported by Korz et al. [19] except that the glucose concentration was 7 g/L or varied as specified in the text. Defined medium consisted in glucose 7 g/L, KH_2PO_4 13.3 g/L, $(NH_4)_2HPO_4$ 4 g/L, $MgSO_4$ 1.2 g/L, citric acid 1.7 g/L, trace metal solution consisted in EDTA 8.4 mg/L, $CoCl_2 \bullet 6\ H_2O$ 2.5 mg/L, $MnCl_2 \bullet 4\ H_2O$ 15 mg/L, $CuCl_2 \bullet 2\ H_2O$ 1.5 mg/L, H_3BO_3 3 mg/L, $Na_2MoO_4 \bullet 2\ H_2O$ 2.5 mg/L, $Zn(CH_3COO)_2 \bullet 2\ H_2O$ 13 mg/L, Fe (III) citrate 100 mg/L, thiamine HCl 4.5 mg/L, and ampicillin 100 mg/L. Fed-batch feeding solution consisted in glucose 600 g/L, $MgSO_4$ 20 g/L, trace metal solution consisted in EDTA 13 mg/L, $CoCl_2 \bullet 6\ H_2O$ 4 mg/L, $MnCl_2 \bullet 4\ H_2O$ 23.5 mg/L, $CuCl_2 \bullet 2\ H_2O$ 2.5 mg/L, H_3BO_3 5 mg/L, $Na_2MoO_4 \bullet 2\ H_2O$ 4 mg/L, $Zn(CH_3COO)_2 \bullet 2\ H_2O$ 16 mg/L, and Fe (III) citrate 40 mg/L. For experiments using the modified feeding solution, the feeding solution was supplemented with 54 g/L of yeast extract.

4.3.3 Protein quantification

Cell lysis buffer (300 µL/pellet) was prepared with 1X Promega Corporation (Madison, WI) Fast Break lysis reagent, 1 mM phenylmethylsulphonyl fluoride (PMSF) (Bio Basic Inc. Markham, On) and 3 U DNAse 1 (Promega Corp.) and cell lysis was carried out on a rocking platform (Boekel Scientific, Feasterville, PA) at room temperature for 30 min. Total and soluble fractions of crude cell lysates were loaded on 4-12% discontinuous SDS-PAGE gels [20]. Albumin standards (Thermo Scientific, Rockford, IL) of 10, 30, 100, and 200 µg/mL were loaded on every gel to provide

quantitative estimation. Gels were stained using Fermentas PageBlue Protein Staining Solution (Glen Burnie, MD) fast protocol followed by overnight destaining in distilled water. Quantification of scanned gels was achieved via densitometry using ImageJ software [21].

4.3.4 Effect of temperature and media on cell growth

Primary inoculum was seeded in 25 mL of defined medium containing 25 g/L of glucose and 100 μg/mL ampicillin in 125 mL Erlenmeyer flasks at 30°C for 18 h in an orbital shaker at 200 rpm to serve as inoculum for the experiments. Enough inoculum from the overnight culture to obtain an OD_{600} of ~0.1 was added to 25 mL of defined medium containing 25 g/L of glucose and 100 μg/mL ampicillin in 125 mL Erlenmeyer flasks. Flasks were then incubated at 28ºC or 37ºC and growth curves were obtained by measuring OD_{600}. The same procedures except without addition of glucose were repeated for growth in 20 g/L LB Lennox medium (25 mL of 20 g/L LB Lennox medium containing 100 μg/mL ampicillin in a 125 mL Erlenmeyer flask).

4.3.5 Effect of temperature on growth and expression

Testing the effect of temperature was done in LB Lennox medium and cultures were prepared as described in the previous section. The cultures were grown either at 28ºC or 37ºC until biomass reached an OD_{600} of 0.6 at which point the cultures were induced with 2 mM isopropyl β-D-1-thiogalactopyranoside (IPTG) (Promega, Madison, WI). Some cultures were then placed on an orbital shaker (200 rpm) at 28ºC while the rest were placed at 37ºC on a second orbital shaker (200 rpm) to get following growth:induction temperature scheme (28:28, 37:37, and 28:37). All of the cultures were

induced for 18 h after which protein quantification was performed as previously mentioned.

4.3.6 Effect of yeast extract induction timing and inducer concentration in defined medium

To investigate the effect of yeast extract, induction timing and inducer concentration on ToxA5.1 expression in defined medium, a fractional factorial design was used. The low, intermediate and high values of the fractional factorial design, as summarized in Table 4-1, were: 0, 5 and 10 g/L for yeast extract; 0.4, 0.8 and 1.2 for the OD_{600} at which the induction was performed, and 0, 1 and 2 mM for the inducer concentration (IPTG).

Table 4-1: Fractional factorial design values for yeast extract, biomass at the time of induction and IPTG concentration.

Order	Experimental Conditions	Parameter Setting		
		Yeast Extract	Optical Density	IPTG
		g/L	OD_{600}	mM
1	- - +	0	0.4	0
2	+ - -	10	0.4	0
3	0 0 0	5	0.8	1
4	- + -	0	1.2	0
5	+ + +	10	1.2	2

Cultures were prepared as previously except that the defined medium contained 10 g/L of glucose. Briefly, the culture was grown to the appropriate induction OD_{600} on an orbital shaker (200 rpm) at 37ºC, then, induction was done.

4.3.7 Fermentation in bioreactors

4.3.7.1 Inoculum preparation

Primary inoculum (Section 4.3.1) was added to four 500 mL Erlenmeyer flasks, each containing 100 mL of defined medium [19] with of 10 g/L of glucose and 100 μg/mL of ampicillin. Experiments were conducted at 30°C for 12 h in an orbital shaker at 200 rpm. The culture was transferred to two 200 mL centrifuge bottles and centrifuged at 2 550 rcf for 20 min at 20°C (Hermle Labortechnik GmbH, Wehingen, Germany). Supernatant fluid was discarded and both pellets were then suspended with 25 mL of defined medium and mixed together, for a total of 50 mL 8-fold concentration. This concentrated solution served as inoculum for the bioreactors and a sufficient amount was added to the bioreactor to obtain approximately 0.150 OD_{600}.

4.3.7.2 Dual-point pH-stat fermentations

Fermentation was performed in New-Brunswick Scientific BioFlo110 3-L bioreactors (Edison, NJ) with a working volume of 1.5 L. The batch phase was carried out in 1.5 L of defined medium containing 7 g/L of glucose. Temperature (28°C) and agitation with two 6-blades Rushton impeller on a shaft (300 rpm) were kept constant via the control module of the bioreactors. During the batch phase, the medium pH was controlled by the addition of NH_4OH (Fisher Scientific), 25% v/v, when the pH dropped lower than the setpoint of 6.6. Dissolved oxygen (DO) was set at 20% air saturation and a constant airflow of 1 vvm was bubbled into the bioreactors. When the oxygen demand could not be satisfied with the air supply, pure oxygen was mixed in the airflow using the BioFlo110 gas mixer module.

Upon glucose exhaustion in the batch medium, a dual-point pH control strategy [22] was implemented using a LabVIEW interface and OPC functions (Object Linking and Embedding (OLE) for Process Control). A pulse of feeding solution corresponding to 10 g glucose /L was injected (for a total of 15 g of glucose per pulse) when the pH reached the desired setpoint of 6.8. A subroutine of the program prevented injection of a second glucose pulse for 5 min to ensure that pH would decrease below 6.8, thus, ensure complete depletion of glucose prior to a new injection. When pH decreased below the lower setpoint of 6.6, NH_4OH (25% v/v) was added to the medium for pH control.

4.3.7.3 Glucose and acetate

The concentrations of glucose and acetate were determined using an Agilent 1200 unit (Agilent Technologies, Foster City, CA) with a Shodex S-1011 column (Showa Denko K.K., Kawasaki, Japan) and a Shodex SG-1011 guard column. Samples of 50 µL were loaded and the mobile phase (H_2SO_4, 5 mM) was run at 0.6 mL/min. Glucose was quantified using a RI detector while acetate was quantified using a UV detector (λ= 210 nm).

4.4 Results

4.4.1 Effects of media and temperature on cell growth

The effect of temperature and medium composition on *E. coli* TG1 growth can be seen on Figure 4-1. Growth at both of the tested temperatures (28 and 37ºC) in LB Lennox medium was faster than in the defined medium. It is interesting to note that the maximal biomass concentration achieved in LB Lennox medium was 1.2 g DCW/L, which was obtained at the lower temperature of 28°C. Similarly, the maximal biomass

level achieved in defined medium was of 1.22 g DCW/L again when the cells were grown at the lower temperature of 28°C. Growth in both media at 37°C yielded a final biomass concentration of 0.9 and 0.84 g DCW/L in the defined and LB Lennox medium, respectively.

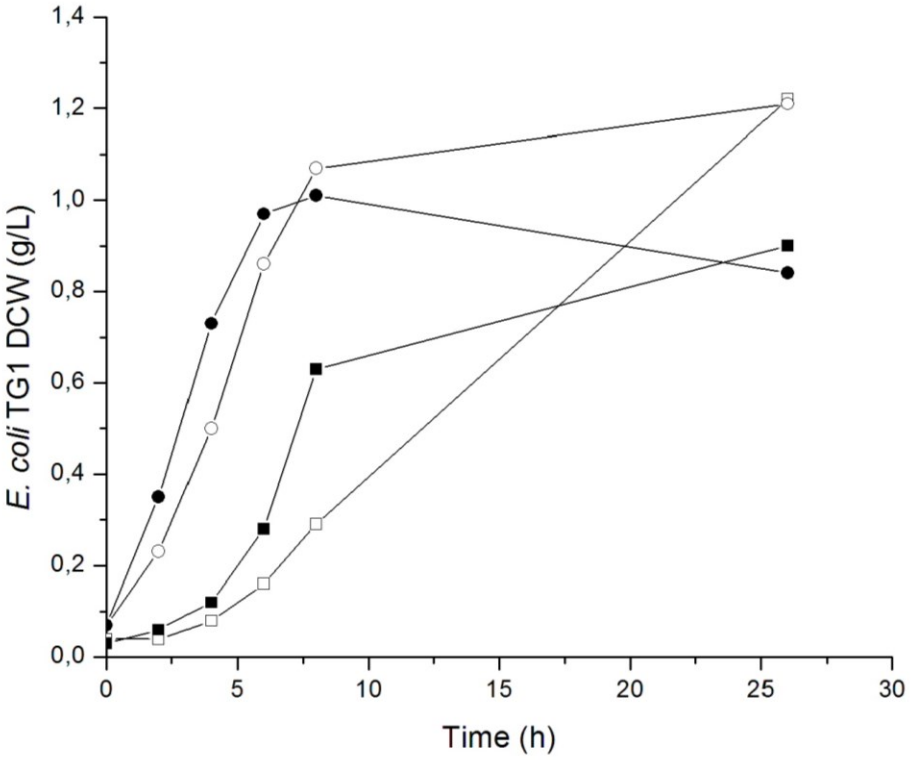

Figure 4-1: Effect of growth temperature and medium composition on *E. coli* TG1+ToxA5.1 growth without induction. Defined medium containing 25 g/L glucose at 28ºC (–□–) and 37ºC (–■–), LB medium at 28°C (–○–) and 37°C (–●–). Standard deviation is not shown for clarity (n=4). The standard deviation average values were of 0.01 g/L for the defined medium and 0.03 g/L for the complex medium.

4.4.2 Protein expression

4.4.2.1 Protein expression in flasks

The effect of temperature on the expression of the recombinant protein ToxA5.1 can be seen on Figure 4-2. It is clear from Figure 4-2 that ToxA5.1 cell content was greater when expression took place at a temperature of 37°C. When cells were grown and

recombinant protein expressed at 28°C, ToxA5.1 cell content was only 19 mg /g DCW, whereas it was 120 mg /g DCW when cells were grown at 28°C and recombinant protein expression was performed at 37°C. The greatest protein cell content was achieved when cells were grown and recombinant proteins were expressed at 37°C. Under these conditions, ToxA5.1 cell content was of 182 mg /g DCW.

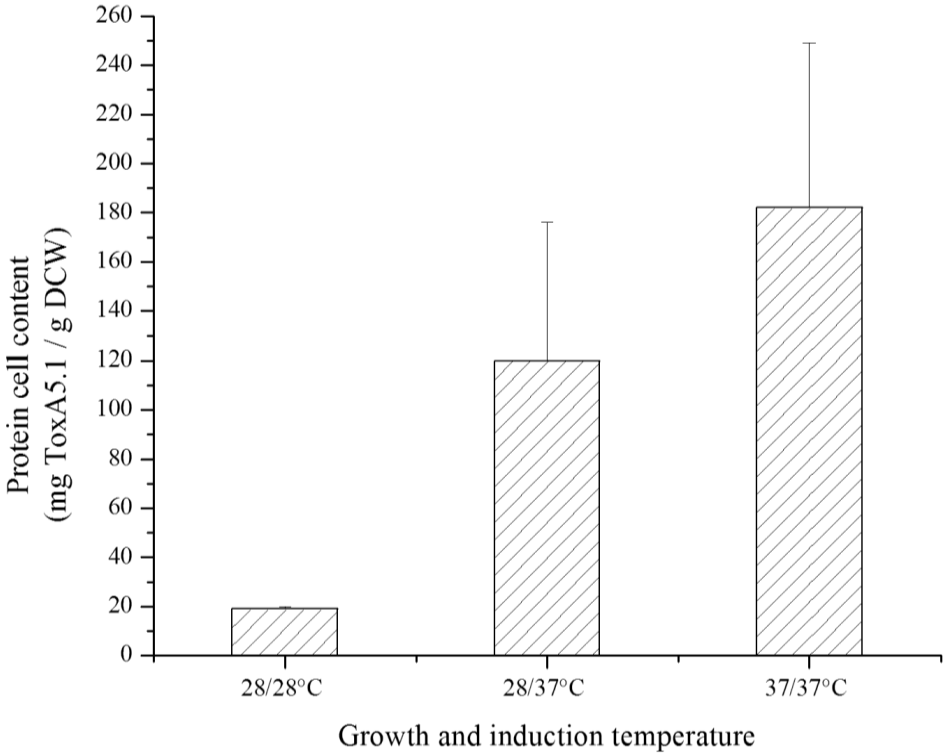

Figure 4-2: ToxA5.1 recombinant protein content in *E. coli* TG1 induced at OD_{600}= 0.6 with 2 mM IPTG for 18 h in LB Lennox medium at different combinations of cell growth/protein expression temperatures. Error bars are showing the highest value of two replicates for each condition.

Effects of yeast extract, biomass concentration at induction time and IPTG concentration were tested using a fractional factorial design. It can be seen from Figure 4-3 that a culture without yeast extract or IPTG led to no protein expression while the presence of IPTG alone resulted in expression of 0.3 mg ToxA5.1/L. The single factor having the greatest effect was yeast extract as expression of 2.7 mg ToxA5.1/L was

observed when it was present at a concentration of 10 g/L. Yeast extract and IPTG concentrations of 5 g/L and 1 mM, respectively, and induction performed at mid-exponential phase (OD_{600} ~ 0.6) resulted in protein expression of 1.7 mg ToxA5.1/L. However it was when yeast extract and IPTG were present at concentrations of 10 g/L and 2 mM, respectively that the highest ToxA5.1 expression of 10 mg /L was obtained.

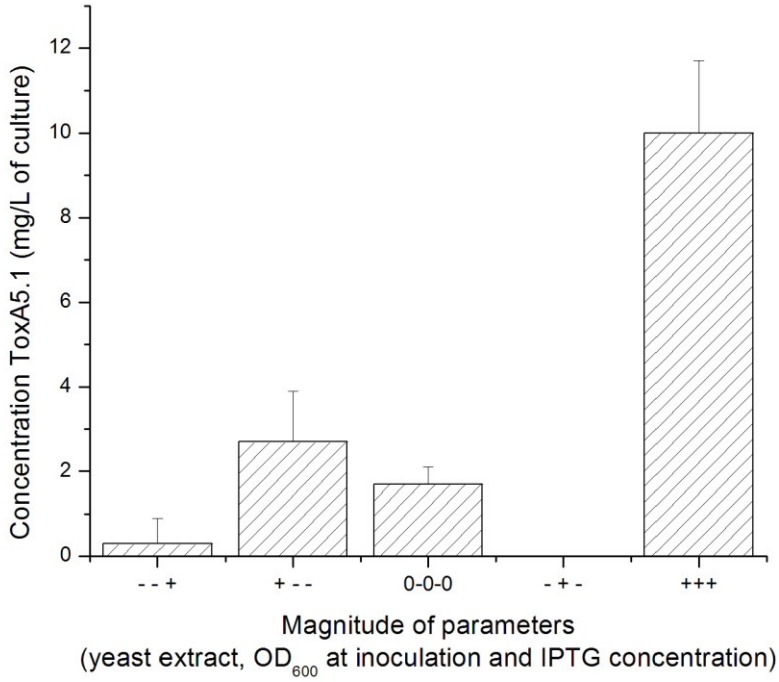

Figure 4-3: Effect of yeast extract, induction timing and inducer concentration on ToxA5.1 expression in defined medium with 5 g/L of glucose. Error bars are 1σ (n=3).

4.4.2.2 Bioreactor protein expression

Several expression conditions were tested during the fed-batch phase in bioreactors and are summarized in Table 4-2. It can be seen from Table 4-2 that a temperature of 28°C with high or medium biomass concentration and an inducer concentration of 1 or 2 mM did not yield a detectable level of ToxA5.1 even after 18 h of induction. Increasing the temperature to 37°C and inducing the culture at a biomass

concentration of 15 g DCW/L with 1 mM IPTG resulted in very little ToxA5.1 expression (< 1 mg/L) after 18h. Only when cells were induced with 1 mM IPTG at 37°C at a biomass of 5 g DCW/L with yeast extract supplemented in the feeding solution did ToxA5.1 expression occurred: after 7 h of induction, 127 mg/L of ToxA5.1 were obtained.

Table 4-2: Summary of conditions tested for the expression of ToxA5.1 in bioreactors.

Induction Temperature	Inducer Concentration	Biomass at time of induction	Final Biomass	ToxA5.1 concentration	Induction duration
ºC	mM	g DCW/L	g DCW/L	mg/L	h
28	1	21	22.5	ND	18
28	2	15	20.1	ND	18
37	1	15	19.5	< 1	18
37	1*	5	12.26	127	7

ND: not detectable

* feeding solution contained 54 g/L yeast extract

A typical fermentation experiment in which *E. coli* TG1 was grown and induced is presented on Figure 4-4. The batch phase medium initially contained 7 g/L of glucose, which were consumed over a period of 8 h as indicated by a decrease in pH value to the lower setpoint of 6.6. Upon reaching this lower setpoint was reached, ammonia was fed to the culture to keep the medium pH above 6.6. The acidic by-products produced during the catabolism of glucose were consumed as indicated by the increase of the pH value from 6.6 to 6.67 in approximately 3 h at which time the batch phase was considered to be completed. During the batch phase, the biomass level was 1.43 g DCW/L and the yield of biomass on glucose ($Y_{X/S}$) was 0.204 g DCW/g glucose. The fed-batch phase was

initiated manually by injecting a pulse of feeding solution containing 15 g of glucose, which caused a rapid pH drop in the fermentation medium. The amount of glucose that was injected upon fed-batch initiation was consumed in approximately 2 h as indicated by an increase in the medium pH. Once the medium pH value reached 6.75, a second pulse of the feeding solution was injected in the culture. The latter glucose pulse was consumed in approximately 1 h and the pH increased to reach a value of 6.8. The biomass concentration of the culture then reached 5 g/L and induction was performed by injecting IPTG in the fermentation broth to achieve a concentration of 1 mM IPTG and increasing the culture temperature from 28°C to 37°C. Upon induction, the feeding solution was replaced by the formulation found in section 4.3.2. This modified feeding solution was added to the fermentation every time the pH reached a value of 6.8 indicating depletion of glucose and of the acidic by-products from the fermentation broth. The fermentation lasted a total of 34 h and a final biomass concentration of 12.26 g DCW/L was obtained. From Table 4-3, it can be observed that during the fed-batch phase, 137 g of glucose and 9.45 g of yeast extract were fed to the culture and the biomass yield on glucose ($Y_{X/S}$) was 0.079 g DCW/g glucose. As shown in Figure 4-5, no recombinant protein was detected at the time of induction and for 1 hour post-induction. ToxA5.1 expression was detected 2 h post-induction and after 7 h of induction a total of 127 mg ToxA5.1/L was obtained resulting, as can be seen in Table 4-4, in ToxA5.1 cell content ($Y_{P/X}$) of 11 mg/g DCW. A yield of ToxA5.1 over glucose ($Y_{P/S}$) of 1.31 mg/g glucose and a productivity of 3.53 mg/L h of ToxA5.1 were calculated.

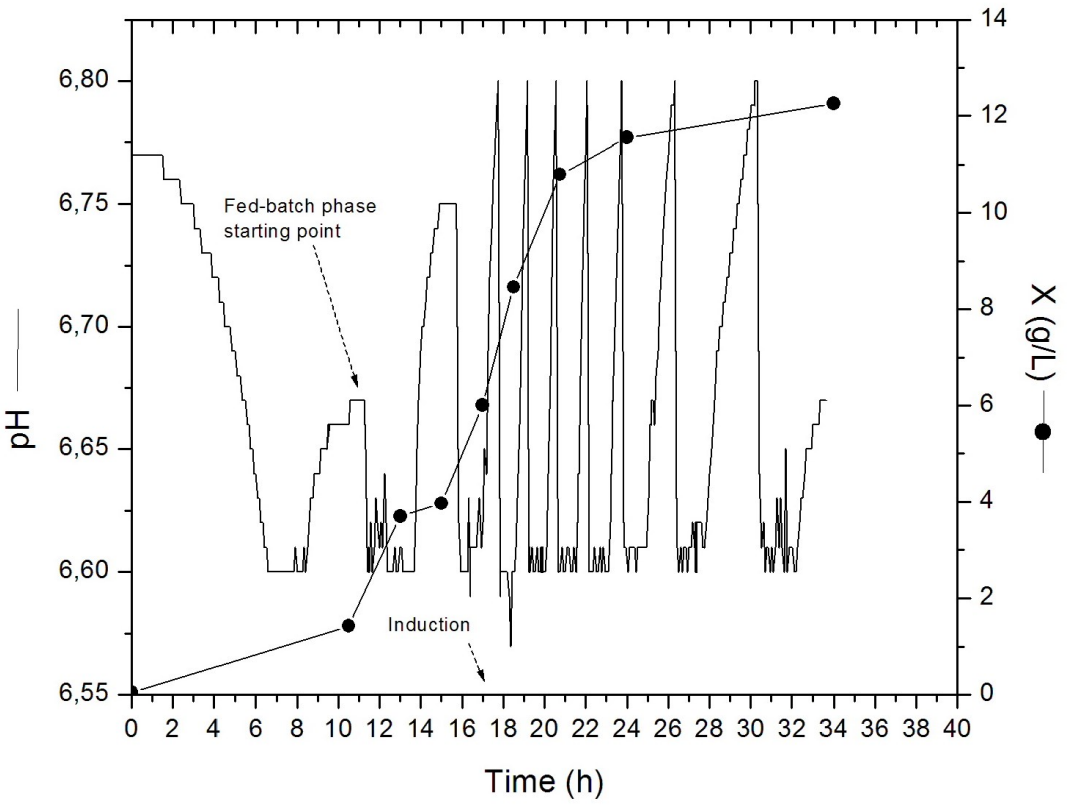

Figure 4-4: Fermentation of *E. coli* TG1 using a dual-point pH-stat control coupled with a feeding pulse.

Table 4-3: Parameters from batch and fed-batch fermentation phases.

		Batch Phase	Fed-Batch phase	Total
Glucose added	(g/L)	7	137	144
X	(g DCW/L)	1.43	10.83	12.26
Yeast extract added	(g/L)	---	9.45	9.45
$Y_{X/S}$	(g DCW/g Glucose)	0.204	0.079	0.085

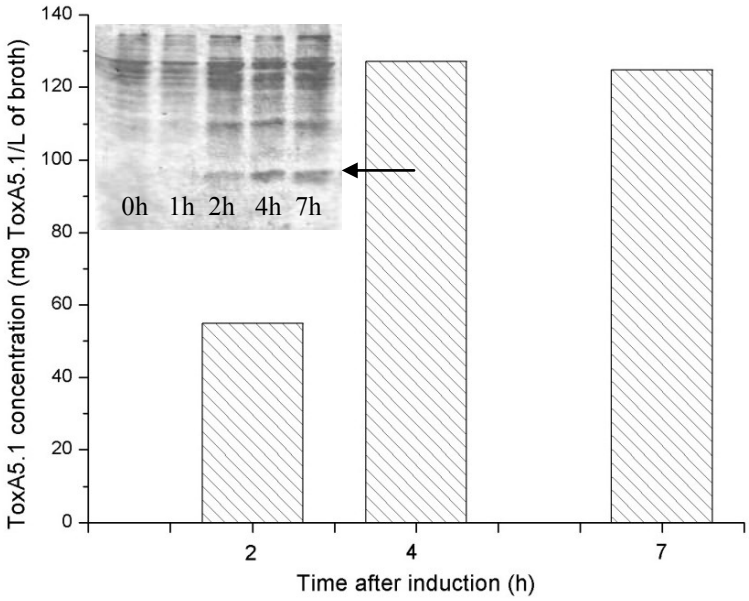

Figure 4-5: Time course expression of recombinant protein ToxA5.1single domain antibody against *C. difficile* toxin A in *E. coli* TG1during fed-batch fermentation.

Table 4-4: Various yield coefficients for ToxA5.1 expression.

$Y_{P/X}$	(mg/g DCW)	11
$Y_{P/S}$	(mg/g S)	1.31
P	(mg/L h)	3.53

4.5 Discussion

4.5.1 Effect of temperature and media on cell growth

Results of Figure 4-1 show that growth in a complex medium such as LB results in a higher growth rate than growth obtained in defined medium. This can be explained by the fact that the complex medium contains growth factors and other trace elements present in the yeast extract. In the complex medium, the temperature did not seem to have a significant effect during the first 10 h but a higher biomass concentration was obtained

at a lower temperature of 28°C than at a temperature of 37°C with final biomass concentrations of 1.21 and 0.84 g DCW/L, respectively. In the defined medium, however, the temperature had an impact early during the growth phase and, after 6 h, the growth rate was larger at 37°C than at 28ºC. However, the same trend can be observed in the defined medium where a greater final biomass was achieved at 28°C. Lower biomass concentration at higher temperature can be explained by the fact that *E. coli* growth follows an Arrhenius type equation with an optimal temperature range between 23°C and 37°C outside which growth rate diminishes drastically [23]. It has been well established that an increase of temperature would lead to an increase of the rates of two opposite reactions: the reactions that lead to cell growth and the endogenous metabolic reactions that consume cell materials to sustain the viability of cells. When the environmental temperature is lower than the optimal temperature, an increase of temperature will result in an increase of the cell growth reaction as opposed to endogenous metabolic reaction, leading to the increase of the overall or net cell growth rate. On the other hand, when the temperature is higher than the optimal temperature, a temperature increase will result in an increase in the endogenous metabolism, leading to a decrease in the new specific cell growth rate [23].

4.5.2 Effect of temperature on cell growth and ToxA5.1 expression

The hypothesis proposed to explain the effect of temperature on cell growth can also be used to understand why the cell protein content is greater at 37°C than it is at 28°C as observed on Figure 4-2. When *E. coli* TG1 cells were grown and gene expression induced at 28°C, ToxA5.1 content was almost 10 times less than when cells were grown and gene expression carried out at 37°C, where a protein concentration of 182 mg

ToxA5.1/ g DCW was obtained. It is reported in the literature that a lower temperature might have an effect on the expression of certain genes [24, 25]. For instance, it was demonstrated that the expression of the OmpA gene, which is also present in the plasmid used in this study, was less efficient at a temperature lower than 28°C when compared to a temperature of 37°C [26]. Similarly, absence of the recombinant protein K1 capsular antigen was reported by Bortolussi and Ferrieri [27] when *E. coli* cells were grown and gene expression performed at a temperature lower than 30°C for a short period of time. When examining results on Figure 4-2, it can be seen that increasing the temperature from 28°C during the growth phase to 37°C during the induction phase did not impair on the ability of the transformed *E. coli* cells to express the recombinant ToxA5.1 gene as ToxA5.1 content of 120 mg/g DCW was obtained when the growth temperature was 28°C and the induction temperature was 37°C.

4.5.3 Effect of yeast extract, induction and inducer

The effect of yeast extract supplementation during the induction phase can clearly be seen on Figure 4-3. The presence of yeast extract had the greatest effect on the protein expression. In addition, even without the inducer present, expression of ToxA5.1 in the presence of yeast extract was of 2.7 mg/L. A synergistic effect of yeast extract and inducer is clearly evidenced and resulted in a protein expression of 10 mg/L. It is interesting to note that a concentration of 10 g/L of yeast extract without inducer resulted in a greater ToxA5.1 expression than a concentration of 5 g/L combined with 1 mM of inducer. As mentioned earlier, yeast extract is comprised of complex nitrogen sources which are building blocks for proteins as well as some growth factors and it is a known fact that protein expression is enhanced when yeast extract is present [17, 28]. Furthermore,

yeast extract can lead to high level of basal expression in some cases, which could explain why ToxA5.1 was expressed even in the absence of inducer as seen in Figure 4-3. It was also observed in previous studies (data not shown) that the plasmid pSJF2H used in this study, which was derived from a high copy number vector, pUC8 [29-31], did not have a tight expression regulation. In other words, when complex medium was used to grow *E. coli* cells, the repressor responsible for preventing recombinant expression, may not fully bind to the operator site on the lac operon, allowing a certain level of transcription of the genes downstream of the promoter [30, 32].

4.5.4 Fermentation in bioreactors

A typical fermentation experiment is shown in Figure 4-4. Using a pH-stat control strategy to feed glucose was successful in achieving a biomass concentration of 21 g/L as can be seen in Table 4-2. Several conditions under which ToxA5.1 was not expressed are reported in Table 4-2. From this table, the importance of temperature, timing and duration of induction as well as supplementation with yeast extract for expression of ToxA5.1 in defined medium can be seen. At the low temperature of 28°C, even after 18 h of induction using 2 mM IPTG at late mid-exponential phase, no detectable amount of ToxA5.1 was found. Increasing the temperature to 37°C during induction at late mid-exponential phase only resulted in very little expression of ToxA5.1. Successful expression of ToxA5.1 was achieved only when induction was performed at the early mid-exponential phase at a temperature of 37°C with inducer concentration of 1 mM IPTG and a supplement of yeast extract in the feeding solution. Under these conditions, it was possible to obtain 127 mg/L of ToxA5.1 in the fermentation culture. It is interesting to note that even if the fermentation lasted over a period of 34 h, the final biomass

concentration reached only 12.26 g DCW/L which is lower than the 27 g/L obtained in previous studies where no induction occurred [22]. This could be explained by the fact that the induction conditions produce a metabolic burden [15] in which most of the cell's energy was diverted towards protein expression, which is detrimental to biomass production, and this phenomenon is reported to be more significant with complex media (e.g. LB) than with minimal medium (e.g. M9) [15].

4.6 Conclusion

It was shown that using a pH-stat control strategy, *E. coli* TG1 expressing the single domain antibody against *C. difficile* enterotoxin A could be grown to a final biomass of 12.26 g DCW/L with ToxA5.1 cell content of 11 mg / g DCW. Temperature increase from 28°C to 37°C and yeast extract supplementation at the time of induction were critical in order to obtain ToxA5.1; under the conditions tested ToxA5.1 was expressed at a concentration of 127 mg/L. It is clear from the results that yeast extract supplementation is required for protein expression when *E. coli* is grown in define medium. Since growth control is not as critical during induction phase, larger concentration of yeast extract, more akin to those used in LB medium should be supplemented at the time of induction. Timing of induction as well as temperature at which induction is done must also be considered as both influences ToxA5.1 titer.

4.7 Acknowledgements

Financial support from the Natural Science and Engineering Council of Canada (NSERC) and The Canada Foundation of Innovation (CFI) is gratefully acknowledged.

4.8 References

1. Bobak, D.A. The molecular pathogenesis of *Clostridium difficile*-associated disease. *Current Infectious Disease Reports* **10**, 111-115 (2008).

2. O'Brien, J.A., Lahue, B.J., Caro, J.J. and Davidson, D.M. The emerging infectious challenge of *Clostridium difficile*-associated disease in Massachusetts hospitals: Clinical and economic consequences. *Infection Control and Hospital Epidemiology* **28**, 1219-1227 (2007).

3. McFarland, L.V., Clarridge, J.E., Beneda, H.W. and Raugi, G.J. Fluoroquinolone use and risk factors for *Clostridium difficile*-associated disease within a veterans administration health care system. *Clinical Infectious Diseases* **45**, 1141-1151 (2007).

4. Pépin, J., Valiquette, L., Alary, M.E., Villemure, P., Pelletier, A., Forget, K., Pépin, K. and Chouinard, D. *Clostridium difficile*-associated diarrhea in a region of Quebec from 1991 to 2003: A changing pattern of disease severity. *Canadian Medical Association Journal* **171**, 466-472 (2004).

5. Cohen, S.H., Gerding, D.N., Johnson, S., Kelly, C.P., Loo, V.G., McDonald, L.C., Pepin, J. and Wilcox, M.H. Clinical practice guidelines for *Clostridium difficile* infection in adults: 2010 update by the Society for Healthcare Epidemiology of America (SHEA) and the Infectious Diseases Society of America (IDSA). *Infection Control and Hospital Epidemiology* **31**, 431-455 (2010).

6. McFarland, L.V. Renewed interest in a difficult disease: *Clostridium difficile* infections - Epidemiology and current treatment strategies. *Current Opinion in Gastroenterology* **25**, 24-35 (2009).

7. McFarland, L.V. Emerging therapies for *Clostridium difficile* infections. *Expert Opinion on Emerging Drugs* **16**, 425-439 (2011).

8. Hussack, G. and Tanha, J. Toxin-specific antibodies for the treatment of *Clostridium difficile*: Current status and future perspectives. *Toxins* **2**, 998-1018 (2010).

9. Hamers-Casterman, C., Atarhouch, T., Muyldermans, S., Robinson, G., Hamers, C., Songa, E.B., Bendahman, N. and Hamers, R. Naturally occurring antibodies devoid of light chains. *Nature* **363**, 446-448 (1993).

10. Hussack, G., Arbabi-Ghahroudi, M., Van Faassen, H., Songer, J.G., Ng, K.K.S., MacKenzie, R. and Tanha, J. Neutralization of *Clostridium difficile* toxin A with single-domain antibodies targeting the cell receptor binding domain. *Journal of Biological Chemistry* **286**, 8961-8976 (2011).

11. Famm, K., Hansen, L., Christ, D. and Winter, G. Thermodynamically Stable Aggregation-Resistant Antibody Domains through Directed Evolution. *Journal of Molecular Biology* **376**, 926-931 (2008).

12. Harmsen, M.M., Van Solt, C.B., Van Zijderveld-Van Bemmel, A.M., Niewold, T.A. and Van Zijderveld, F.G. Selection and optimization of proteolytically stable llama single-domain antibody fragments for oral immunotherapy. *Applied Microbiology and Biotechnology* **72**, 544-551 (2006).

13. Lee, S.Y. High cell-density culture of *Escherichia coli*. *Trends in Biotechnology* **14**, 98-105 (1996).

14. Shiloach, J. and Fass, R. Growing *E. coli* to high cell density - A historical perspective on method development. *Biotechnology Advances* **23**, 345-357 (2005).

15. Bentley, W.E., Mirjalili, N., Andersen, D.C., Davis, R.H. and Kompal a, D.S. Plasmid-encoded protein: The principal factor in the 'metabolic burden' associated with recombinant bacteria. *Biotechnology and Bioengineering* **35**, 668-681 (1990).

16. Yildir, C., Önsan, Z.I. and Kirdar, B. Optimization of starting time and period of induction and inducer concentration in the production of the restriction enzyme EcoRI from recombinant *Escherichia coli* 294. *Turkish Journal of Chemistry* **22**, 221-226 (1998).

17. Nancib, N., Branlant, C. and Boudrant, J. Metabolic roles of peptone and yeast extract for the culture of a recombinant strain of *Escherichia coli*. *Journal of Industrial Microbiology* **8**, 165-169 (1991).

18. Arbabi-Ghahroudi, M., Mackenzie, R. and Tanha, J. Selection of Non-aggregating V(H) Binders from Synthetic V (H) Phage-Display Libraries. *Methods in Molecular Biology* **525**, 1-30 (2009).

19. Korz, D.J., Rinas, U., Hellmuth, K., Sanders, E.A. and Deckwer, W.D. Simple fed-batch technique for high cell density cultivation of *Escherichia coli*. *Journal of Biotechnology* **39**, 59-65 (1995).

20. Laemmli, U.K. Cleavage of structural proteins during the assembly of the head of bacteriophage T4. *Nature* **227**, 680-685 (1970).

21. Abràmoff, M.D., Magalhães, P.J. and Ram, S.J. Image processing with imageJ. *Biophotonics International* **11**, 36-41 (2004).

22. Parisien, A., Dembélé, S., Thibault, J. and Lan, C., Q., (in preparation).

23. Herendeen, S.L., VanBogelen, R.A. and Neidhardt, F.C. Levels of major proteins of *Escherichia coli* during growth at different temperatures. *Journal of Bacteriology* **139**, 185-194 (1979).

24. Robbe-Saule, V., Carreira, I., Kolb, A. and Norel, F. Effect of growth temperature on Crl-dependent regulation of σs activity in *Salmonella enterica* serovar Typhimurium. *Journal of Bacteriology* **190**, 4453-4459 (2008).

25. Kovářová, K., Zehnder, A.J.B. and Egli, T. Temperature-dependent growth kinetics of *Escherichia coli* ML 30 in glucose-limited continuous culture. *Journal of Bacteriology* **178**, 4530-4539 (1996).

26. Afonyushkin, T., Moll, I., Bläsi, U. and Kaberdin, V.R. Temperature-dependent stability and translation of *Escherichia coli* ompA mRNA. *Biochemical and Biophysical Research Communications* **311**, 604-609 (2003).

27. Bortolussi, R., Ferrieri, P. and Quie, P.G. Influence of growth temperature of *Escherichia coli* on K1 capsular antigen production and resistance to opsonization. *Infection and Immunity* **39**, 1136-1141 (1983).

28. Grossman, T.H., Kawasaki, E.S., Punreddy, S.R. and Osburne, M.S. Spontaneous cAMP-dependent derepression of gene expression in stationary phase plays a role in recombinant expression instability. *Gene* **209**, 95-103 (1998).

29. Chambers, S.P., Prior, S.E., Evans, R.A., Sherwood, R.F. and Minton, N.P. Plasmid pMTL153: A high copy number version of pAT153 and its use to obtain high expression of the *Pseudomonas* carboxypeptidase G2 gene. *Applied Microbiology and Biotechnology* **29**, 572-578 (1988).

30. Nielsen, B.L., Willis, V.C. and Lin, C.Y. Western blot analysis to illustrate relative control levels of the lac and ara promoters in *Escherichia coli*. *Biochemistry and Molecular Biology Education* **35**, 133-137 (2007).

31. Hoedemaeker, F.J., Signorelli, T., Johns, K., Kuntz, D.A. and Rose, D.R. A single chain Fv fragment of P-glycoprotein-specific monoclonal antibody C219. Design, expression, and crystal structure at 2.4 Å resolution. *Journal of Biological Chemistry* **272**, 29784-29789 (1997).

32. Griffiths, A.J.F., Miller, J.H., T.Suzuki, D., Lewontin, R.C. and Gelbart., W.M. An Introduction to genetic analysis. (W.H. Freeman, New York; 2000).

Chapter 5: Enhanced recovery of single domain antibody ToxA5.1 against *Clostridium difficile* toxin A using synergistic selective lysis of *Escherichia coli* TG1cells

Albert Parisien[1], Christian Euler [1], Kristin Chow [1], Greg Hussack[2], Jules Thibault[1] and Christopher Q. Lan[1]*

[1] Chemical and Biological Engineering Department, University of Ottawa, Ottawa, ON, Canada K1N 6N5

[2] Institute for Biological Sciences, National Research Council Canada, 100 Sussex Drive Ottawa, ON, Canada, K1A 0R6

*Corresponding author: Christopher Q. Lan, Christopher.Lan@uottawa.ca

5.1 Abstract

Synergistic selective cell lysis combining thermolysis and Triton X-100 was investigated as a possible lysis scheme for recovering ToxA5.1, a thermostable single domain antibody neutralizing *Clostridium difficile* toxin A (TcdA), from *Escherichia coli* TG1 periplasmic space. Results showed that when *E. coli* cells were exposed to a temperature of 60°C and a 1% w/v concentration of Triton X-100, it was possible to recover over 95% of the target protein initially present in the cells. Furthermore, synergistic selective lysis yielded a supernatant fluid in which our target protein was enriched by 27% compared to a total cell lysis scheme. ELISA showed that synergistic lysis at 50 or 70°C for 15 min with 1% Triton X-100 concentration had no effect on the activity of the purified ToxA5.1 indicating that synergistic selective cell lysis is a suitable method of recovering thermostable proteins.

Keywords*:* His6-tagged recombinant protein, Synergistic lysis, Triton X-100, Protein recovery

5.2 Introduction

Discovered in 1993 [1], *camelidae* single domain antibody (sdAb), termed VHH, have a structure similar to that of human variable domain (VH). These molecules are comprised of three complementary determining regions (CDR) providing antigen binding and four framework regions constituting the core structure of the molecule [2]. SdAb have several unique properties, which make them very promising therapeutic agents. These antibodies are highly soluble, which makes production of a high concentration product likely since no precipitation would occur. They can withstand extreme pH, proteases and a high temperature environment [2-8]. Producing sdAb is relatively less expensive than monoclonal antibodies (mAb). Since they do not require extensive folding to be functional and, therefore, can be produced in prokaryotic cells (e.g. *E. coli*) or in eukaryotic microbial cells (e.g. yeasts), capital and operation costs of downstream processes are less expensive and scale-up is easier compared to that of mammalian cells [5, 6, 9].

The first step of downstream processing is usually cell lysis which provides access to the recombinant protein in order to proceed with further purification. There currently exist a variety of different techniques for microbe cell envelope destruction. The most widely used large-scale methods of cell disruption are concussion (such as a bead milling) or liquid shearing (high pressure homogenization) [10]. These techniques, which are causing total cell lysis, result in the disruption of the whole cell envelope and, consequently, to the release of all cellular materials. While being effective and of low cost, they release all of the cellular content in the lysis solution and the desired product require extensive purification in downstream processing [11].

There are three layers in the cell envelope of Gram-negative bacteria such as *E. coli:* a cytoplasmic membrane, a peptidoglycan layer and an outer membrane made of lipopolysaccharides and phospholipids [12]. With total lysis techniques, these three layers are disrupted and cellular material are released into the liquid phase. Consequently, lysis solution viscosity rises significantly. Furthermore, native proteins, which are present in large number, may greatly hinder target protein recovery. As a result, recovery of recombinant proteins from high cell density cultures (HCDC) could be particularly challenging.

Several strategies have been investigated to selectively lyse cells. Most of those techniques use chemicals (chemolysis) to remove or destabilize the outer membrane of Gram-negative bacteria [13-16], and, therefore, enable selective protein release from the periplasmic space. It was demonstrated that the addition of certain surfactants, when carefully controlled, could increase the efficiency and selectivity of periplasmic leakage. Of these surfactants, Triton X-100 [16-19], glycine [14, 15, 17, 20] and guanidine hydrochloride [16, 21], which are relatively inexpensive and are not protein based, have been investigated in different scenarios. Furthermore, chemolysis using the combination of different chemical agents, e.g., Triton X-100 and guanidine hydrochloride [16] or Triton X-100 and glycine [17] have studied with promising results. However, the addition of large quantities of chemical agents as required by chemolysis in large-scale operations might increase the recovery costs, cause problems in downstream processing, and draw environmental concerns.

Heat treatment, known as thermolysis, has also been proposed as a selective cell lysis strategy. It exploits the fact that, when cells are exposed to high temperature, the

outer membrane lipopolysaccharide (LPS) of Gram-negative bacteria, which are responsible ensuring membrane stability, will be released enabling selective release of periplasmic proteins [22]. The use of biological methods for cell wall disruption can also result in selective lysis and can be performed in mild conditions. However, lytic enzymes are very costly and Gram-negative bacteria must be pre-treated to disrupt the outer membrane for efficient enzymatic reaction. It is therefore not a viable option for large scale operations [12].

Thermolysis of *E. coli* at 80°C for 120 minutes was shown to release 90% of a hyperthermophilic esterase [23]. It was revealed through electron microscopy that fragmentation and holes appeared in the membrane after heat treatment, proving that thermolysis is an effective method for the breakdown of the *E. coli* cellular envelope. It was pointed out that thermolysis has the added advantage of denaturing and precipitating most native *E. coli* proteins. It was reported that proteins were released after 20 minutes of treatment at 90°C [24]. It was also demonstrated that protein release was more effective with short treatments at high temperatures than longer treatments at low temperatures [24].

Thermolysis, as demonstrated in the aforementioned examples, requires treatment at temperature of 80^{o}C for 120 minutes or 90^{o}C for 20 minutes to be effective. Therefore only applicable to hyperthermostable proteins [11] and cannot be used for heat-sensitive protein recovery [11, 23]. ToxA5.1, the protein of our interest, is a periplasmic recombinant protein [25]. Its thermostability has been demonstrated by circular dichroism experiments, which revealed that 90% of ToxA5.1 was still properly folded at a temperature of 70°C[25]. Furthermore, 50% degradation of ToxA5.1 was observed at 73°C and unfolding of more

than 90% of ToxA5.1 was observed at a temperature of 85°C and, therefore, temperature above 70°C should not be used.

In this paper, we studied the feasibility of using synergistic lysis on recombinant *E. coli* TG1 expressing ToxA5.1. Synergistic lysis is, in essence, a combination of thermolysis and chemolysis utilizing Triton X-100. Temperature is used to disrupt membrane integrity enabling solubilization of the membrane by Triton X-100. The objective was to create a selective lysis approach that operates efficiently at a temperature that would not cause denaturation of our target protein and, at the same time, avoid the excessive use of chemicals.

5.3 Material and Methods

5.3.1 Cell growth and protein expression

Escherichia coli TG1 bearing the plasmid for ToxA5.1 expression gene [25] was grown on agar plates, which consisted in 20 g/L LB Lennox (Fisher Scientific, Pittsburgh, PA) and 100 mM ampicillin (Fisher Scientific) and used to inoculate sterile modified LB media, which consisted in of 20 g/L LB Lennox broth (Fisher Scientific), 6 g/L enzymatic tryptone (Fluka, St. Louis, MO), 5 g/L yeast extract (Oxoid, Lenexa, KS), and 100 mM ampicillin in a shaker at 37ºC and 200 rpm for 18 h. The culture was then used as inoculation for fresh cultures in identical medium. Once the OD_{600} of the culture reached 0.6, it was induced for protein expression using 2 mM isopropyl β-D-1-thiogalactopyranoside (IPTG) (Promega, Madison, WI) at 37 ºC and 200 rpm for 18 h.

5.4 Cell Lysis

5.4.1 Small volume synergistic lysis

A 1 mL-sample of the induced overnight culture was lysed using Promega FastBreak cell lysis buffer chemical lysis and kept at 4°C for protein analysis in order to calculate recovery and selectivity. This sample was used to calculate the total amount of ToxA5.1 present in the overnight culture and the fraction of the total ToxA5.1 measured in the chemical lysis lysate. Synergistic lysis was performed in a Precision water bath model 2835, (Thermo Electron Corp., Waltham, MA) that was pre-heated to the appropriate temperature (37°C, 50°C, 60°C or 70°C). A 1 mL-sample of overnight induced culture was placed in a 1.5 ml micro-centrifuge tube, and the appropriate amount of Triton X-100 to achieve a concentration of 0-4% w/v was added. During the lysis period ranging from 5 to 60 minutes, samples were hand-shaken 5 times every 5 min. Upon completion of the lysis, samples were removed from the water bath and spun at 12 800 rcf for 2 minutes in a tabletop micro-centrifuge (ICE Micromax, Thermo Electron corp.) to pellet the insoluble material. Supernatant fluids were removed and kept at 4°C for protein analysis. These supernatant fluids contained ToxA5.1 released by synergistic lysis.

5.4.2 Synergistic lysis in Erlenmeyer flasks

Samples for the total chemical lysis were taken and treated in the same manner as for the small volume experiments. Samples of 10 mL of the induced overnight culture were transferred to 125-mL Erlenmeyer flasks and Triton X-100 was added to the cultures to the final desired concentration on a w/v basis. Flasks were placed in a reciprocating water bath (BlueM Magni Whirl, Fisher Scientific) at the appropriate

temperature of 37, 40, 50, 60 or 70°C with gentle shaking. Once in the shaker, the samples were allowed to equilibrate to the desired temperature and then incubated for the specified duration of the lysis scheme. Following this period, 1 mL-samples were removed from each culture. These samples were centrifuged at 12800 rcf for 2 minutes. Supernatant fluids were removed and kept at 4°C for protein analysis. These supernatant fluids contained ToxA5.1 released by synergistic lysis.

5.4.3 Protein quantification and activity determination

For sample analysis, appropriate dilutions of synergistic lysis supernatant fluid and of initial induced supernatant fluid obtained from overnight cultures were loaded on 4-15% discontinuous SDS-PAGE gels [26] along with the initial clarified cell lysate with purified and quantified ToxA5.1 serving as standards for protein quantification. Gels were run at 180 V for 50 min. Proteins were stained using Fermentas PageBlue Protein Staining Solution (Glen Burnie, MD) (fast procedure) as per manufacturer's recommendations. Quantification of scanned gels was achieved via densitometry using ImageJ software [27].

To assess the activity of purified ToxA5.1 recovered using nickel nanoparticles[28] after synergistic lysis at 50 and 70°C using 1% w/v Triton X-100, ELISA was performed on the samples and on a ToxA5.1 control recovered after chemical lysis. The control was the same ToxA5.1 obtained from chemical lysis after overnight expression and purified using the commercial Novagen His-Bind column (EMD Millipore, Billerica, MA). Briefly, the column was equilibrated with 10 mL of 1X binding buffer (0.5 M NaCl Fisher Scientific, 20 mM Tris-HCl Fisher Scientific , 5 mM imidazole Alfa Aesar Ward Hill, MA, pH 7.9), then, 5 mL of clarified cell lysate, obtained using the Promega

FastBreak cell lysis system according to the manufacturer recommended protocol, was loaded on the column. The column was then washed with 10 mL of binding buffer and 10 mL of wash buffer (0.5 M NaCl, 60 mM imidazole, 20 mM Tris-HCl, pH 7.9). ToxA5.1 was eluted using 5 mL of elution buffer (1 M imidazole, 0.5 M NaCl, 20 mM Tris-HCl, pH 7.9). ELISA was carried out as follows. First, a 96-well plate was coated overnight with *C. difficile* toxin A (2.5 μg/mL diluted in PBS (8 g NaCl, 0.2 g KCl, 1.44 g Na_2HPO_4, and 0.24 g KH_2PO_4 per litre), 100 μL/well, 4°C). The plate was then blocked with 1% casein (diluted in PBS, 200 μL/well) for 2 h at 37°C. The primary antibodies (ToxA5.1, 100 μL/well) were serially diluted in PBS from a starting concentration of 0.5 μg/mL (31 nM), incubated at room temperature for 1 h, and then followed by 5 washes with PBS-Tween 20 (0.05%). Secondary antibody (rabbit anti-His6-HRP IgG, Cedarlane Laboratories, Burlington, ON) diluted 1:2500 in PBS was added at 100 μL/well, incubated for 1 h at room temperature, and then washed 5 X with PBS-T. HRP substrate (KPL substrate kit Mandel Scientific, Guelph, ON) was added (100 μL/well) for 3 min. The reaction was stopped by the addition of 100 μL/well of 1 M phosphoric acid and plates were read at the 450 nm wavelength.

5.4.4 Calculations of ToxA5.1 recovery and selectivity

Recovery and selectivity were calculated using densities measured from SDS-PAGE gels.

The recovery of ToxA5.1 was calculated using Equation 1:

$$\text{Recovery} = \frac{V_{SLS} \times C_{SLS}}{V_{ITL} \times C_{ITL}} \times 100 \qquad (1)$$

where V_{SLS} is the volume of supernatant fluid of the broth after synergistic lysis treatment, C_{SLS} is the concentration of ToxA5.1 in the supernatant fluid after synergistic lysis, V_{ITL} is the initial sample volume, and C_{ITL} is the total concentration of ToxA5.1 in the initial sample from chemical lysis.

Each lane, which corresponded to a sample of supernatant fluid, contained all of the proteins in *E. coli*, i.e., both native and recombinant and selectivity was calculated using Equation 2:

$$\text{Selectivity} = \left(\frac{\dfrac{\text{ToxA5.1 band intensity}_{SLS}}{\text{Total lane intensity}_{SLS}}}{\dfrac{\text{ToxA5.1 band intensity}_{ITL}}{\text{Total lane intensity}_{ITL}}} \right) \times 100 \qquad (2)$$

where ToxA5.1 band intensity$_{SLS}$ was the intensity of the ToxA5.1 band in a lane, i.e., recombinant protein, in the synergistic lysis supernatant fluid, Total lane intensity$_{SLS}$ was the intensity of all of the proteins in the lane, i.e. native and recombinant proteins, in the synergistic lysis supernatant fluid, ToxA5.1 band intensity$_{ITL}$ was the intensity of the ToxA5.1 band in the total lysate lane i.e. recombinant protein in the initial chemical lysis sample, and Total lane intensity$_{ITL}$ was the intensity of all of the proteins in the lane i.e. native and recombinant proteins in the initial chemical lysis sample. Selectivity was defined as the ratio of ToxA5.1 proportion with respect to the other proteins after synergistic lysis on ToxA5.1 proportion in chemical lysis.

5.5 Results

5.5.1 Synergistic lysis experiments in micro-centrifuge tubes

Initial synergistic lysis screening experiments were performed at 37, 50, and 70°C using 0, 0.5, 1, and 2 w/v % Triton X-100. The 37°C samples, even at the 4% Triton X-100 concentration, did not yield detectable lysis and therefore are not presented. From Figure 5-1, it can be seen that at 50°C, recovery of ToxA5.1 increase with Triton X-100 concentration up to 1%, then decreased at a concentration of 2%. The highest recovery at 50°C, which was 73%, was obtained after 60 min of lysis with 1% Triton X-100. Selectivity, which is expressed as the increase in percentage of the ratio ToxA5.1/total protein from synergistic lysis compared to total chemical lysis ToxA5.1/total cell protein, seemed to level off 125% as can be seen in Figure 5-1. This indicates that the synergistic lysis supernatant fluid contained 25% more ToxA5.1 with respect to the other proteins than those of the total chemical lysis. Furthermore, the selectivity did not seem to be dependent on the duration of lysis. For the 70°C experiments, the highest recovery, which was 83%, was achieved after 2 min, using a Triton X-100 concentration of 0.5%. It is interesting to note that recoveries at 70°C were decreasing with the inverse in Triton X-100 concentrations at all of the tested Triton X-100 concentrations. Selectivity seemed to be enhanced at higher Triton X-100 concentrations as the highest selectivity was obtained after 6 min at 2%. An extra set of experiments was performed at 60°C using Triton X-100 concentrations of 0, 1, and 2%. On Figure 5-1 it can be seen that recoveries of around 50% could be achieved after 6 min in all of the Triton X-100 concentration tested at 60°C. It is interesting to note that a high selectivity of 140% was achieved at this temperature after 10 min when 1% Triton X-100 was used.

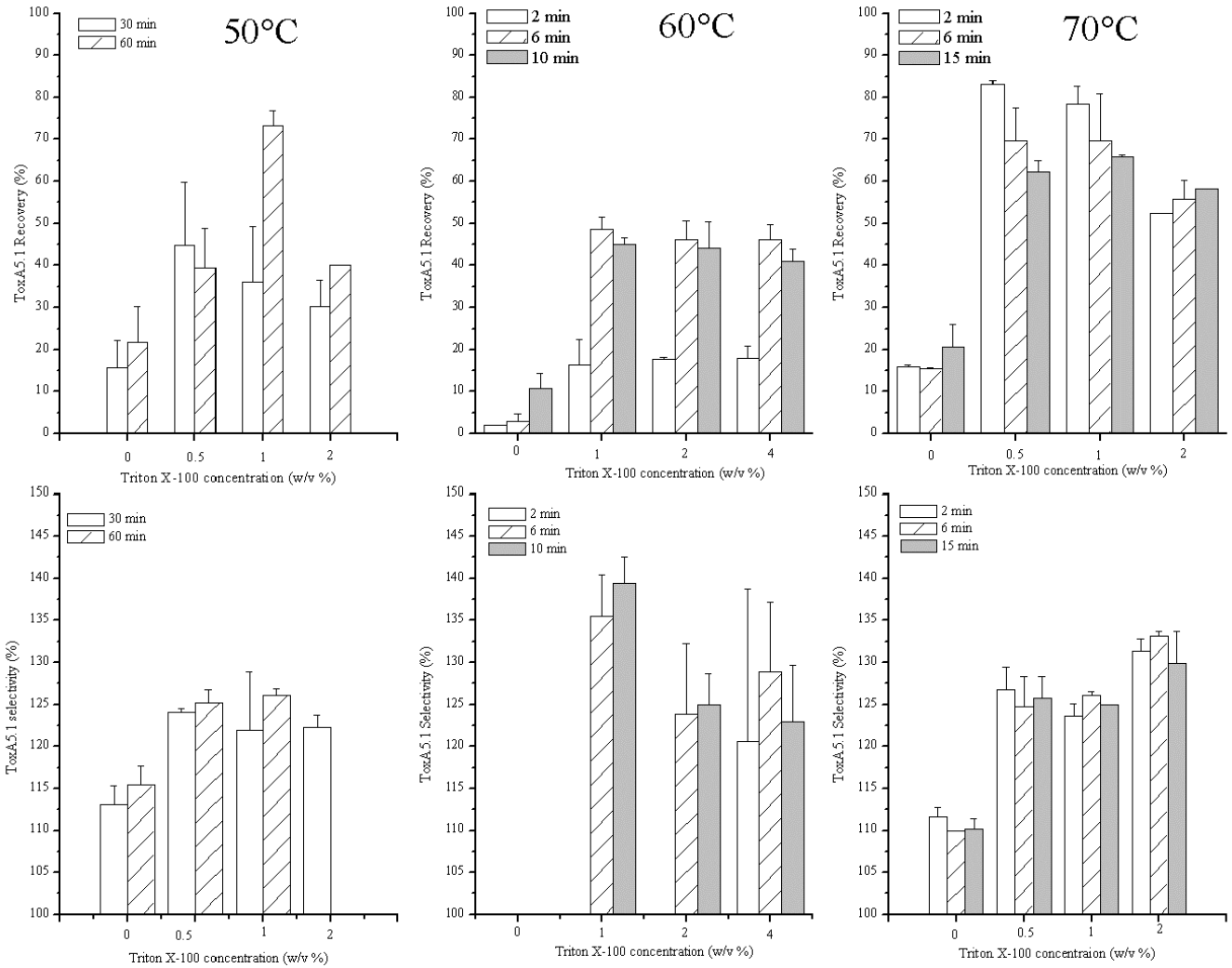

Figure 5-1: Recovery and selectivity obtained from synergistic lysis of one mL-sample of bacterial culture grown in modified LB Lennox broth performed in micro-centrifuge tube under various temperature, Triton X-100 concentration and lysis duration. Error bars are 1σ (n=3).

5.5.2 Synergistic lysis in Erlenmeyer flasks

5.5.2.1 Time course profiles for the synergistic lysis

Effects of synergistic lysis were tested on larger volumes of induced cultures in Erlenmeyer flasks with controlled shaking. Time course profiles for ToxA5.1 recovery at temperatures of 37, 50, 60, and 70°C and with a Triton X-100 concentration of 1% obtained after 5, 15, 30, and 60 min are presented in Figure 5-2. The trends observed for recoveries in Erlenmeyer flasks were comparable to those observed in micro-centrifuge tubes. The 37°C samples showed a low recovery of approximately 10% while, for the 50°C samples, recovery of ToxA5.1 increased from 27% after 5 min of lysis to approximately 80% after 15 min and remained constant thereafter. Selectivity at that temperature increased from 100% after 5 min of lysis to 153% after 15 min, 167% after 30 min and 177% after 60 min as seen in Figure 5-3. For synergistic lysis performed at 60°C, the highest recovery, which was of 95%, was achieved after 5 min. Recovery followed a downward trend, as lysis progressed, reaching a lower value of 76% after 60 min. For synergistic lysis performed at 70°C, recovery after 5 min was 76% and, as for the lysis performed at 60°C, the recovery was lower, as time progressed, reaching 53% after 60 min. Selectivity at that temperature was 166% after 5 min and decreased to 155% after 60 min.

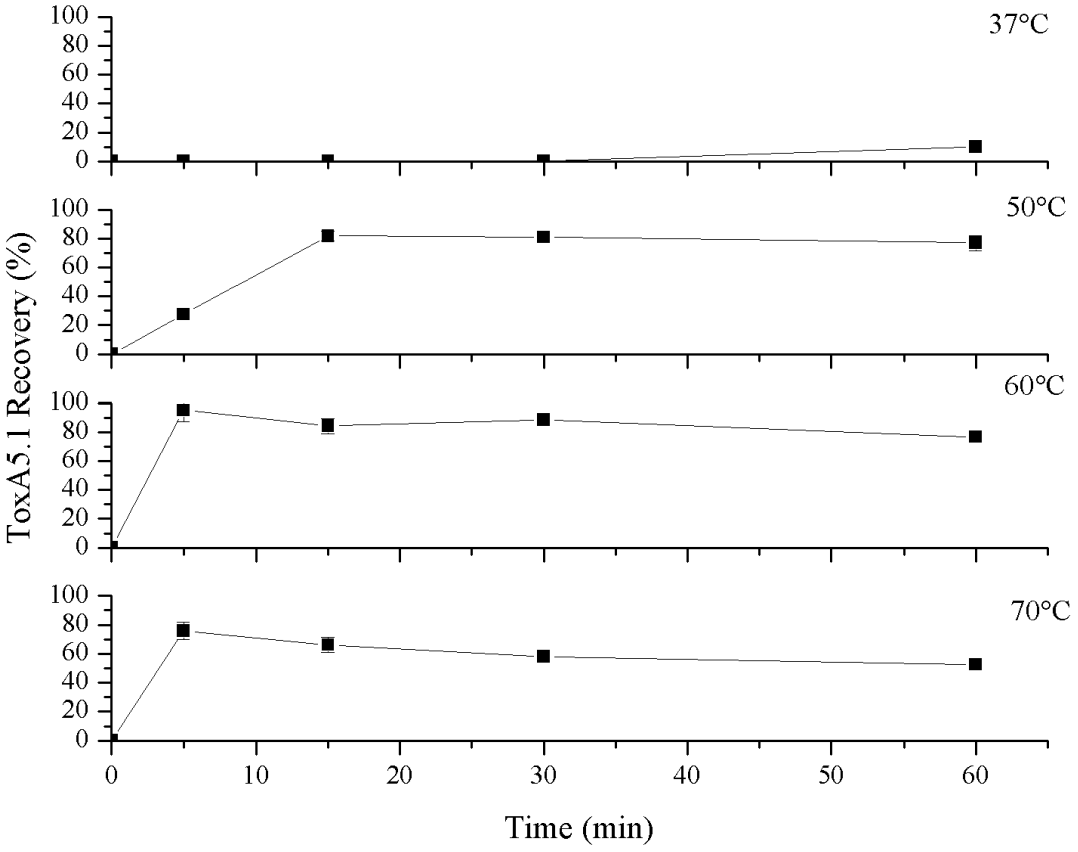

Figure 5-2: Time course profiles of the recovery of ToxA5.1 sdAb using synergistic lysis in Erlenmeyer flask at various temperatures and with Triton X-100 at 1% w/v. Error bars are 1σ (n=3).

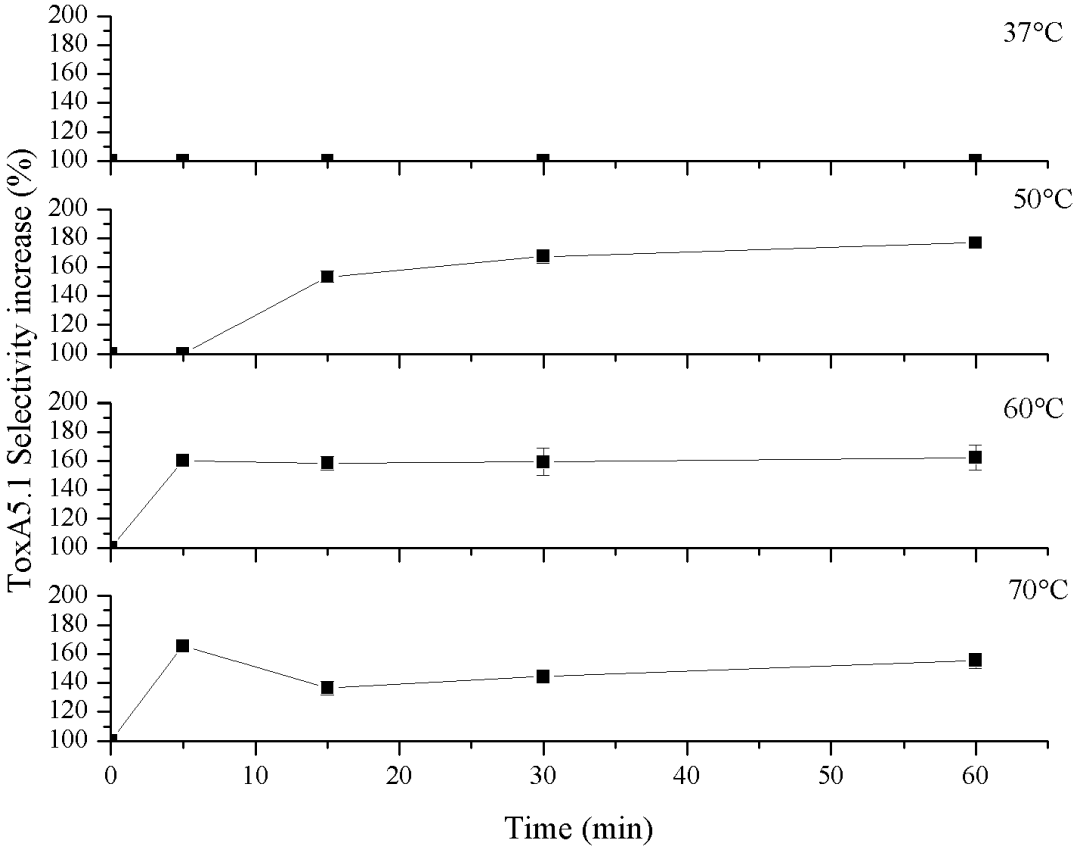

Figure 5-3: Time course profiles of the selectivity of ToxA5.1 sdAb in lysate supernatant fluids using synergistic lysis in Erlenmeyer flasks at various temperatures and with Triton X-100 at 1% w/v. Errors bars are 1σ (n=3).

5.5.2.2 Fixed length synergistic lysis

Using information gathered during the micro-centrifuge tube and time course experiments, the synergistic lysis was repeated in Erlenmeyer flasks at temperature of 40, 50, and 60°C with a Triton X-100 concentration of 0, 1, and 2% and samples were taken after 20 min of lysis since short duration did not yield satisfactory results while longer duration would not be practical at large scale. As can be seen on Figure 5-4 the highest recovery for these experiments, which was of 95%, was achieved with the 60°C and 1% Triton X-100 combination. It is interesting to note that samples at 40 and 50°C and 1% Triton X-100 yielded recoveries of 63 and 60% respectively. The Triton X-100

concentration increase resulted in lower recoveries for all of the tested temperatures but had a lesser effect at 60°C where the recovery was 85%. Selectivity for ToxA5.1 following these lysis experiments can be seen Figure 5-5. The best combination of temperature and Triton X-100 concentration was again 60°C and 1% which achieved a selectivity of 127%. Increasing the Triton X-100 concentration from 1% to 2% did not result in a selectivity increase at 40°C but rather yielded a small increase at 50°C where the selectivity increased from 109% to 114%.

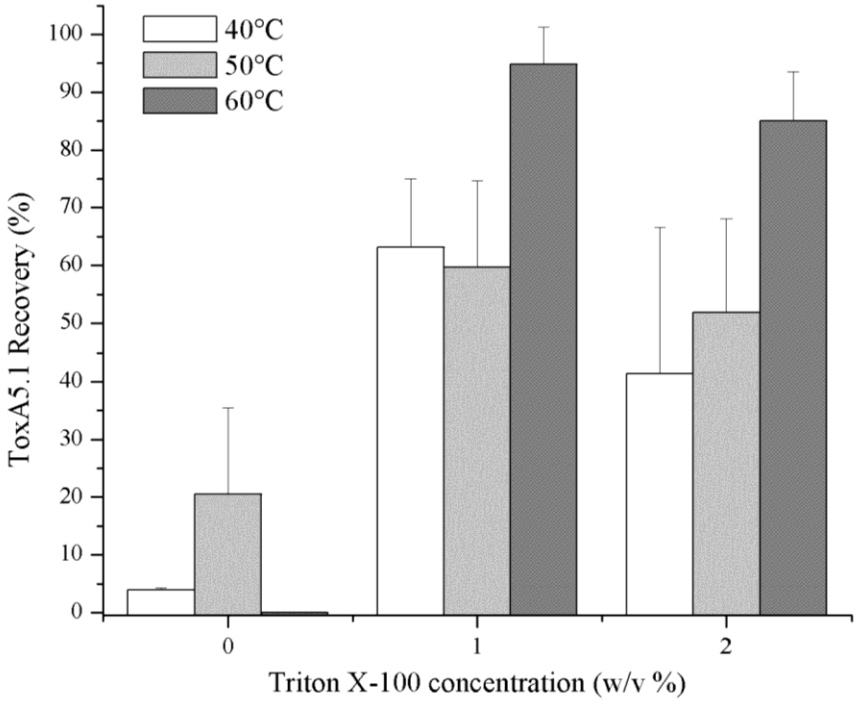

Figure 5-4: Recovery of ToxA5.1 from modified LB broth after synergistic lysis of 20 minutes at temperatures of 40, 50, and 60°C under Triton X-100 concentrations of 0, 1, and 2% w/v. Error bars are 1σ (n=3).

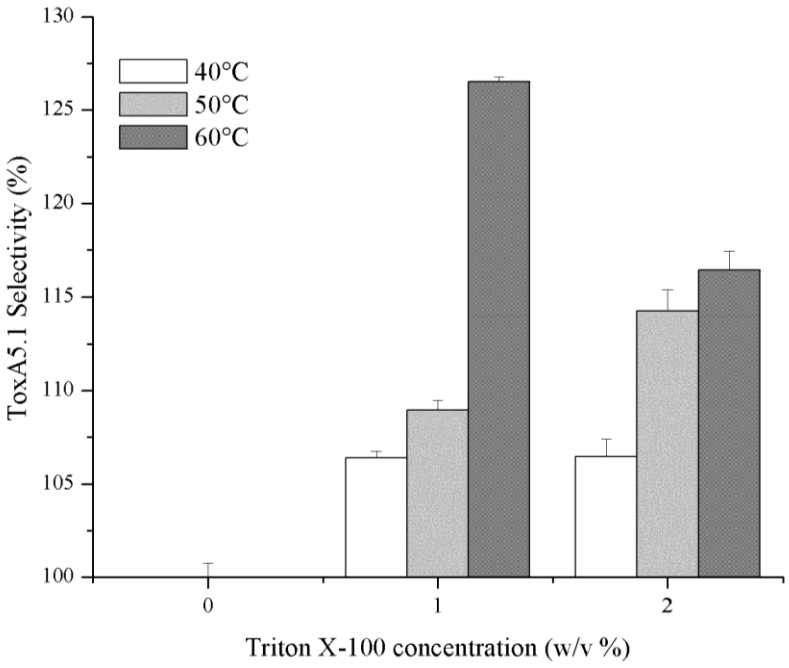

Figure 5-5: Selectivity of ToxA5.1 from modified LB broth sdAb lysate supernatant fluids after synergistic lysis of 20 minutes at temperatures of 40, 50, and 60°C under Triton X-100 concentrations of 0, 1, and 2% w/v. Error bars are 1σ (n=3).

5.5.3 Effect of synergistic lysis on ToxA5.1 activity

Following synergistic lysis at 50 and 70°C with 1% Triton X-100, ToxA5.1 was purified from the supernatant fluid using magnetic nanoparticles. Activity of the purified ToxA5.1 against the intended target, *C. difficile* toxin A, was tested using ELISA. As can be seen in Figure 5-6, both samples of ToxA5.1 purified after synergistic lysis were still able to bind toxin A and the activity they displayed was comparable to that of the control sample, which was purified after the cells were chemically lysed using the FastBreak buffer.

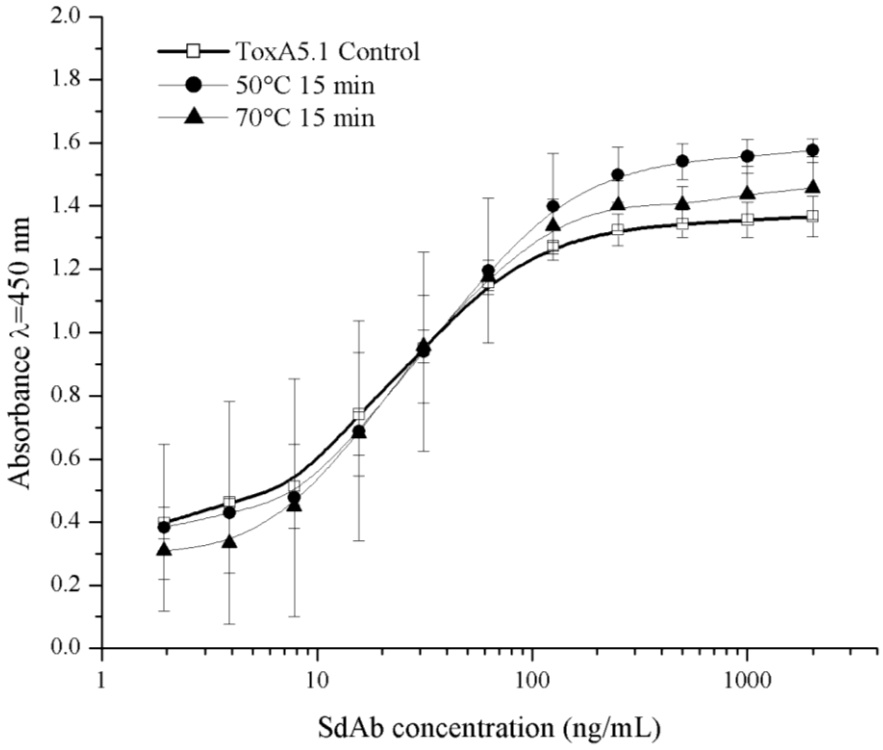

Figure 5-6: Activity of ToxA5.1 purified using nickel nanoparticles after synergistic lysis at 50 or 70°C with 1% Triton X-100 compared to a ToxA5.1 control obtained after using the Promega FastBreak cell lysis system and purified using a Novagen His-Bind column.

5.6 Discussion

5.6.1 Synergistic lysis experiments in micro-centrifuge tubes

Since our protein of interest, ToxA5.1, is thermostable and transported to the periplasmic space after its expression in the *E. coli* cytoplasm, synergistic lysis using heat and Triton X-100 was investigated as a mean of recovering the recombinant protein. During the initial experiments, concentrations up to 4% Triton X-100 did not cause any sign of lysis at 37°C for 60 min. As can be seen on Figure 5-1, at the lower temperature of 50°C it took longer to achieve higher recovery for all of the Triton X-100 concentrations tested, although the 60 min samples yielded higher recoveries. This can be

explained by the fact that lower temperatures are less effective at removing LPS and, therefore, more time is required to disrupt cell membrane integrity [22]. The concentration of Triton X-100 seemed to have maximal effectiveness at 1%, the concentration at which the highest recovery was observed in all of the tested temperatures. This might be due to the fact that Triton X-100, as other surfactants, has a critical micelle concentration (CMC) defined as the concentration above which Triton X-100 will start forming micelles. In water systems, the CMC for Triton X-100 is 0.22-0.24 mM [29] which translates to approximately 1.5 w/v %. The CMC could explain why at 2% Triton X-100 concentration the recovery of ToxA5.1 was less. If Triton X-100 forms micelles, it would suggest that less Triton X-100 is available to solubilize the cell membranes. At 60°C, the recovery of ToxA5.1 seemed to be independent of time after 6 min and independent of Triton X-100 concentration from 1 to 4%. It is not clear why at 60°C, the Triton X-100 concentration did not seem to affect recovery. It is hypothesized that the CMC increases with temperature as it was reported that micelle size of Triton X-100 varies with respect to temperature. Micelle diameter observed at 35°C was 54 Å and it increased to 85 Å at 55°C [30]. If the micelle size does increase, it might suggest a higher CMC since larger diameter micelles would imply a higher concentration of Triton X-100 would be available in the system for membrane solubilization. For the synergistic lysis performed at 70°C, the highest recovery was achieved after two minutes at a Triton X-100 concentration of 0.5%. This suggests that thermolysis was quite rapid at that temperature and that Triton X-100 concentration plays a lesser role is lysing cells. At 70°C product recovery showed a downward trend as synergistic lysis progressed and this was true for all of the Triton X-100 concentrations tested. This result could be explained by the

denaturating effect of temperature on proteins [11, 23]. Even if ToxA5.1 is thermostable, its melting temperature of 73°C [25] is very close to the tested temperature some ToxA5.1 could have been denaturated and, thus, removed from the supernatant fluid upon centrifugation.

For selectivity, the best conditions at 50 and 60°C were with 1% Triton X-100, which is close to the CMC, indicating that a high concentration of readily available Triton X-100, i.e. not forming micelles, is required for synergistic lysis. It can be said that synergistic lysis increases the ratio of ToxA5.1 over native proteins in the supernatant fluid when compared to the ratio of ToxA5.1 over native proteins in the chemical lysate.

5.6.2 Synergistic lysis in Erlenmeyer flasks

The synergistic lysis experiment recovery results derived from Erlenmeyer flasks experiments, shown in Figure 5-2, were comparable to the results obtained in micro-centrifuge tubes at a 1% Triton X-100 concentration. At 37°C, no apparent lysis occurred until 60 min after the lysis was induced and only 10% recovery was obtained using 1% Triton X-100. This recovery could be due to cell autolysis and confirms that Triton X-100 alone was not sufficient to induce cell lysis as it has been already reported [31]. The trend for the 50°C synergistic lysis in flasks also followed the trend observed in micro-centrifuge tubes. The ToxA5.1 recovery was only 27% after 5 min but reached 82% after 15 min. The recovery was constant thereafter with 80% after 30 min and 77% after 60 min. As for selectivity, it seemed to be higher in flasks than in micro-centrifuge tubes. This might be the result of improved mixing offered by the reciprocating water bath which would better distribute Triton X-100 and enhanced the selective removal of the cell membrane. The selectivity for the 50°C experiments increased with the duration of

the lysis to reach a maximum of 177% as seen on Figure 5-3. This increase in selectivity over time might be the result of native protein denaturation. The highest ToxA5.1 recovery using 1% Triton X-100 was achieved at 60°C. At this temperature, 95% of the ToxA5.1 initially present was recovered in the supernatant fluid. It is interesting to note that this recovery was achieved in only 5 min. For this temperature, selectivity remained constant at around 160% indicating that the ratio of ToxA5.1 to native protein remained constant throughout the lysis cycle. The synergistic lysis performed at 70°C yielded high recovery early in the lysis, as expected, since this temperature rapidly disrupts membrane integrity [11] exposing the inner surface of the membrane to the solubilizing action of Triton X-100. However, recovery decreased as time progressed which might indicate that not only native proteins were denaturated but also our target protein ToxA5.1. The selectivity time course at 70°C seemed to support this fact as, after 5 min, selectivity was 166% but after 15 min it had decreased to 136% indicating that some ToxA5.1 might have become denaturated. Selectivity, however, increased thereafter to reach 155% after 60 min. From Figure 5-2 and Figure 5-3, it is clear that longer lysis duration is desirable at a temperature of 50°C but at temperatures of 60 and 70°C shorter lysis cycles should be considered.

The third set of experiments, which were 20 min synergistic lysis experiments, described in Figure 5-4 and Figure 5-5, were consistent with the previous experiments with regards to recovery in the sense that highest recovery was achieved at 60°C using 1% Triton X-100. However, in these experiments, samples at 40°C showed signs of synergistic lysis that yielded a ToxA5.1 recovery of 63% when 1% Triton X-100 was used. Furthermore, selectivity observed for these was lower than the ones seen in

previous experiments. It is hypothesized that the state of the overnight culture might have influenced the results. Figure 5-6 shows that neither exposure of 15 min to a temperature of 50 or 70°C nor Triton X-100 addition resulted in ToxA5.1 activity loss even after a lysis period of 15 minutes. It can be seen from the ELISA data that both samples recovered after synergistic lysis were still able to bind and neutralize *C. difficile* toxin A possibly with great affinity, especially at higher sdAb concentrations, than that of the control ToxA5.1 recovered after chemical lysis.

5.7 Conclusion

In conclusion, it was shown that synergistic cell lysis could provide an effective and selective lysis scheme for thermostable proteins expressed in periplasmic space. Using a synergistic cell lysis can minimize the number of biological contaminants typically released during total cell lysis. By lessening this contamination, broth viscosity as well as the presence of native proteins can be controlled and, thus, facilitates downstream processing. Selective lysis becomes useful especially when high cell density cultures need to be lysed. The amount of genetic material released during total lysis makes it for a highly viscous broth that hampers protein purification. There exist a compromised between temperature and lysis duration where lower temperature requires longer lysis duration. It was also shown that 95% of the initially present ToxA5.1 could be recovered and furthermore, it was possible to increase the concentration of ToxA5.1 by 127% in the resulting supernatant fluid after synergistic lysis at 60°C using 1% Triton X-100. Triton X-100 concentration should be at or slightly below the critical micelle concentration to effectively solubilize cell membranes that are exposed after heat treatment. Finally, activity levels of ToxA5.1, recovered after synergistic lysis at

temperatures of 50 and 70°C in the presence of 1% Triton X-100 for 15 minutes, were comparable to that of a ToxA5.1 control obtained via chemical lysis, making synergistic lysis a suitable method for extracting ToxA5.1 before further downstream processing.

5.8 Acknowledgements

Financial support from the Natural Science and Engineering Council of Canada (NSERC) and The Canada Foundation of Innovation (CFI) is gratefully acknowledged.

5.9 References

1. Hamers-Casterman, C., Atarhouch, T., Muyldermans, S., Robinson, G., Hamers, C., Songa, E.B., Bendahman, N. and Hamers, R. Naturally occurring antibodies devoid of light chains. *Nature* **363**, 446-448 (1993).

2. Harmsen, M.M. and De Haard, H.J. Properties, production, and applications of camelid single-domain antibody fragments. *Applied Microbiology and Biotechnology* **77**, 13-22 (2007).

3. Saerens, D., Frederix, F., Reekmans, G., Conrath, K., Jans, K., Brys, L., Huang, L., Bosmans, E., Maes, G., Borghs, G. and Muyldermans, S. Engineering camel single-domain antibodies and immobilization chemistry for human prostate-specific antigen sensing. *Analytical Chemistry* **77**, 7547-7555 (2005).

4. Muyldermans, S. Single domain camel antibodies: Current status. *Reviews in Molecular Biotechnology* **74**, 277-302 (2001).

5. Holliger, P. and Hudson, P.J. Engineered antibody fragments and the rise of single domains. *Nature Biotechnology* **23**, 1126-1136 (2005).

6. Gibbs, W.W. Nanobodies. *Scientific American* **293**, 78-83 (2005).

7. Arbabi-Ghahroudi, M., Tanha, J. and MacKenzie, R. Prokaryotic expression of antibodies. *Cancer and Metastasis Reviews* **24**, 501-519 (2005).

8. Goldman, E.R., Andersen, G.P., Liu, J.L., Delehanty, J.B., Sherwood, L.J., Osborn, L.E., Cummins, L.B. and Hayhurst, A. Facile generation of heat-stable antiviral and antitoxin single domain antibodies from a semisynthetic llama library. *Analytical Chemistry* **78**, 8245-8255 (2006).

9. Gasser, B. and Mattanovich, D. Antibody production with yeasts and filamentous fungi: On the road to large scale? *Biotechnology Letters* **29**, 201-212 (2007).

10. Majors, R.E. Sample preparation for large-scale protein purification. *LC-GC Europe* **19**, 82-92 (2006).

11. Ren, X., Yu, D., Han, S. and Feng, Y. Thermolysis of recombinant *Escherichia coli* for recovering a thermostable enzyme. *Biochemical Engineering Journal* **33**, 94-98 (2007).

12. Harrison, S.T.L. Bacterial cell disruption: A key unit operation in the recovery of intracellular products. *Biotechnology Advances* **9**, 217-240 (1991).

13. Allen, J.R., Patkar, A.Y., Frank, T.C., Donate, F.A., Yuk, C.C., Shields, J.E. and Gustafson, M.E. Use of glycol ethers for selective release of periplasmic proteins from Gram-negative bacteria. *Biotechnology Progress* **23**, 1163-1170 (2007).

14. Hammes, W., Schleifer, K.H. and Kandler, O. Mode of action of glycine on the biosynthesis of peptidoglycan. *Journal of Bacteriology* **116**, 1029-1053 (1973).

15. Kaderbhai, N., Karim, A., Hankey, W., Jenkins, G., Venning, J. and Kaderbhai, M.A. Glycine-induced extracellular secretion of a recombinant cytochrome expressed in *Escherichia coli*. *Biotechnology and Applied Biochemistry* **25**, 53-61 (1997).

16. Naglak, T.J. and Wang, H.Y. Recovery of a foreign protein from the periplasm of *Escherichia coli* by chemical permeabilization. *Enzyme and Microbial Technology* **12**, 603-611 (1990).

17. Yang, J., Moyana, T., Mackenzie, S., Xia, Q. and Xiang, J. One hundred seventy-fold increase in excretion of an FV fragment-tumor necrosis factor alpha fusion protein (sFV/TNF-α) from *Escherichia coli* caused by the synergistic effects of glycine and Triton X-100. *Applied and Environmental Microbiology* **64**, 2869-2874 (1998).

18. Choi, J.I. and Lee, S.Y. Efficient and economical recovery of poly(3-hydroxybutyrate) from recombinant *Escherichia coli* by simple digestion with chemicals. *Biotechnology and Bioengineering* **62**, 546-553 (1999).

19. Mörbe, J.L. and Riesenberg, D. Release of miniantibodies from *E. coli* cells into the supernatant at low and high cell densities. *Microbiological Research* **152**, 385-394 (1997).

20. Jang, K.H., Seo, J.W., Song, K.B., Kim, C.H. and Rhee, S.K. Extracellular secretion of levansucrase from *Zymomonas mobilis* in *Escherichia coli*. *Bioprocess Engineering* **21**, 453-458 (1999).

21. Anand, H., Balasundaram, B., Pandit, A.B. and Harrison, S.T.L. The effect of chemical pretreatment combined with mechanical disruption on the extent of disruption and release of intracellular protein from *E. coli*. *Biochemical Engineering Journal* **35**, 166-173 (2007).

22. Tsuchido, T., Katsui, N. and Takeuchi, A. Destruction of the outer membrane permeability barrier of *Escherichia coli* by heat treatment. *Applied and Environmental Microbiology* **50**, 298-303 (1985).

23. Ren, X., Yu, D., Yu, L., Gao, G., Han, S. and Feng, Y. A new study of cell disruption to release recombinant thermostable enzyme from *Escherichia coli* by thermolysis. *Journal of Biotechnology* **129**, 668-673 (2007).

24. Watson, J.S., Cumming, R.H., Street, G. and Tuffnell, J.M. in Separations in Biotechnology (eds. M. S. Verrall & M.J. Hudson) pp:105-109 (Ellis Horwood Ltd, London; 1987).

25. Hussack, G., Arbabi-Ghahroudi, M., Van Faassen, H., Songer, J.G., Ng, K.K.S., MacKenzie, R. and Tanha, J. Neutralization of *Clostridium difficile* toxin A with single-domain antibodies targeting the cell receptor binding domain. *Journal of Biological Chemistry* **286**, 8961-8976 (2011).

26. Laemmli, U.K. Cleavage of structural proteins during the assembly of the head of bacteriophage T4. *Nature* **227**, 680-685 (1970).

27. Abràmoff, M.D., Magalhães, P.J. and Ram, S.J. Image processing with imageJ. *Biophotonics International* **11**, 36-41 (2004).

28. Parisien, A., Al-Zarka, F., Hussack, G., Baranova, E.A., Thibault, J. and Qingdao Lan, C. Nickel nanoparticles synthesized by a modified polyol method for the purification of histidine-tagged single-domain antibody ToxA5.1. *Journal of Materials Research* **27**, 2884-2890 (2012).

29. Hait, S.K. and Moulik, S.P. Determination of Critical Micelle Concentration (CMC) of Nonionic Surfactants by Donor-Acceptor Interaction with Iodine and Correlation of CMC with Hydrophile-Lipophile Balance and Other Parameters of the Surfactants. *Journal of Surfactants and Detergents* **4**, 303-309 (2001).

30. Streletzky, K. and Phillies, G.D.J. Temperature dependence of Triton X-100 micelle size and hydration. *Langmuir* **11**, 42-47 (1995).

31. Schnaitman, C.A. Solubilization of the cytoplasmic membrane of *Escherichia coli* by Triton X-100. *Journal of Bacteriology* **108**, 545-552 (1971).

Chapter 6: Nickel nanoparticles synthesized by a modified polyol method for the purification of histidine-tagged single domain antibody ToxA5.1 (Published in Journal of Materials Research, 2012)

Albert Parisien[1], Fady Al-Zarka[1], Greg Hussack[2], Elena A. Baranova[1], Jules Thibault[1], and Christopher Q. Lan[1]*

[1]University of Ottawa, Department of Chemical and Biological Engineering
161 Louis-Pasteur, Ottawa, Ontario, Canada K1N 6N5
[2]Institute for Biological Sciences, National Research Council Canada,
100 Sussex Drive Ottawa, ON, Canada, K1A 0R6

* To whom all correspondence should be addressed
University of Ottawa, Department of Chemical and Biological Engineering
161 Louis-Pasteur, Ottawa, Ontario, Canada K1N 6N5
Christopher.Lan@uottawa.ca

6.1 Abstract

Nickel nanoparticles (NNP) synthesized by a modified polyol method using ethylene glycol as a reducing agent, palladium chloride as a nucleating agent, and polyvinylpyrrolidone (PVP) as a protective agent were investigated as a potential magnetic adsorbent for the purification of hexahistidine (His6-tagged) recombinant proteins. The synthesis resulted in nanoparticles having an average diameter of 68 ± 28 nm. The XRD pattern confirmed the presence of nickel metal, as well as the presence of un-reacted $Ni(OH)_2$. Magnetic characterization showed that a magnetization saturation of 39.3 electromagnetic unit (emu)/g at 20 000 Oersted (Oe) was reached rapidly and that the material exhibited ferromagnetic behavior. Protein purification results showed that the synthesized nickel nanoparticles were highly selective for binding to a His6-tagged recombinant protein single domain antibody ToxA5.1. In addition, NNP were used for four adsorption cycles without significant binding capacity losses. These particles have shown great potential as being easily synthesized, cost-effective, and highly selective magnetic adsorbents for the purification of His6-tagged recombinant proteins.

KEYWORDS: Magnetic, adsorption, purification

6.2 Introduction

Purification and recovery of recombinant proteins, after cell disruption, is achieved by techniques ranging from gel chromatography, ion exchange chromatography and affinity chromatography to electrophoresis, precipitation and membrane separation [1, 2]. A versatile affinity chromatography approach for recombinant protein recovery is immobilized metal ion affinity chromatography (IMAC), which provides high recovery and selectivity to His6-tagged recombinant proteins. Another approach is the use of magnetic affinity adsorbents (MAA) for their ability to retain the selectivity and recovery characteristics of IMAC with the additional advantage of being easily recovered using a magnetic field. These particles, however, are very expensive, making cost-effectiveness a major concern in their commercial large scale applications.

Several essential attributes are desired from inorganic magnetic core materials: (i) good response to the applied external magnetic field; (ii) small size (diameter) that provides large surface area for protein binding; (iii) reasonable price; and (iv) ease of manufacturing [3, 4]. The ability of magnetic particles to aggregate rapidly in the presence of a magnetic field makes the utilization of nanoparticles ideal for separation. Furthermore, nickel nanoparticles (NNP) are characterized by their large surface area and fast binding/adsorption kinetics in comparison to microparticles [3], making them well suited for protein purification.

It has been well established that nickel nanoparticles exhibit excellent magnetic behavior [5-7] and nickel has been one of the most commonly used metal ions in IMAC [8, 9]. The polyol process in which metal salt precursors are reduced in a polyalcohol solvent has been used to produce a variety of elemental metal nanoparticles which have

applications in many fields such as magnetic resonance imaging (MRI), catalysis or solar cells [10]. In previous studies, it has been shown that a layer of NiO was formed on the surface of the NNP synthesized by the modified polyol method [6], probably by oxidization of Ni when the synthesized NNP were exposed to air. In another study, Lee et al. [11] investigated the use of a complex type of nanoparticles that have a Ni core and a NiO shell for selective binding and magnetic separation of His-tagged green fluorescent protein (GFP). Furthermore, a magnetically recyclable protein separation system using three-layer magnetic nanocomposite spheres was investigated [12]. The magnetic nanocomposite spheres had a uniform hematite (α-Fe_2O_3) core, which was coated with a dense silica shell and, then, a porous silica shell. The porous silica shell was loaded with large amounts of NiO, which served as binding sites for selectively purifying His-tagged GFP. The selective binding of His-tagged proteins to nickel oxide surfaces was also explored for bioactive protein nanoarrays [12].

In this research, we investigated the potential of nickel nanoparticles (NNP) synthesized using a modified polyol method [5, 13] to serve as magnetic adsorbents for the purification a His6-tagged recombinant protein, ToxA5.1, a single domain antibody neutralizing *Clostridium difficile* enterotoxin A [14].

6.3 Materials and Methods

6.3.1 Synthesis of nickel nanoparticles

Nickel nanoparticles were synthesized using a modified polyol method [5, 13] by mixing 0.4 g $Ni(OH)_2$ (Acros Organics, Fisher Scientific, Pittsburgh, PA), 160 mL ethylene glycol (EG) (Fisher Scientific) and 0.1268 g of polyvinylpyrrolidone (PVP) (Fisher Scientific) to get a 1:0.5 w/w ratio of Ni:PVP, at room temperature in a 1 L three-

neck boiling flask for 30 min after which the solution was heated to 190ºC. Once the $Ni(OH)_2$ in EG mixture reached 190ºC, a $PdCl_2$ solution was quickly added to the flask. The $PdCl_2$ (Sigma Aldrich, St. Louis, MO) solution was prepared by mixing 0.0076 g $PdCl_2$ in 40 mL EG in a beaker at room temperature for 45 min. Upon addition of the $PdCl_2$ solution, the initial mixture of $Ni(OH)_2$ in EG changed from a light green color to black within 15 min indicating the formation of metallic Ni. After 2 h of refluxing, the suspension was left to cool at room temperature and, then, the NNP were separated from the spent EG solvent using a magnet. The recovered NNP were thoroughly washed three times with 99% ethanol and separated using a magnet. The washed particles were then suspended in 10 mL of 99% ethanol and stored at room temperature.

6.3.2 Characterization of Ni nanoparticles

XRD: The structure of Ni nanoparticles was determined by X-ray diffraction (XRD), using an Ultima IV powder XRD (Rigaku, The Woodlands, Tx) with a copper source from 20º to 80º 2θ with a step of 0.02º 2θ.

SEM: Scanning electron microscopy (SEM) was performed on the synthesized nickel nanoparticles using a JSM-7500F FESEM (JEOL, Peabody, MA) instrument. To prepare the sample, 500 µL of particles suspended in ethanol was sonicated for 5 min in a Fisher Scientific FS140 ultrasonic cleaner (135 W and 42 kHz ± 6%) and a drop of the suspension was applied onto a carbon-coated copper grid. Average size and size distribution of the particles were calculated using ImageJ software [15] based on the measurement of 260 particles distributed over 2 different areas of the sample (2 different images).

Magnetic characterization: The magnetic measurements were obtained using a Quantum Design SQUID magnetometer MPMS-XL7 operating at 300 K for DC-applied fields ranging from −7 to 7 T. ZFC/FC analyses were performed on powdered samples of 17 mg of nanoparticles, wrapped in a polyethylene membrane.

Nickel quantification: Nickel from NNP was quantified using an iCE3300 Atomic absorption apparatus (Thermo Scientific.) following appropriate sample dilutions. Quantification of the nickel was obtained from the average of 5 measurements of 4 s each at a wavelength of 232 nm. Samples were prepared by pipetting 500 μL of NNP suspended in ethanol into a beaker and subjecting them to a magnetic field to remove the ethanol. The NNP were dissolved by adding sequentially 1 mL of concentrated hydrochloric acid (Fisher Scientific), 1 mL of concentrated nitric acid (Fisher Scientific) and 2 mL of deionized water. Upon dissolution, the solution was transferred to a 50 mL volumetric flask and the total solution volume was adjusted to 50 mL using deionized water.

6.3.3 Protein purification and regeneration of Ni nanoparticles

Escherichia coli TG1 cells bearing the plasmid for ToxA5.1 gene expression [14], were grown from a starting patch in sterile modified LB media consisted of 20 g LB Lennox broth (Fisher Scientific), 6 g enzymatic tryptone (Fluka, St. Louis, MO) and 5 g yeast extract (Oxoid, Lenexa, KS) for 1000 mL of distilled water overnight in a shaker at 37ºC and 200 rpm. Fresh sterile modified LB broth was inoculated with enough of the overnight culture to get an $OD_{600\ nm}$ of 0.1 and grown at 37°C until $OD_{600\ nm}$ reached 0.6 at which point recombinant protein expression was induced using 2 mM isopropyl β-D-1-thiogalactopyranoside (Promega, Madison, WI) at 37ºC for 18 h. Bacterial lysis was

performed using the Promega Fastbreak lysis system following the protocol provided by the manufacturer. The bacterial lysate was centrifuged at a relative centrifugal force (RCF) of 1150 for 10 min. The clarified lysate was used for the purification experiment.

For the purification experiments, 500 μL of the NNP suspension was added to a 2 mL micro-centrifuge tube. The tube was inserted in a Promega magnetic holder for 1 min. The ethanol was removed and the NNP were suspended in 300 μL of wash-bind buffer, which contained 100 mM HEPES and 10 mM imidazole (pH 7.5), by quick vortexing followed by sonication for 10 s to ensure dispersion prior to the binding step. The well-dispersed NNP suspension is referred to as NNP slurry from now on. One mL of clarified bacterial lysate was added to the micro-centrifuge tube containing the NNP slurry. To ensure proper binding, the tube was placed on a platform rocker (Boekel Scientific, Feasterville, PA) to mix for 2 min. The tube was then inserted in the magnetic holder for 1 min at which point the NNP were separated from the bulk liquid by aggregation on the tube wall. The supernatant fluid was then removed and kept at 4°C for analysis of the unbound fraction (UBF), which represents the proteins that did not bind to the NNP. The tube was then removed from the magnetic holder and the NNP were suspended in 300 μL of wash-bind buffer and mixed for 10 s. The tube was then inserted into the magnetic holder again to separate the NNP from the supernatant fluid which was discarded. The washing step was repeated two more times. After the third wash, the NNP were suspended in 100 μL of the elution buffer (100 mM HEPES and 500 mM imidazole, pH 7.5) to elute the adsorbed proteins. The suspension was sonicated for 10 s and put on a Boekel scientific rocking platform (Feasterville, PA) for 2 min. The tube was inserted into the magnetic stand for 1 min and the supernatant fluid containing the recombinant

protein was removed and kept at 4ºC until analyzed. The NNP were then washed three times using 1000 µL of wash-bind buffer each time. This completed the first purification with pristine NNP. The same procedures were repeated three more times for a total of four binding cycles with the same NNP and every time, the starting material was clarified lysate obtained from the 18 h induced culture. An additional elution was performed on the NNP after completing the fourth cycle by using elution buffer containing 1.0 M, 1.5 M or 2.0 M imidazole.

For protein gel analysis, samples of appropriate dilutions were loaded on 4-15% discontinuous SDS-PAGE gels [16]. Gels were run at 190 V for 45 min. Proteins were stained using the Fermentas PageBlue Protein Staining Solution (Glen Burnie, MD) fast procedure as per manufacturer's recommendations. Quantification of scanned gels was achieved via densitometry using ImageJ software [15].

To confirm that the purified protein was indeed the target protein and to assess the activity of purified ToxA5.1 via NNP, an ELISA was performed in comparison with a control. The control was the same ToxA5.1 but purified using the commercial Novagen His-Bind column (EMD Millipore, Billerica, MA). Briefly, the column was equilibrated with 10 mL of 1X binding buffer (0.5 M NaCl Fisher Scientific, 20 mM Tris-HCl Fisher Scientific , 5 mM imidazole Alfa Aesar Ward Hill, MA, pH 7.9), then, 5 mL clarified cell lysate were loaded on the column. The column was then washed with 10 mL of binding buffer and 10 mL of wash buffer (0.5 M NaCl, 60 mM imidazole, 20 mM Tris-HCl, pH 7.9). ToxA5.1 was eluted using 5 mL of elute buffer (1 M imidazole, 0.5 M NaCl, 20 mM Tris-HCl, pH 7.9). ELISA was carried out as follows. First, a 96-well plate was coated overnight with *C. difficile* toxin A (2.5 µg/mL diluted in PBS, 100 µL/well, 4°C).

The plate was then blocked with 1% casein (diluted in PBS, 200 µL/well) for 2 h at 37°C. The primary antibodies (ToxA5.1, 100 µL/well) were serially diluted in PBS from a starting concentration of 0.5 µg/mL (31 nM), incubated at room temperature for 1 h, and then followed by 5 washes with PBS-Tween 20 (0.05%). Secondary antibody (rabbit anti-His6-HRP IgG, Cedarlane Laboratories, Burlington, ON) diluted 1:2500 in PBS was added at 100 µL/well, incubated for 1 h at room temperature, and then washed 5 X with PBS-T. HRP substrate (KPL substrate kit Mandel Scientific, Guelph, ON) was added (100 µL/well) for 3 min. The reaction was stopped by the addition of 100 µL/well of 1 M phosphoric acid and plates were read at 450 nm wavelength.

6.3.4 Calculations of binding capacities and ToxA5.1 recovery

The quantity of ToxA5.1 adsorbed per unit amount of NNP (q_n in mg/g) at the n^{th} separation cycle was calculated using Equation 1:

$$q_n = \frac{\left(V_{broth} \times C_{broth}\right) - \left(V_{UBF} \times C_{UBF}\right)}{M_p} + q_{residual,\ n-1} \qquad (1)$$

where V_{broth} is the volume of initial broth (L), C_{broth} the concentration of ToxA5.1 in the initial broth (mg/L), V_{UBF} the volume of the unbound fraction (L), C_{UBF} the concentration of ToxA5.1 in the unbound fraction (mg/L), M_p the mass of nickel nanoparticles (NNP) expressed as g of Ni.

The quantity of ToxA5.1 remaining on the NNP after the elution ($q_{residual}$ in mg/g) of the n^{th} cycle is calculated using Equation 2:

$$q_{residual,\,n} = q_n - \frac{V_{eluate} \times C_{eluate}}{M_p} \quad (2)$$

where V_{eluate} is the volume of the eluate fraction (L) and C_{eluate} the concentration of ToxA5.1 in the eluate fraction (mg/L).

The protein percentage recovery is calculated using Equation 3:

$$\text{Recovery} = \frac{V_{eluate} \times C_{eluate}}{V_{broth} \times C_{broth}} \times 100 \quad (3)$$

6.4 Results and discussion

6.4.1 NNP characteristics

6.4.1.1 XRD

The structure of the resulting NNP was confirmed by XRD as shown in Figure 6-1. The diffraction lines of (1 1 1), (2 0 0), and (2 2 0) planes from the XRD profile confirm that nickel nanoparticles with the face-centered cubic (fcc) structure [17] were obtained. The XRD pattern also showed the presence of the $Ni(OH)_2$ phase with characteristic diffraction peaks at 33º, 38.5º, 52º, 59º, and 62.5º 2θ corresponding to (1 0 0), (1 0 1), (1 0 2), (1 1 0), and (1 1 1) crystalline planes [17] indicating incompleteness of the reduction reaction in EG. The addition of PVP helped in slowing down the reduction of $Ni(OH)_2$ to Ni by interacting with the nickel precursor [18] and controlling the size of the nanoparticles formed in the reaction which could explain the presence of unreacted $Ni(OH)_2$. Using the full-width at half maximum of Ni (111) reflection and the Scherrer formula [19], the crystallite size of Ni was calculated to be 24.3 nm.

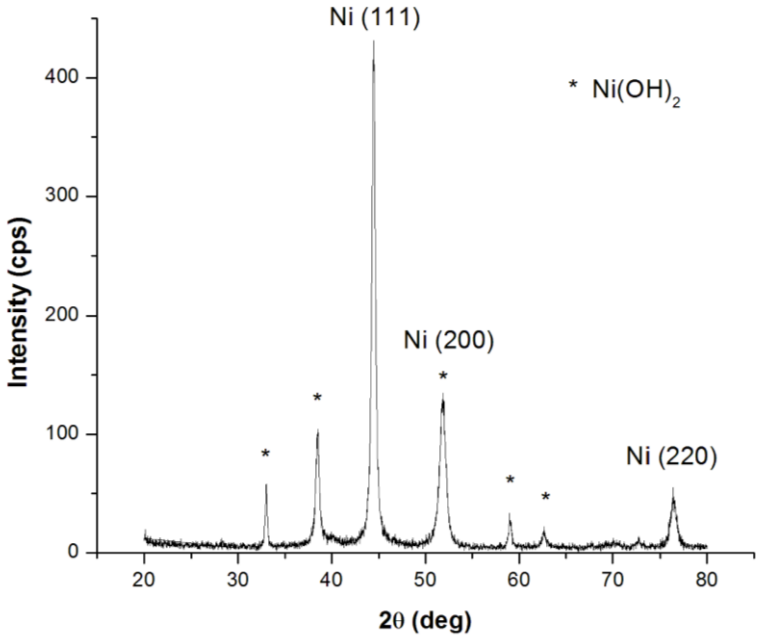

Figure 6-1: XRD pattern of the nickel nanoparticles (1% atomic Ni:Pd, 1:0.5 w/w Ni:PVP).

6.4.1.2 SEM

Figure 6-2 shows a SEM micrograph of the resulting NNP and the corresponding histogram, respectively. It is seen that NNP form large agglomerates consisted of small spherical-shaped particles. It should be further noted that the ability of NNP to form agglomerates is beneficial for the intended application, i.e., purification of proteins from clarified or unclarified fermentation broth. As a matter of fact, it is much more difficult to separate dispersed nanoparticles from broth than to separate their larger counterparts [3]. The re-agglomeration of some nanoparticles when mixing is stopped can greatly facilitate the separation of particles from the suspension and, as a result, be beneficial to large-scale application without significant loss of binding surface area. From the SEM micrograph, the average NNP diameter was calculated to be 68 ± 28 nm; it was also found that 95.6% of the particles were in the range of 20-120 nm and 60.6% in the range of 40-80 nm. When comparing the measured diameter to the crystallite diameter

calculated from the XRD data it can be said that the NNP are constituted of several crystallites of 24.3 nm average size.

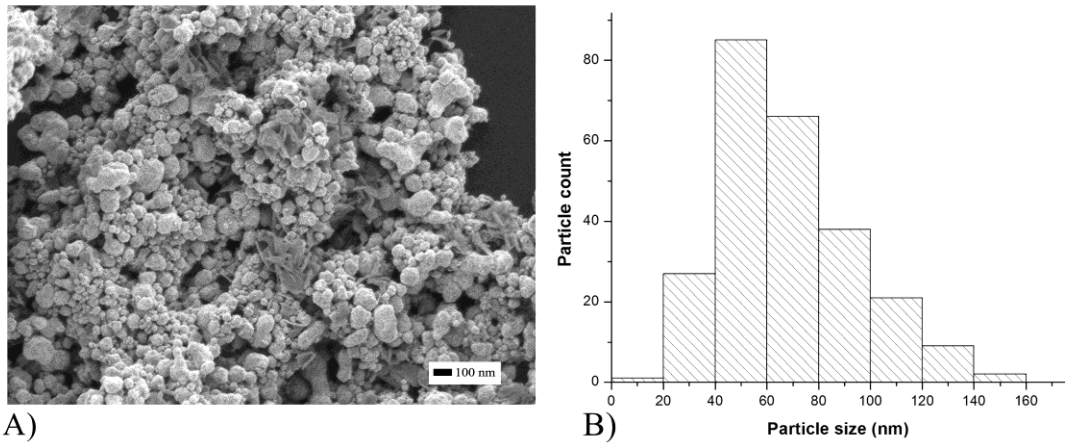

Figure 6-2: SEM of nickel nanoparticles at magnification of 40 000 (A) and nickel nanoparticles size distribution measured on 260 particles over two distinct areas of the sample (B). Average size of NNP was 68 ± 28 nm.

The magnetic behavior of the synthesized NNP was measured using superconducting quantum interference device (SQUID) magnetometer. The NNP were subjected to field dependent magnetization at 300 K. Figure 6-3A shows that a magnetization saturation of 39.3 emu g^{-1} at 20 000 Oe was reached rapidly. Figure 6-3B shows the weak ferromagnetic behavior of the NNP as indicated by the hysteresis loop between -1000 and 1000 Oe. This behavior is desired for a magnetic adsorbent [12]as high magnetization values enable fast and easy removal from solution and the low coercivity enables rapid dispersion of the NNP upon removal of the magnetic field. The magnetic properties of the NNP were also confirmed by visually observing that it took less than 5 s after applying a magnet to the suspension of NNP contained in a 2 mL micro-centrifuge tube to obtain a clear solution.

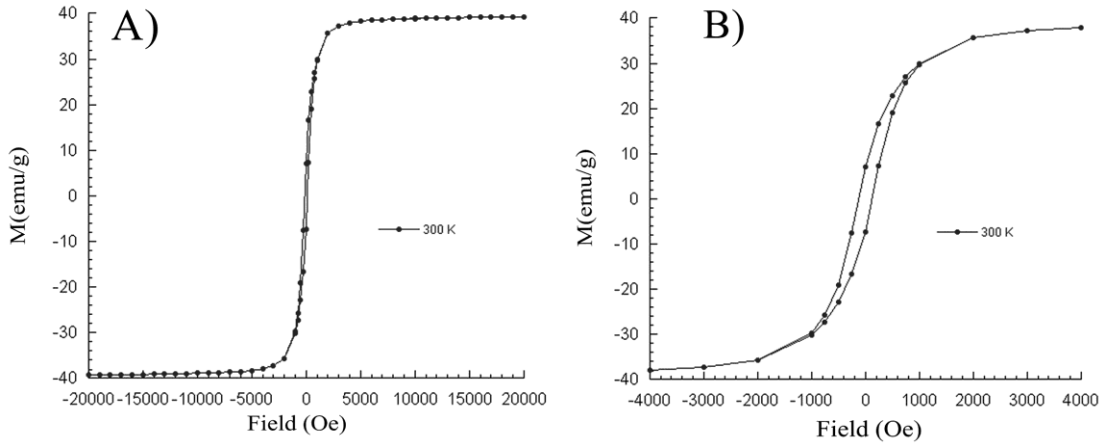

Figure 6-3: Field-dependent measurements (SQUID) for the nickel nanoparticles at 300 K from the field range of -20000 to 20000 Oe (A) and from -4000 to 4000 Oe to show the hysteresis loop (B).

6.4.2 Selective binding of the His-tagged ToxA5.1 by the NNP

In this study, the synthesized NNP were tested as magnetic affinity adsorbent for the purification of His6-tagged single domain antibody ToxA5.1 [14] from whole lysate of recombinant *E. coli* TG1 cells overexpressing the protein after clarification of the cell lysate (CCL) by centrifugation. Protein purification experiments were carried out using the pristine particles (the 1st cycle) as well as recycled particles, i.e., NNP after elution and regeneration. For each purification cycle, the NNP went through the following steps sequentially: 1) binding by mixing the NNP with CCL; 2) three washes using wash-bind buffer; and 3) elution using buffer containing 0.5 M imidazole. No special regeneration step was included in the experiments other than washing three times the used NNP with 1000 μL of the wash-bind buffer. Samples of the clarified cell lysate (CCL), unbound fraction (UBF), and the eluate were all subjected to SDS-PAGE gel analysis. As shown on the electrophoresis gel in Figure 6-4, lane 1 is the CCL sample and lanes 2-5 are the UBF samples from the 1st, 2nd, 3rd, and 4th purification cycles, respectively. Lanes 6-9 are

samples of eluates from the first to the fourth purification cycles. It is clear that the band representing ToxA5.1 (~16 kDa molecular weight) was absent from lanes 2 to 4 (the UBF samples of the 1st to 3rd purification cycle) and was very faint in lane 5 (the UBF sample of the fourth purification cycle), indicating that undetectable (lanes 2 to 4) or trace amount (lane 5) of ToxA5.1 were remaining in the UBF. Comparing the protein bands in lane 1 (CCL) to lanes 2 to 5 (UBF), it is clear that a lower number of protein was present in the UBF samples than that in the CCL sample, indicating that some of the native proteins present in the CCL were adsorbed on to the NNP and, therefore, absent from the UBF. This observation could be explained by binding of some native proteins with natural metal-binding motifs, e.g., proteins with histidine clusters or motifs rich in Glu, Asp, Tyr, Cys, Arg, Lys or Met [20] on their surfaces or proteins that bind to heterologously expressed His-tagged proteins [21] which in our study was ToxA5.1. Non-specific binding of native proteins to the NNP by mechanisms other than affinity interaction between the His-tag and the nickel ions could also occur. Possible non-specific binding mechanisms include weak physical forces such as van der Waals forces and hydrophobic interaction between proteins and the PVP layer surrounding the NNP.

Figure 6-4 also shows that only ToxA5.1 was detected in lanes 6 to 9, indicating that the eluates contained undetectable level of contaminating proteins. This seems to highlight the fact that the experimental washing procedure was sufficient to remove the loosely bound non-specific proteins and, therefore, this prevented them from contaminating the eluate. These results demonstrated that ToxA5.1 recovery from the clarified whole cell lysate using NNP was highly selective under the tested conditions.

It is worth mentioning that both binding of ToxA5.1 onto the NNP in the binding step and elution of proteins from the NNP occurred rapidly and that an equilibrium was established within 5 min in both cases (data not shown). The rapid binding and elution of NNP can be explained by the fact that 1) NNP are very small with an average diameter of 68 nm and 2) binding was limited to the surface of the particles. On the contrary, with conventional adsorbents such as ion changers, most binding sites are located inside the pores of the particles, requiring slow intra-porous diffusion for binding and elution.

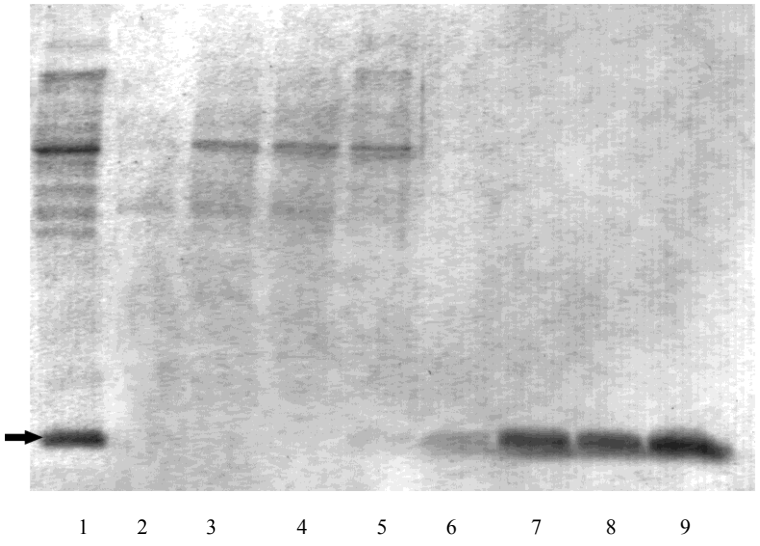

Figure 6-4: SDS-PAGE analysis of successive purification cycles of ToxA5.1 single domain antibody. Lane 1: clarified cell lysate arrow showing ToxA5.1 single domain antibody, Lanes 2-5:UBF of first, second, third, and fourth purification cycles using pristine or regenerated NNP, Lanes 6-9: eluates from the first to the fourth purification cycles.

To confirm the NNP-purified protein was the targeted His6-tagged ToxA5.1 and that the antibody still had the ability to bind to the target toxin, ELISA was performed. As shown in Figure 6-5 the ELISA binding data indicated that the purified protein were indeed active ToxA5.1 as they bound to the *C. difficile* toxin A coated on the plate. Furthermore, the binding curve of the NNP purified ToxA5.1 was very similar to the

control, which was obtained with ToxA5.1 purified using the commercial Novagen His Bind column (EMD Millipore, Billerica, MA) following the manufacturer's protocol. These results indicated that purification using NNP did not degrade nor affect the folding or functionality of ToxA5.1. If the purification scheme would have affected the integrity of ToxA5.1, the NNP purified curve would have been shifted to the right as a higher concentration of ToxA5.1 would have been needed to obtain the same absorbance reading as the control sample.

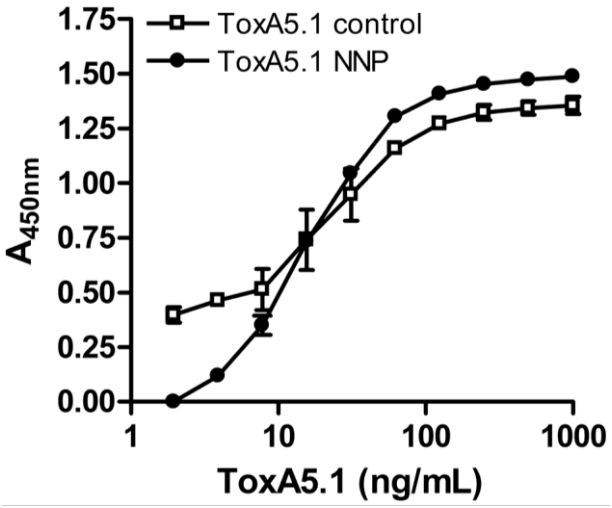

Figure 6-5: ELISA demonstrating NNP-purified ToxA5.1 retains its ability to bind *C. difficile* toxin A. Included in the ELISA was a control preparation of ToxA5.1 purified using a commercially available affinity resin.

The high selectivity displayed by the NNP to His6-tagged antibodies and the clear separation of the His6-tagged antibody using imidazole elutions indicated that specific metal chelation by the His-tag, which is analogous to IMAC, was probably at play on the surface or interstitial layers of the NNP. It is worth mentioning that in a previous study [22],

it was confirmed via surface characterization using Fourier transform infrared spectroscopy and X-ray photoelectron spectroscopy that the NNP synthesized by the modified polyol method possessed an external layer of NiO. It is hypothesized that the binding of the recombinant His6-tagged protein ToxA5.1 to the NNP can be attributed to the interaction of an electron donating group at the surface of the protein with metal, which is in our case the histidine tag and nickel, via coordination bonding as how it occurs in conventional IMAC [20, 23]

The observation that the NNP, which had a NiO surface layer, could selectively purify His-tagged ToxA5.1 is compatible with the results of Lee et al. [11], who used a different and more complex approach to synthesize Ni/NiO core/shell nanoparticles. The capacity of NiO surfaces to selectively bind His-tagged proteins was also demonstrated by Kim et al. [12], who used magnetic nanocomposite spheres decorated with NiO for selective purification of His-tagged GFP and by the work of Nam et al. [24], who developed bioreactive protein nanoarrays exploiting the selective binding of His-tagged proteins to nickel oxide surfaces formed by dip-pen nanolithography.

6.4.3 Reusability of the NNP

As shown in lanes 2 to 5 of Figure 6-4, the residual ToxA5.1 in UBF became noticeable only after the fourth purification cycle, indicating that the used NNP recovered from previous cycles were able to capture almost all the ToxA5.1 in the following cycles and that the loss of proteins to the UBF became observable only after three cycles. Given the fact that no optimized regeneration steps were involved in the adsorption/elution cycles, these results suggest that the NNP are reusable. The development of an optimized

regeneration step using specially designed regeneration buffer is underway, which is expected to further improve the reusability of the particles.

It is to be noted that the eluate from the first cycle using pristine NNP as shown in lane 6 of Figure 6-4 contained less target protein than the eluates from the subsequent purification cycles (i.e., the 2^{nd}-4^{th} cycles), which are shown in lanes 7 to 9 of Figure 6-4. The protein concentrations in eluates were 6 mg ToxA5.1/L for the first purification cycle and 18, 22, and 21 mg ToxA5.1/L for the 2^{nd}, 3^{rd}, and 4^{th} purification cycles, corresponding to recoveries of 14%, 41%, 50% and 48%, respectively. Since only undetectable levels of ToxA5.1 were left in the UBF after the binding step (lanes 2-5 in Figure 6-4) and the washing supernatant fluids (data not shown), it is reasonable to assume that most of the missing proteins remained on the NNP, which were not eluted using the elution buffer containing 0.5 M imidazole. This observation implies that the development of a more efficient elution procedure (e.g., elution in a column rather than in a stirred container), or a combination of the two, is necessary for better elution efficiency. It should also be noted that both adsorption and elution were carried out in well mixed test tubes. Therefore, results of the binding and elution steps reflect the distribution of protein between the adsorbent and the aqueous solution when equilibrium was established in the corresponding conditions. Using packed or fluidized columns for elution, which is a common practice in ion exchange and affinity absorption, is also expected to increase product recovery and NNP reusability.

6.5 Conclusion

In conclusion, we have demonstrated that nickel nanoparticles synthesized using a straightforward, modified polyol method could serve as a selective and effective magnetic adsorbent for the purification of a His6-tagged recombinant protein from clarified cell lysates. The results show that the NNP had an average diameter of 68 nm, exhibited ferromagnetic behavior, were highly selective to the His6-tagged proteins and were reusable without a significant loss in binding capacity. ELISA binding data also demonstrated that the purification scheme utilizing the NNP did not cause any degradation, unfolding or loss of activity of the target protein ToxA5.1. Studies are underway to improve the efficiency and reusability of processes employing such particles.

6.6 Acknowledgements

The authors wish to thank Dr. Yun Liu for the SEM pictures, Dr. Tara Kell for the XRD scan and Dr. Muralee Murugesu's laboratory for the SQUID measurements. Financial support from the Natural Science and Engineering Council of Canada (NSERC) and The Canada Foundation of Innovation (CFI) is gratefully acknowledged.

6.7 References

1. Langer, E. and Ranck, J. Capacity bottleneck squeezed by downstream processes. *BioProcess Int* **4**, 14-18 (2006).

2. Low, D., O'Leary, R. and Pujar, N.S. Future of antibody purification. *Journal of Chromatography B: Analytical Technologies in the Biomedical and Life Sciences* **848**, 48-63 (2007).

3. Franzreb, M., Siemann-Herzberg, M., Hobley, T.J. and Thomas, O.R.T. Protein purification using magnetic adsorbent particles. *Applied Microbiology and Biotechnology* **70**, 505-516 (2006).

4. Horák, D., Babič, M., Macková, H. and Beneš, M.J. Preparation and properties of magnetic nano- and microsized particles for biological and environmental separations. *Journal of Separation Science* **30**, 1751-1772 (2007).

5. Ai, F., Yao, A., Huang, W., Wang, D. and Zhang, X. Synthesis of PVP-protected NiPd nanoalloys by modified polyol process and their magnetic properties. *Physica E: Low-Dimensional Systems and Nanostructures* **42**, 1281-1286 (2010).

6. Couto, G.G., Klein, J.J., Schreiner, W.H., Mosca, D.H., de Oliveira, A.J.A. and Zarbin, A.J.G. Nickel nanoparticles obtained by a modified polyol process: Synthesis, characterization, and magnetic properties. *Journal of Colloid and Interface Science* **311**, 461-468 (2007).

7. Zhang, H., Ding, J., Chow, G., Ran, M. and Yi, J. Engineering magnetic properties of Ni nanoparticles by non-magnetic cores. *Chemistry of Materials* **21**, 5222-5228 (2009).

8. Porath, J. and Olin, B. Immobilized metal ion affinity adsorption and immobilized metal ion affinity chromatography of biomaterials. Serum protein affinities for gel-immobilized iron and nickel ions. *Biochemistry* **22**, 1621-1630 (1983).

9. Porath, J. Immobilized metal ion affinity chromatography. *Protein Expression and Purification* **3**, 263-281 (1992).

10. Carroll, K.J., Reveles, J.U., Shultz, M.D., Khanna, S.N. and Carpenter, E.E. Preparation of elemental Cu and Ni nanoparticles by the polyol method: An experimental and theoretical approach. *Journal of Physical Chemistry C* **115**, 2656-2664 (2011).

11. Lee, I.S., Lee, N., Park, J., Kim, B.H., Yi, Y.W., Kim, T., Kim, T.K., Lee, I.H., Paik, S.R. and Hyeon, T. Ni/NiO core/shell nanoparticles for selective binding and magnetic separation of histidine-tagged proteins. *Journal of the American Chemical Society* **128**, 10658-10659 (2006).

12. Kim, J., Piao, Y., Lee, N., Park, Y.I., Lee, I.H., Lee, J.H., Paik, S.R. and Hyeon, T. Magnetic nanocomposite spheres decorated with NiO nanoparticles for a magnetically recyclable protein separation system. *Advanced Materials* **22**, 57-60 (2010).

13. Bai, L., Fan, J., Cao, Y., Yuan, F., Zuo, A. and Tang, Q. Shape-controlled synthesis of Ni particles via polyol reduction. *Journal of Crystal Growth* **311**, 2474-2479 (2009).

14. Hussack, G., Arbabi-Ghahroudi, M., Van Faassen, H., Songer, J.G., Ng, K.K.S., MacKenzie, R. and Tanha, J. Neutralization of *Clostridium difficile* toxin A with single-domain antibodies targeting the cell receptor binding domain. *Journal of Biological Chemistry* **286**, 8961-8976 (2011).

15. Abràmoff, M.D., Magalhães, P.J. and Ram, S.J. Image processing with imageJ. *Biophotonics International* **11**, 36-41 (2004).

16. Laemmli, U.K. Cleavage of structural proteins during the assembly of the head of bacteriophage T4. *Nature* **227**, 680-685 (1970).

17. Cullity, B.D. Elements of X-Ray Diffraction, Edn. 3rd. (Addison-Wesley publishing Co., Reading, MA; 1956).

18. Chou, K.S. and Huang, K.C. Studies on the chemical synthesis of nanosized nickel powder and its stability. *Journal of Nanoparticle Research* **3**, 127-132 (2001).

19. West, A.R. Solid state chemistry and its applications (Wiley, New York; 1984).

20. Gaberc-Porekar, V. and Menart, V. Perspectives of immobilized-metal affinity chromatography. *Journal of Biochemical and Biophysical Methods* **49**, 335-360 (2001).

21. Block, H., Maertens, B., Spriestersbach, A., Brinker, N., Kubicek, J., Fabis, R., Labahn, J. and Schäfer, F. in *Methods in Enzymology* **463,** 439-473 (2009).

22. Baranova, E.A., Cally, A., Allagui, A., Ntais, S. and Wüthrich, R. Nickel particles with increased catalytic activity towards hydrogen evolution reaction. *Comptes Rendus Chimie* **16**, 28-33 (2013).

23. Chen, C.W., Liu, H.L., Lin, J.C. and Ho, Y. Molecular dynamics simulations of metal ion binding to the His-tag motif. *Journal of the Chinese Chemical Society* **52**, 1281-1290 (2005).

24. Nam, J.M., Han, S.W., Lee, K.B., Liu, X., Ratner, M.A. and Mirkin, C.A. Bioactive protein nanoarrays on nickel oxide surfaces formed by dip-pen nanolithography. *Angewandte Chemie - International Edition* **43**, 1246-1249 (2004).

Chapter 7: Effect of polyvinylpyrrolidone:nickel ratio on properties and performance of nickel nanoparticles for purification of histidine-tagged recombinant protein (ToxA5.1)

Albert Parisien, Aatika Ahmed, Jules Thibault, and Christopher Q. Lan[1]*

[1] Chemical and Biological Engineering Department, University of Ottawa, ON, Canada; K1N 6N5

*Corresponding author: Christopher Q. Lan, Christopher.Lan@uottawa.ca

7.1 Abstract

Nickel nanoparticles (NNP) synthesized via a modified polyol method using a solution containing ethylene glycol as a reducing agent, palladium chloride as a nucleating agent (1% atomic ratio with nickel), and polyvinylpyrrolidone (PVP) as a protective agent at 1:0, 1:0.5, 1:1 and 1:5 mass ratio (Ni:PVP) were investigated as possible magnetic adsorbents for the purification of a hexahistidine (His6-tagged) recombinant protein. The synthesis yielded particles having average diameters of 131 ± 80 nm, 69 ± 28 nm, 54 ±15 nm and 47 ± 20 nm for the solutions initially containing mass ratios of 1:0, 1:0.5, 1:1 and 1:5 Ni:PVP, respectively. XRD profiles confirmed the presence of nickel nanoparticles as well as the presence of a residual amount of unreacted $Ni(OH)_2$. The nanoparticles exhibited a strong magnetic behavior and were suited for (His6) recombinant protein purification. Results showed that these four types of nickel nanoparticles were highly selective and were used for five adsorption cycles following simple regeneration steps with only minor binding efficiency losses. These particles have shown great potential for His6-taggedtagged protein purification as they are easily synthesized, cost-effective, and highly selective magnetic adsorbents.

Keywords: Modified Polyol method, Magnetic Adsorbent, His6-tagged recombinant protein, Nickel nanoparticles

7.2 Introduction

Magnetic separation and purification of organic compounds, proteins, nucleic acids and cells from complex reaction mixtures are becoming more popular for large scale production in bioindustrial purification and extraction processes [1]. Nickel, which is one of the preferred metal in immobilized metal ion affinity chromatography (IMAC) purification[2, 3] for His6-tagged protein purification, has been shown to possess magnetic properties[4-7]. Furthermore, nickel nanoparticles synthesized using a modified polyol method[4, 8] have been shown to be a suitable magnetic adsorbent with high specificity for the purification of the His6-tagged ToxA5.1 protein[9]. In the modified polyol method for the synthesis of nanoparticles, polyvinylpyrrolidone (PVP) is used as a protective agent to control the growth rate of the nickel nanoparticles as well as to minimize agglomeration of the particles. To this effect, PVP was investigated by several researchers [4-6, 10, 11] and was used in our studies to help control the size and agglomeration of the nickel nanoparticles in order to increase the surface area available for His6-taggedprotein binding. In this paper, we report on the effect of different nickel-to-PVP ratios (1:0, 1:0.5 ,1:1 and 1:5) on the morphology, size distribution and performance of nickel nanoparticles (NNP) for the purification of ToxA5.1, a His6-tagged recombinant protein which targets and neutralizes *Clostridium difficile* enterotoxin A [12].

7.3 Material and Methods

7.3.1 Cell growth and protein expression

Escherichia coli TG1 bearing the plasmid for ToxA5.1 expression gene [12] was grown on agar plates containing 20 g/L LB Lennox (Fisher Scientific, Pittsburgh, PA) and 100 mM ampicillin (Fisher Scientific) and used to inoculate sterile modified LB medium consisted in 20

g/L LB Lennox broth (Fisher Scientific), 6 g/L enzymatic tryptone (Fluka, St. Louis, MO), 5 g/L yeast extract (Oxoid, Lenexa, KS), and 100 mM ampicillin in a shaker flask at 37ºC and 200 rpm for 18 h. The culture was then used to inoculate fresh cultures in identical medium. Once the OD_{600} of the culture reached 0.6, it was induced for protein expression using 2 mM isopropyl β-D-1-thiogalactopyranoside (Promega, Madison, WI) at 37ºC and 200 rpm for 18 h. Bacterial lysis was performed using the Promega Fastbreak lysis system (Madison, WI) following the protocol provided by the manufacturer. The bacterial lysate was centrifuged at 3280 rcf for 20 minutes at 20°C. The cleared lysate was used for the purification experiment.

7.3.2 Synthesis of nickel nanoparticles (NNP)

The nickel nanoparticles were synthesized using a modified polyol method[4, 8] by mixing 0.4 g $Ni(OH)_2$ (Acros Organics, Fisher Scientific, Pittsburgh, PA) and appropriate amounts of polyvinylpyrrolidone (PVP) (Fisher Scientific) to get Ni:PVP w/w ratios of 1:0.5, 1:1, and 1:5 in 160 mL ethylene glycol (EG) (Fisher Scientific) in a 1-L three-neck boiling flask on a stirrer plate for 30 min, followed by refluxing in a heated oil bath. Synthesis without PVP was performed in the same manner as the previous syntheses. $PdCl_2$ catalyst solution (Sigma Aldrich, St. Louis, MO) was prepared by mixing vigorously on a stirrer plate for 45 min 0.0076 g $PdCl_2$ in 40 mL ethylene glycol. Once the oil bath reached 190ºC, all of the $PdCl_2$ solution was added to the boiling flask. Upon injection of the catalyst solution, the initial colloidal solution of $Ni(OH)_2$ changed color rapidly to become black within 15 min. This color change was observed in all of the syntheses. After 2 h of refluxing, the suspension was left to cool at room temperature and a magnet was applied to the suspension for 1 min to cause the particles to aggregate. The residue solvent (i.e., the supernatant fluid) was discarded to an organic waste container. The

boiling flask was then washed with 99% ethanol to recover the synthesized particles. The ethanol-nickel particle suspension was centrifuged at 1150 rcf in a bench top centrifuge (Hermle, Madison, NJ) for 10 min. The same magnet was applied to the centrifuge tube to induce particle aggregation, after which the ethanol was removed. Two additional washes were performed using 25 mL of 99% ethanol each. The rinsed particles were then suspended in 10 mL of 99% ethanol and stored at room temperature. The resulting NNP from Ni:PVP 1:0, 1:0.5, 1:1, and 1:5 will be referred to as 0 PVP, 0.5 PVP, 1 PVP and 5 PVP for the remainder of the text.

7.3.3 Protein purification

For the purification experiments, 500 µL of the 10 mL NNP and ethanol suspension was added to a 2-mL micro-centrifuge tube. The tube was inserted in a Promega magnet stand for 1 min. The ethanol was removed using a pipette and the NNP were suspended in 300 µL of wash-bind buffer (100 mM HEPES and 10 mM imidazole, pH 7.5) by quick vortexing and sonication (Fisher Scientific ultrasonic cleaner, model FS140, 135 w 42 kHz ± 6%) for 10 s to ensure dispersion prior to the binding step. After dispersion, 300 µL of cleared bacterial lysate was added to the centrifuge tube containing the NNP. To ensure proper binding, the tube was placed on a platform rocker for 2 min. The tube was then inserted in the magnetic holder and the supernatant fluid was removed and kept at 4°C for further analysis. This fraction will be referred to as the unbound fraction (UBF) from now on. The tube was removed from the magnet and the NNP were suspended in 150 µL of wash-bind buffer and hand-mixed for 10 s. The tube was inserted in the magnetic holder for 2 min and the supernatant fluid was removed and discarded. This washing step was repeated once more for a total of two washes. After the second wash, the NNP were suspended in 100 µL of elution buffer (100 mM HEPES and 1.5 M imidazole, pH

7.5), sonicated for 10 s and put on a rocker platform for 2 min. The tube was inserted in the magnet stand for 30 s and the supernatant fluid containing the recombinant protein was kept at 4°C for analysis. This fraction will be referred to as the eluate from now on. Each replicate of NNP was then regenerated by three successive washes using 600 µL of wash-bind buffer each time. This completed the first purification cycle with pristine NNP. The same procedures were repeated on four other cleared lysate samples for a total of five binding cycles with the same NNP and, every time, the starting material was the cleared lysate obtained after overnight expression.

The UBF contained the protein that did not bind to NNP and thus, it included most of the native proteins as well as a small amount of our specific recombinant His6-tagged protein (ToxA5.1) that did not bind to the given amount of NNP. On the other hand, the eluate represented the sample which contained proteins that specifically bounded to the nickel nanoparticles.

7.3.4 Protein quantification

For sample analysis, UBF samples of appropriate dilutions were loaded on 4-15% discontinuous SDS-PAGE gels [13] along with the initial clarified cell lysate and purified and quantified ToxA5.1 serving as standard for protein quantification. Gels were run at 180 V for 50 min. Proteins were stained using Fermentas PageBlue Protein Staining Solution (Glen Burnie, MD) fast procedure as per manufacturer's recommendations. Quantification of scanned gels was achieved via densitometry using ImageJ software [14].

7.3.5 Characterization of nanoparticles

The atomic structure of the nickel nanoparticles was determined using X-ray diffraction (XRD), which was performed on the synthesized nickel nanoparticles using an Ultima IV powder XRD (Rigaku, The Woodlands, TX) with a copper source from 20 to 60 degrees. To prepare the samples for scanning, the NNP suspension was dispersed by vortexing and 15 µL of sample was placed on a holder. Ethanol was allowed to evaporate before scanning.

7.3.6 Morphology and size distribution of the nickel nanoparticles

Scanning electron microscopy (SEM) was performed on the synthesized nickel nanoparticles using a JSM-7500F FESEM (JEOL, Peabody, MA) instrument. To prepare the sample, 500 µL of the particles suspended in ethanol was sonicated for 5 minutes to break up large aggregates and a drop of the suspension was transferred immediately onto a carbon-coated copper grid. Average size and size distribution of the particles were calculated using ImageJ software [14] based on the measurement of 147, 253, 174, and 414 particles for 1:0, 1:0.5, 1:1 and 1:5 Ni:PVP mass ratio, respectively, and distributed over 2 different areas of each sample (2 different images per sample).

7.3.7 Calculations of ToxA5.1 recovery and binding capacities

The quantity of ToxA5.1 adsorbed per unit amount of NNP (q_n in mg/g Ni) at the n^{th} separation cycle was calculated using Equation 1:

$$q_n = \frac{\left(V_{bm} \times C_{bm}\right) - \left(V_{UBF} \times C_{UBF}\right)}{M_p} \qquad (1)$$

where V_{bm} is the volume of binding mixture (L), C_{bm} the concentration of ToxA5.1 in the initial binding mixture (mg/L), V_{UBF} the volume of the unbounded fraction (L), C_{UBF} the concentration of ToxA5.1 in the unbounded fraction (mg/L), M_p the mass of nickel nanoparticles (NNP) expressed as g of Ni.

Specific binding was calculated using Equation 2:

$$\text{Specific binding} = \frac{\left(V_{bm} \times C_{bm}\right)_{\text{before binding}} - \left(V_{bm} \times C_{bm}\right)_{\text{after binding}}}{\left(V_{bm} \times C_{bm}\right)_{\text{before binding}}} \times 100 \quad (2)$$

Protein recovery was calculated using Equation 3:

$$\text{Recovery} = \frac{V_e \times C_e}{V_{bm} \times C_{bm}} \times 100 \quad (3)$$

where V_e is the volume of the eluate fraction (L) and C_e the concentration of ToxA5.1 in the eluate fraction (mg/L).

From the size distribution and the frequency of each particle diameter, the total volume in m^3 for these 100 particles was calculated using Equation 4. Using the density of bulk nickel and the volume, the number of particles per kg of NNP calculated as shown in Equation 5:

$$\text{Volume of 100 particles} = \sum_{i=1}^{100} \frac{4}{3} \pi \left(\frac{D_i}{2}\right)^3 \quad (4)$$

$$\frac{\text{Number of particles}}{\text{kg of NNP}} = \frac{100}{\rho_{Ni} \times \text{Volume of 100 particles}} \quad (5)$$

Where D_i is the diameter (m) and ρ_{Ni} is the density of bulk nickel in kg/m^3.

The surface area per unit mass for each type of NNP was calculated using Equation 6

$$\text{Surface area per unit mass} = \frac{\sum_{i=1}^{100} 4\pi\left(\frac{D_i}{2}\right)^2}{\left(\sum_{i=1}^{100} \frac{4}{3}\pi\left(\frac{D_i}{2}\right)^3\right) \times \rho_{Ni}} \qquad (6)$$

7.4 Results

7.4.1 The surface structure of NNP

The surface structure of the resulting NNP was confirmed by XRD as shown in Figure 7-1. The diffraction lines of (1 1 1) and (2 0 0) planes from the XRD profile confirmed that nickel nanoparticles with the face-centered cubic (fcc) structure[15] were obtained for all of the tested Ni:PVP syntheses. The XRD patterns also show the presence of a $Ni(OH)_2$ phase with characteristic diffraction peaks at 33º and 38.5º 2θ corresponding to (1 0 0) and (1 0 1) crystalline planes[15], indicating incompleteness of the reduction reaction in EG for all of the four syntheses. Using the full-width at half maximum of Ni (111) reflection and Scherrer formula[16], the crystallite size of Ni was calculated for the resulting four syntheses to be 30.1, 24.3, 25.9, and 21.8 nm, respectively, as shown in Table 7-1. When comparing the diameters measured from the SEM micrographs in Figure 7-2 to the crystallite diameters calculated from the XRD data, it can be said that the resulting NNP are constituted of several crystallites.

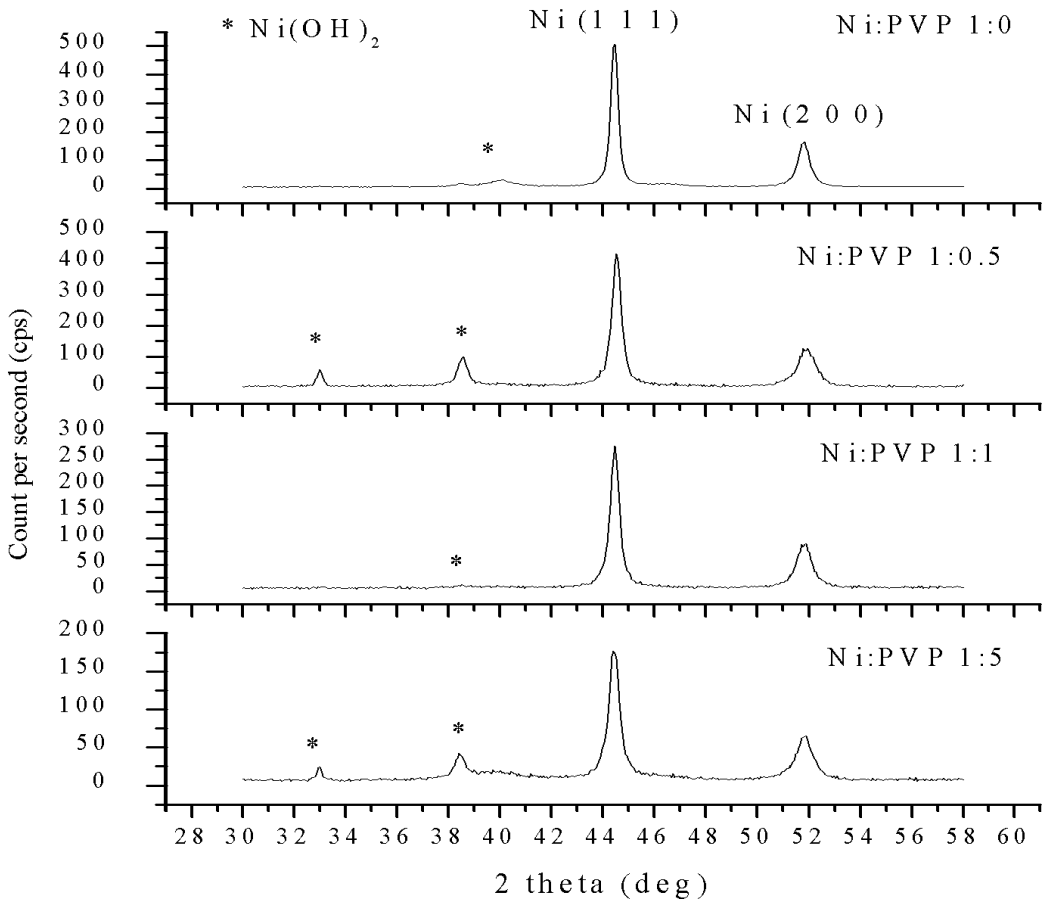

Figure 7-1: XRD pattern of NNP synthesized from $Ni(OH)_2$, 1% atomic Ni:Pd and different w/w Ni:PVP ratio of 1:0, 1:0.5, 1:1, and 1:5 in ethylene glycol under reflux at 190°C for 2h.

Table 7-1 : Physical properties of synthesized nickel nanoparticles.

Ni:PVP	Crystallite Size* nm	Measured diameter nm	Surface area m^2/ kg	N Particles/kg x 10^{-17}
1:0	30.1	131 ± 80	2 737	0.35
1:0.5	24.3	69 ± 28	6 990	3.55
1:1	25.9	54 ± 15	10 004	8.35
1:5	21.8	47 ± 20	9 755	9.79

*Crystallite sizes calculated using the Scherrer formula from XRD data and average diameter calculated using the arithmetic average of measured particles from SEM micrographs. Surface area and number of particles were calculated from SEM measurements.

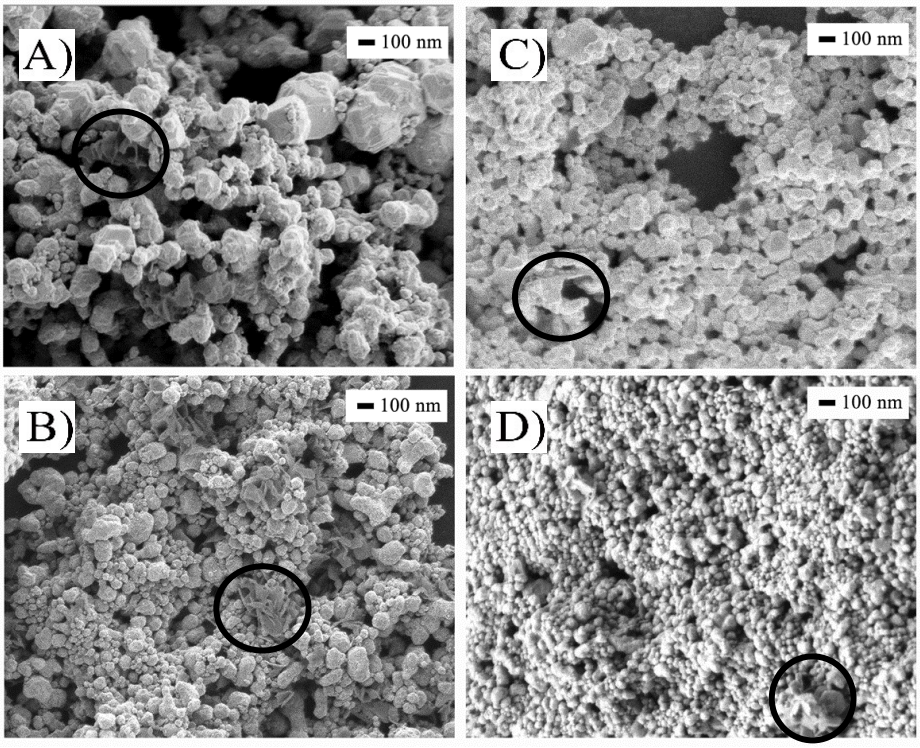

Figure 7-2: SEM of nickel nanoparticles (1% atomic Ni:Pd) in ethylene glycol under reflux for 2h. (A) 1:0 w/w Ni:PVP (B) 1% atomic Ni:Pd, 1:0.5 w/w Ni:PVP (C) 1% atomic Ni:Pd, 1:1 w/w Ni:PVP (D) 1% atomic Ni:Pd, 1: 5 w/w Ni:PVP .

7.4.2 NNP morphology and size distribution

Figure 7-2 shows SEM micrographs of the nickel nanoparticles synthesized using various concentrations of PVP. It is to be noted that, as illustrated in Figure 7-2, all of the samples observed under SEM contained sheath-like structures as indicated by circles, which are suspected to be unreacted $Ni(OH)_2$ [17]. However, the NNP are predominantly globular-shaped particles. The size and shape of these agglomerates varied among NNP with different nickel-to-PVP ratios. The 0 PVP NNP formed the largest particles as shown in Figure 7-2A. As shown on Figure 7-3, these NNP had an average diameter of 131 ± 80 nm, with some particles as large as 600 nm, calculated from measurements taken from 147 individual particles over two different

images for each synthesis. Furthermore, on Figure 7-3 it can be seen that these NNP had a broad size distribution when compared to the NNP obtained with the other NNP synthesized using nickel-to-PVP ratios of 0.5:1, 1:1, and 1:5, respectively. The 0.5 PVP NNP formed moderate sized particles as shown in Figure 7-2B, with an average particle diameter of 69 ± 28 nm calculated from measures taken from 253 individual particles over two different images of the sample. Figure 7-3 shows that these NNP had smaller size distributions than the NNP containing 0 PVP. The 1 PVP NNP formed even smaller particles as shown Figure 7-2C. These NNP were also more evenly distributed in size compared to 0 PVP and 0.5 PVP NNP with an average diameter of 54 ±15 nm calculated from measures taken from 174 individual particles over two different images of the sample. From Figure 7-3 it can be seen that the 5 PVP NNP had the smallest average diameter of 47 ± 20 nm calculated from measures taken from 414 individual particles over two different images of the sample. From the distributions of each NNP synthesis, a surface area per kg of NNP was calculated. As shown in Table 7-1, the surface area per unit mass of particles increased with decreasing NNP diameter for the 0 and 0.5 PVP NNP. Although the average diameter of the 1 PVP NNP was smaller than that of the 5 PVP, it possessed a larger surface area. For each synthesis, the surface area was calculated to be 2 737, 6 990, 10 004, and 9 755 m^2/kg for 0 PVP, 0.5 PVP, 1 PVP, and 5 PVP NNP, respectively. As expected, the number of particles per kg of NNP was inversely proportional to the particle diameter as shown in Table 7-1 where 1 kg of the 0 PVP NNP would contain 0.349×10^{17} particles while 1 kg of the 5 PVP NNP would contain 9.79×10^{17} particles.

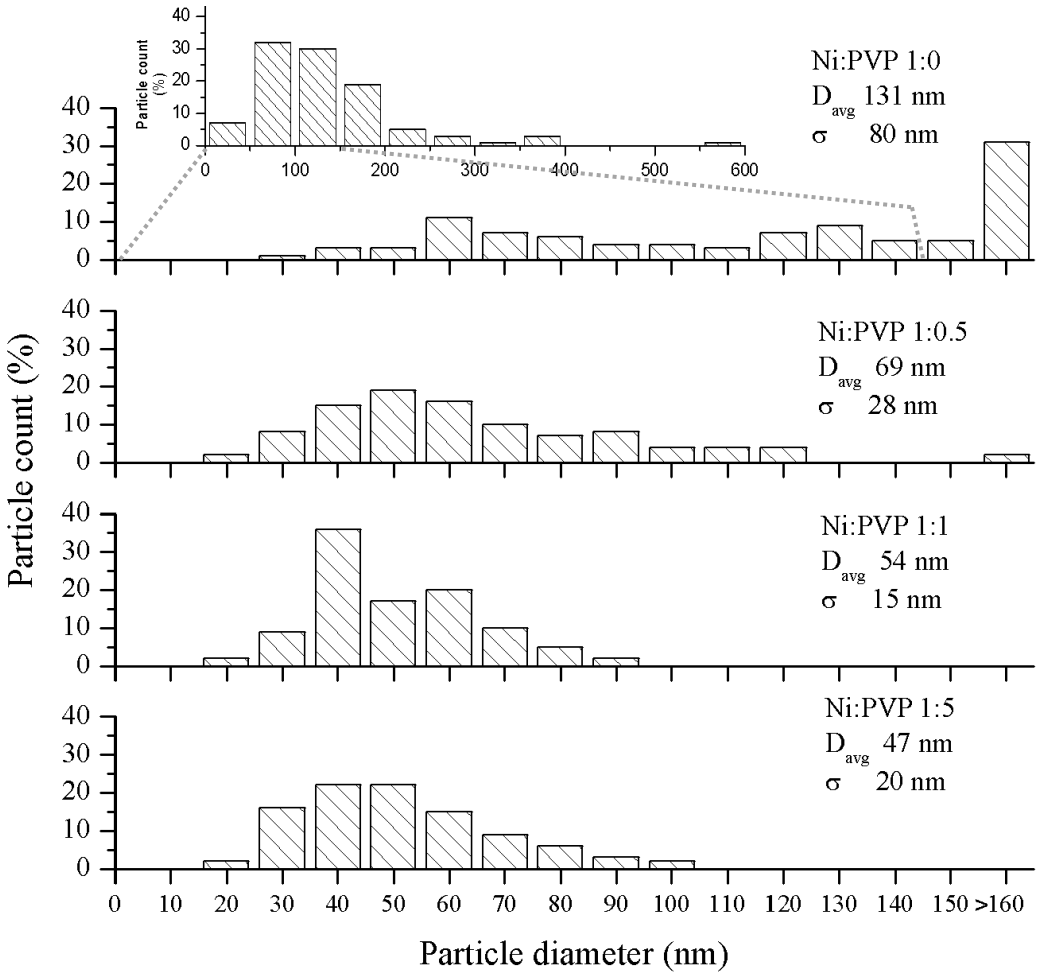

Figure 7-3: Particle size distribution for NNP synthesized via a modified polyol using various Ni:PVP mass ratio.

7.4.3 Protein purification

The SDS-Page electrophoresis gels shown on Figure 7-4 confirmed that all of the NNP synthesized were able to selectively purify the target protein, i.e., ToxA5.1 His6-tagged protein. As can be seen from Figure 7-4, the target protein (indicated by the arrow) that was present in the initial clarified lysate (Lane 1) was absent or very faint in the UBF of the first binding cycle using pristine NNP (Lane 2). The band became darker progressively in Lanes 3-6, which stand for the UBF of the four successive regeneration cycles. The target protein can be seen in Lanes 7-11. It to note that when PVP is used in the synthesis (Figure 7-4B, C and D in the boxes) the

eluates seem to contain a high molecular weight protein that gets co-purified with the target protein.

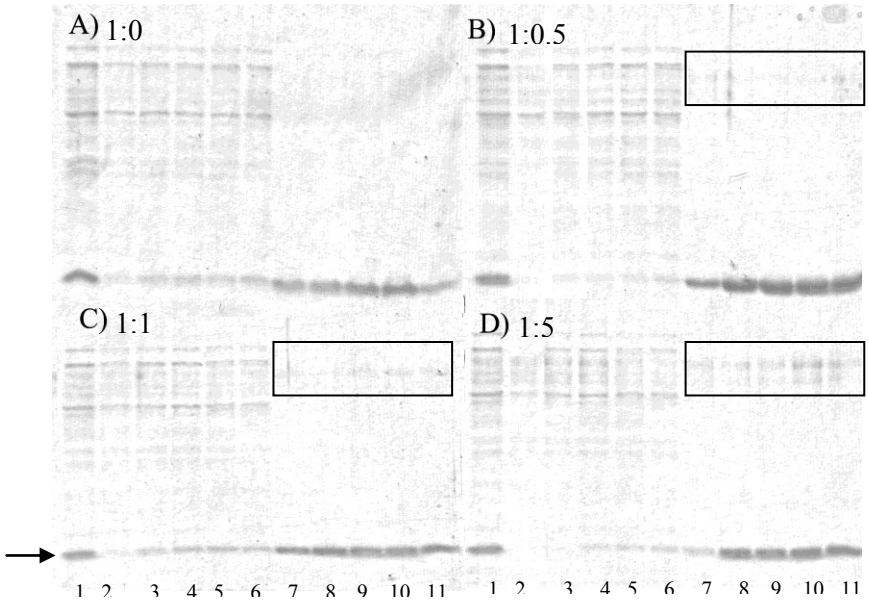

Figure 7-4: SDS-PAGE gels of the unbounded fraction (UBF) and eluate obtained from the purification of ToxA5.1 using various Ni:PVP w/w ratio nickel nanoparticles (NNP): A) 1:0, B) 1:0.5, C) 1:1, and D) 1:5. Lane 1 is the initial cleared lysate containing ToxA5.1 protein (indicated by the arrow). Lanes 2-6 are the UBF following binding using pristine NNP, then NNP regenerated for the 1st, 2nd, 3rd, and 4th time. Lanes 7-11 are the eluate of the pristine NNP, then NNP regenerated for the 1st, 2nd, 3rd, and 4th time.

The concentration of ToxA5.1 from UBF of each regeneration cycle normalized with respect to the amount of NNP used can be seen on Figure 7-5. Consistent with Figure 7-4, 0.5 PVP NNP contained the least amount of ToxA5.1 in the UBF while 0 PVP NNP bounded the least amount of ToxA5.1. It can be noted that after the second cycle, the 0.5, 1, and 5 PVP sample tended towards equilibrium as the amount of ToxA5.1 in the UBF seemed to reach a plateau while the 0 PVP sample had a lower concentration in the UBF after the fourth binding.

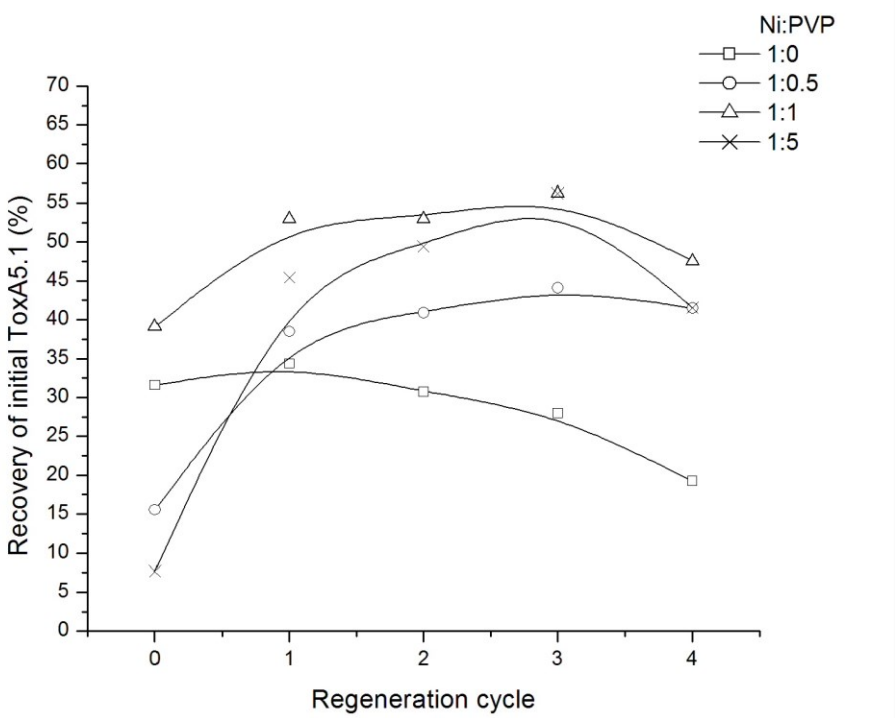

Figure 7-5: Concentration of ToxA5.1 in the unbounded fraction following regeneration cycles.

As seen on Figure 7-6, the amount of ToxA5.1 that was bound to the NNP after the initial binding step varied from 13.4 for the 0 PVP NNP to 14.9 mg ToxA5.1/ g of Ni for the 5 PVP NNP. Figure 7-6 also shows that the amount of ToxA5.1 binding to the NNP tends towards equilibrium as indicated by the plateaus of proteins calculated to be on the NNP. It is to be noted that discrepancies in the material balance around the NNP and ToxA5.1 exists as the material balance suggest that the NNP could accumulate more than 67 mg ToxA5.1 / g of NNP over the course of the five purification cycles (data not shown). It is hypothesized that the un-accounted protein could have been removed by the multiple washes and regeneration cycles even though no ToxA5.1 protein could be detected in these samples. Even at below than detectable level, the amount of ToxA5.1 present in the large volumes of wash and regeneration buffers would still amount to a significant quantity.

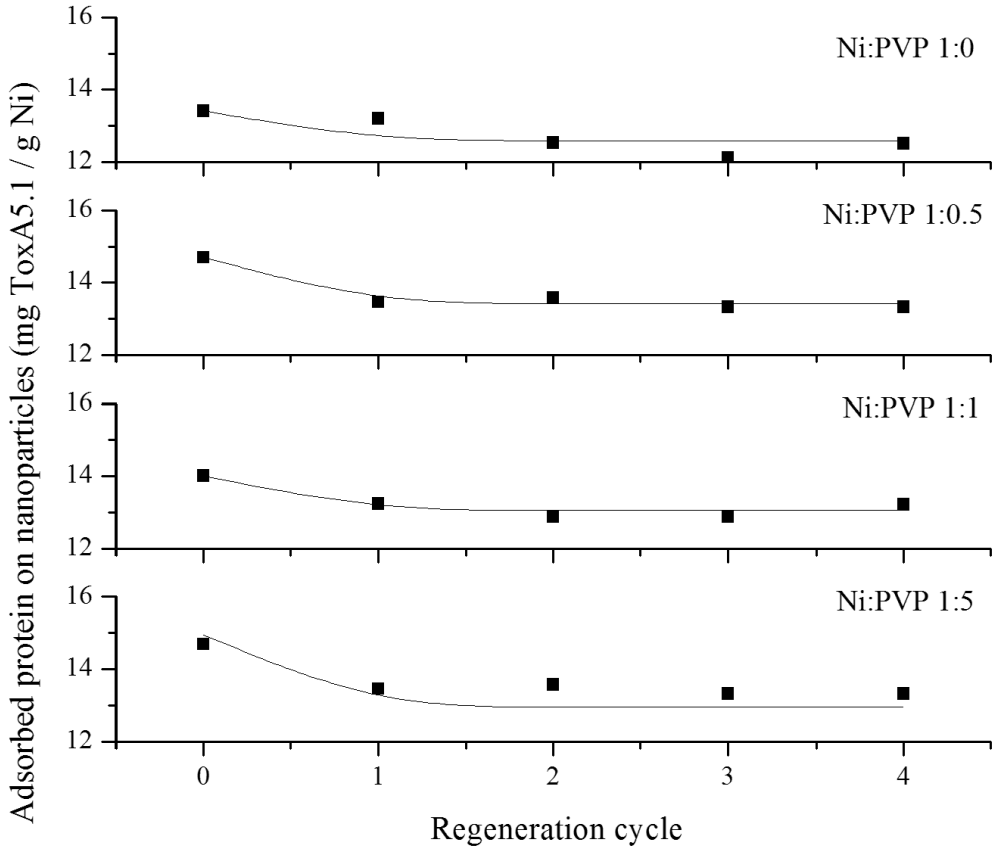

Figure 7-6: ToxA5.1 bounded on nickel nanoparticles following regeneration cycles.

From Figure 7-7 it can be seen that the concentration of ToxA5.1 in the eluates after the first regeneration cycle reached a plateau for a given set of NNP with 0.10, 0.24, 0.15, 0.21 mg ToxA5.1 / mL of eluate for 0, 0.5, 1, and 5 PVP NNP, respectively. It is interesting to note that, for the 0.5 and 5 PVP NNP, the first elution, using pristine NNP, seemed to yield a lower concentration of ToxA5.1. Nevertheless, after the first regeneration, the concentrations for the subsequent elutions were fairly constant. Recovery values of ToxA5.1 initially present in the binding mixture for the various NNP can be found in Table 7-2. It can be seen that average recovery for pristine NNP was, on average, 5% between all of the NNP which was lower than the subsequent cycles. The highest recovery was achieved with the 0.5 PVP NNP with an

average of 12.7% for the 4 regeneration cycles i.e. not considering the first cycle with pristine NNP while average recoveries of 5.1, 7.7, and 10.5% were achieved with the 0, 1, and 5 PVP NNP, respectively. Interestingly, specific bindings were quite high for all of the NNP with an average of 87.5, 99.4, 92.9, 95.2% for 0, 0.5, 1, and 5 PVP NNP, respectively, as can be seen in Table 7-2, with the highest specific binding achieved with the 0.5 PVP NNP while 0 PVP NNP yielded the lowest specific binding.

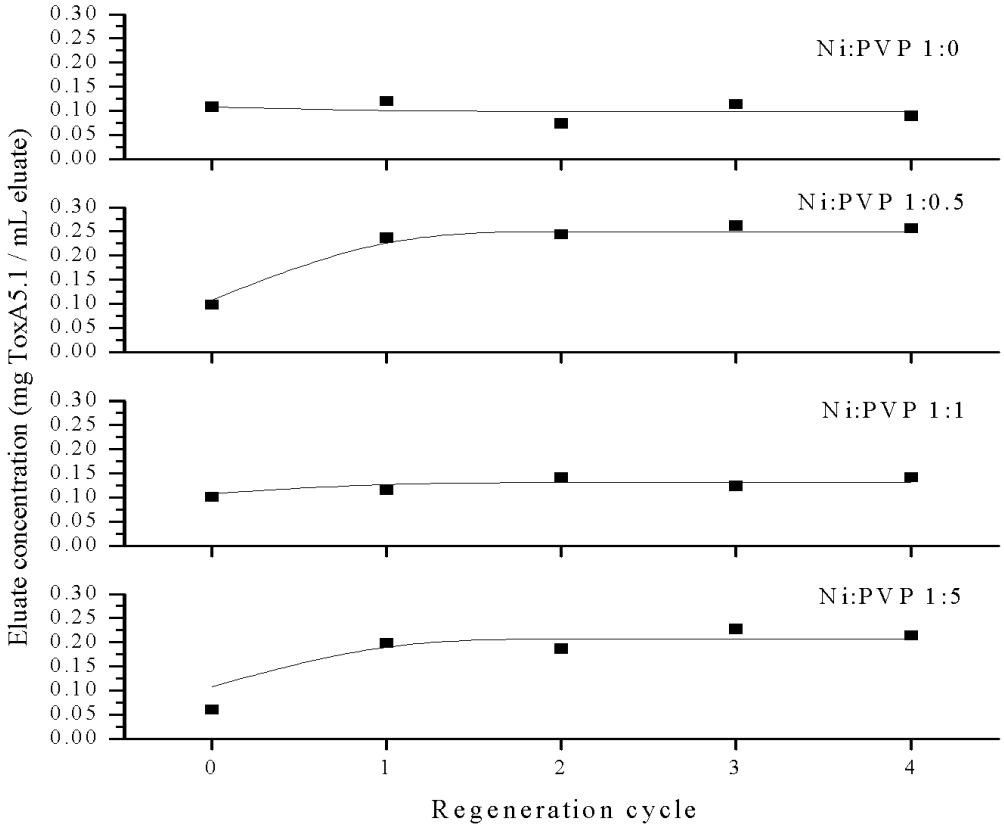

Figure 7-7: Eluate concentrations of various Ni:PVP w/w ratio nickel nanoparticles protein recovery products.

Table 7-2: Recovery of the initially present ToxA5.1 using various nickel nanoparticles.

Regeneration cycle	Ni:PVP w/w ratio							
	1:0		1:0.5		1:1		1:5	
	Specific Binding %	Recovery %	Specific Binding %	Recovery %	Specific Binding %	Recovery %	Specific Binding %	Recovery %
0	92 .1	5 .5	99 .8	5 .0	96 .4	6 .0	99 .6	3 .1
1	91 .3	6 .1	99 .0	12 .1	92 .3	6 .8	98 .4	10 .1
2	84 .7	3 .8	100 .0	12 .4	91 .6	8 .4	93 .7	9 .5
3	84 .0	5 .8	99 .3	13 .4	90 .4	7 .3	92 .4	11 .6
4	85 .3	4 .6	99 .1	13 .1	93 .8	8 .4	92 .2	10 .9

7.5 Discussion

7.5.1 Synthesis and morphology of the Ni nanoparticles

Although nickel nanoparticles were obtained in all of the syntheses, as shown in Figure 7-1, none of the synthesis were successful at fully reducing all of the $Ni(OH)_2$ initially present. For the synthesis in which PVP was used, the presence of $Ni(OH)_2$ could be explained by the fact that PVP acts as a protecting agent and controls the rate of formation of nickel nanoparticles [11], thus slowing down the reaction rate and leaving some $Ni(OH)_2$ unreacted. However, $Ni(OH)_2$ was also present in the 0 PVP NNP synthesis and it is not clear what caused the incomplete reaction. From the XRD data, the crystallite sizes for all of the synthesized NNP were calculated using the Scherrer equation and, when comparing the crystallite size to the diameter obtained via measurements performed on the SEM micrographs, it is clear that the

nanoparticles are composed of several crystallites. The agglomeration observed in the micrographs of Figure 7-2, far from being detrimental to the purification process, was advantageous when using magnetic purification. The nanoparticles still offer a larg surface area for binding compared to micrometer particles while agglomerates make for a faster separation[18]. It was observed during the purification experiments that NNP that were evenly dispersed and smaller in size (i.e. 1 and 5 PVP NNP) were harder to separate from the binding mixture when inserted in the magnetic stand as they took longer to travel to the micro-centrifuge tube wall. This might be due to the fact that increasing the PVP ratio in the synthesis reduced particle size [6, 19], which makes it harder to be subjected to the magnetic field and may also to help stabilize the suspension [5]. From the micrographs, it is clear that PVP has an effect on size and morphology of the NNP. An increase in the PVP ratio results in smaller and more evenly dispersed NNP because, as mentioned earlier, PVP controls the growth rate of the nickel crystals.

Even though particles agglomerated, they could still be dispersed by mixing and the re-agglomeration of some nanoparticles when mixing is stopped can greatly facilitate the separation of particles from the suspension and, as a result, be beneficial to large scale application of the particles without a significant loss of binding surface area. As expected, the surface area increases when particles are smaller in diameter, as can be seen in Table 7-1 but it is interesting to note that the surface area of the 1 PVP NNP was greater than that of the 5 PVP. This might be due to the slightly broader size distribution of the latter (Figure 7-3) which is accounted for in the surface area calculation. The number of particles per kg of NNP, which was expected to be larger with a smaller particle diameter, indeed followed this trends where 1 kg of 5 PVP NNP would contain over 28 times the number of particles contained in 1 kg of the 0 PVP NNP.

7.5.2 Protein purification

As can be seen from Figure 7-4, all of the synthesized NNP proved to be efficient and selective binding adsorbents. The specific binding capacity of all of the PVP containing NNP were well above 95% (Table 7-2) showing that the NNP were indeed able to effectively bind the His6-tagged proteins. Specific binding and recovery of the NNP were comparable with some commercially available magnetic matrices which were tested and yielded specific binding capacities varying between 50.6 and 98% while recoveries varied between 4.4 and 80.2% [20]. The reusability of the NNP has been shown in Figure 7-4 where similar quantities of ToxA5.1 were purified for 5 cycles with the NNP. The first binding step using pristine NNP, however, yielded much lower recovery rates than the subsequent cycles. It is hypothesized that, during the first binding cycle, ToxA5.1 binds strongly to the surface of the NNP. Since the elution process is not as efficient as it could be, not all of the ToxA5.1 is removed from the surface and remains tightly bounded. In subsequent binding cycles, it is hypothesized that multi-layer binding occurred.

It is interesting to note that 0.5 PVP NNP yielded higher recoveries. It is not clear why this is the case. It is hypothesized that a balance must be struck between particle size and available binding sites. Increased PVP concentrations might yield lower diameter particles but could also contribute to surface coating on the NNP. This coating may have prevented the formation of NiO at the surface of the nickel that is responsible for the interaction between the His6 tag and the adsorbent. It was reported, in a previous study [21] , that NiO was indeed present at the surface of the same 0.5 PVP NNP used in this study for His6-tagged protein binding.

In general, the recovery of ToxA5.1 would need to be improved by either developing a more efficient elution buffer or by carrying out adsorption and elution in packed beds of the NNP adsorbents.

7.6 Conclusion

In conclusion, nickel nanoparticles synthesized using the modified polyol method were established to be selective and effective magnetic adsorbents for the purification of hexahistidine-tagged recombinant protein ToxA5.1. It was further demonstrated that the Ni:PVP mass ratio had a significant effect on the morphology and size distribution of NNP. All four types of NNP synthesized under different Ni:PVP ratios were found to be effective in binding ToxA5.1 His6-tagged recombinant protein very specifically and strongly. It is clear from the achieved recovery and the specific binding results that a better elution scheme still needs to be developed.

7.7 Acknowledgements

The authors would like to thank Dr. Tara Kell for the XRD scans. Financial support from the Natural Science and Engineering Council of Canada (NSERC) and The Canada Foundation of Innovation (CFI) is gratefully acknowledged.

7.8 References

1. Benelmekki, M., Montras, A., Martins, A.J., Coutinho, P.J.G. and Martinez, L.M. Magnetophoresis behaviour at low gradient magnetic field and size control of nickel single core nanobeads. *Journal of Magnetism and Magnetic Materials* **323**, 1945-1949 (2011).

2. Porath, J. IMAC-Immobilized metal ion affinity based chromatography. *Trends in Analytical Chemistry* **7**, 254-259 (1988).

3. Porath, J. Immobilized metal ion affinity chromatography. *Protein Expression and Purification* **3**, 263-281 (1992).

4. Ai, F., Yao, A., Huang, W., Wang, D. and Zhang, X. Synthesis of PVP-protected NiPd nanoalloys by modified polyol process and their magnetic properties. *Physica E: Low-Dimensional Systems and Nanostructures* **42**, 1281-1286 (2010).

5. Couto, G.G., Klein, J.J., Schreiner, W.H., Mosca, D.H., de Oliveira, A.J.A. and Zarbin, A.J.G. Nickel nanoparticles obtained by a modified polyol process: Synthesis, characterization, and magnetic properties. *Journal of Colloid and Interface Science* **311**, 461-468 (2007).

6. Li, P., Guan, J., Zhang, Q. and Zhao, W. Preparation and characterization of monodisperse nickel nanoparticles by polyol process. *Journal Wuhan University of Technology, Materials Science Edition* **20**, 35-37 (2005).

7. Zhang, H., Ding, J., Chow, G., Ran, M. and Yi, J. Engineering magnetic properties of Ni nanoparticles by non-magnetic cores. *Chemistry of Materials* **21**, 5222-5228 (2009).

8. Bai, L., Fan, J., Cao, Y., Yuan, F., Zuo, A. and Tang, Q. Shape-controlled synthesis of Ni particles via polyol reduction. *Journal of Crystal Growth* **311**, 2474-2479 (2009).

9. Parisien, A., Al-Zarka, F., Hussack, G., Baranova, E.A., Thibault, J. and Qingdao Lan, C. Nickel nanoparticles synthesized by a modified polyol method for the purification of histidine-tagged single-domain antibody ToxA5.1. *Journal of Materials Research* **27**, 2884-2890 (2012).

10. Carroll, K.J., Reveles, J.U., Shultz, M.D., Khanna, S.N. and Carpenter, E.E. Preparation of elemental Cu and Ni nanoparticles by the polyol method: An experimental and theoretical approach. *Journal of Physical Chemistry C* **115**, 2656-2664 (2011).

11. Chou, K.S. and Huang, K.C. Studies on the chemical synthesis of nanosized nickel powder and its stability. *Journal of Nanoparticle Research* **3**, 127-132 (2001).

12. Hussack, G., Arbabi-Ghahroudi, M., Van Faassen, H., Songer, J.G., Ng, K.K.S., MacKenzie, R. and Tanha, J. Neutralization of *Clostridium difficile* toxin A with single-domain antibodies targeting the cell receptor binding domain. *Journal of Biological Chemistry* **286**, 8961-8976 (2011).

13. Laemmli, U.K. Cleavage of structural proteins during the assembly of the head of bacteriophage T4. *Nature* **227**, 680-685 (1970).

14. Abràmoff, M.D., Magalhães, P.J. and Ram, S.J. Image processing with imageJ. *Biophotonics International* **11**, 36-41 (2004).

15. Cullity, B.D. Elements of X-Ray Diffraction, Edn. 3rd. (Addison-Wesley publishing Co., Reading, MA; 1956).

16. West, A.R. Solid state chemistry and its applications (Wiley, New York; 1984).

17. Xu, L., Ding, Y.S., Chen, C.H., Zhao, L., Rimkus, C., Joesten, R. and Suib, S.L. 3D flowerlike α-nickel hydroxide with enhanced electrochemical activity synthesized by microwave-assisted hydrothermal method. *Chemistry of Materials* **20**, 308-316 (2008).

18. Franzreb, M., Siemann-Herzberg, M., Hobley, T.J. and Thomas, O.R.T. Protein purification using magnetic adsorbent particles. *Applied Microbiology and Biotechnology* **70**, 505-516 (2006).

19. Liu, D., Ren, S., Wu, H., Zhang, Q. and Wen, L. Morphology control in synthesis of nickel nanoparticles in the presence of polyvinylpyrrolidone (PVPK30). *Journal of Materials Science* **43**, 1974-1978 (2008).

20. Nejadmoghaddam, M.R., Chamankhah, M., Zarei, S. and Zarnani, A.H. Profiling and quantitative evaluation of three Nickel-Coated magnetic matrices for purification of recombinant proteins: Helpful hints for the optimized nanomagnetisable matrix preparation. *Journal of Nanobiotechnology* **9** (2011).

21. Baranova, E.A., Cally, A., Allagui, A., Ntais, S. and Wüthrich, R. Nickel particles with increased catalytic activity towards hydrogen evolution reaction. *Comptes Rendus Chimie* **16**, 28-33 (2013).

Chapter 8: Binding characterization of hexahistidine-tagged recombinant protein ToxA5.1 against *Clostridium difficile* toxin A on nickel nanoparticles synthesized by a modified polyol method.

Albert Parisien, Aatika Ahmed, Jules Thibault, and Christopher Q. Lan[1]*

[1] Chemical and Biological Engineering Department, University of Ottawa, ON, Canada; K1N 6N5

*Corresponding author: Christopher Q. Lan, Christopher.Lan@uottawa.ca

8.1 Abstract

Magnetic purification of recombinant proteins is increasing in popularity. A novel magnetic affinity adsorbent, nickel nanoparticles (NNP) synthesized via a modified polyol method, was shown to be suitable for hexahistidine tagged protein purification of ToxA5.1, a single domain antibody neutralizing C*lostridium difficile* toxin A. Using clarified cell lysate and a range of protein concentrations typically found in cell expression systems, binding experiments were performed under various imidazole concentrations. From the experimental data, two models were derived based on a modified Langmuir isotherm and a modified Freundlich isotherm models to characterize the specific binding capacity of the NNP without and with the presence of imidazole.

Keywords: Modified Polyol method, Magnetic Adsorbent, His6-tagged recombinant protein, Nickel nanoparticles

8.2 Introduction

Purification and recovery of recombinant proteins, following intentional cell lysis, can be achieved using techniques ranging from gel chromatography, ion exchange chromatography and affinity chromatography to electrophoresis, precipitation and membrane separation [1, 2]. In recent years, the use of magnetic affinity adsorbents (MAA) for the purification of bio-molecules has increased in popularity [3-5]. The principle of magnetic separation is simple. Magnetic core particles are covered with a functional group which acts as the affinity ligand with one of the most widely used affinity ligands being nickel. The nickel interacts with the polyhistidine tag that is fused to a wide range of recombinant proteins enabling selective purification. Typically, a magnetic affinity adsorbent is comprised of an inorganic magnetic core particle covered by a polymer matrix with polystyrene (PS) or poly(methyl methacrylate) (PMMA) being historically most frequently used matrices for magnetic microparticles [4]. Recovery and purification of hexahistidine (His6-tagged) recombinant proteins using magnetic affinity adsorbents typically involve the following steps: 1) Cell lysis to expose intracellular proteins, 2) Application of magnetic bead slurry to capture the recombinant proteins, 3) Washing of the magnetic beads to remove native and partially bounded proteins, and 4) Elution of the tightly bounded protein(s) often done by imidazole displacement.

The evaluation of the ability of different magnetic adsorbents for recovery of a variety of recombinant proteins has been carried out by many researchers [6-9].

The adsorption usually follows a Langmuir-type binding equilibrium as shown in Equation 1:

$$q = \frac{q_0 C}{K + C} \qquad (1)$$

where q is the equilibrium loading of the magnetic adsorbent (mg/g), q_0 is the maximum binding capacity of the adsorbent (mg/g), C is the equilibrium bulk-phase protein concentration (mg/L), and K is the Langmuir constant (mg/L) which represents the ratio of the adsorption rate constant over the desorption rate constant.

It is clear that larger binding capacities are desirable since more proteins are recovered per gram of adsorbent while smaller values of K indicate a more stable complex. Franzeb *et al.* [10] looked at over 30 scientific papers reporting on protein purification using magnetic adsorbent and extracted isotherm data. Experiments were of two types: 1) Mono systems where only the target protein was present in a buffer, and 2) Feedstock systems where the target protein was mixed with other proteins in solution such as whey or *E. coli* lysate. Surprisingly, only one fifth of the publications were about feedstock systems, which would actually provide a more representative binding kinetics that would be useful in practical applications. It is clear from data reported that feedstock systems exhibited lower q_0 values than mono component systems with maximal loading values ranging between 8 and 180 mg/g compared to mono systems that had values ranging between 42 and 800 mg/g [10]. Values for the dissociation constant were also affected by the type of system with values between 0.001 and 0.43 g/L for mono component systems and between 0.00077 and 0.047 for feedstock systems. Mono component systems may be used in screening experiments to

determine the best adsorbent for the targeted protein but if separation is planned to be used with feedstocks, then, further testing is required to obtain representative binding kinetics.

In this paper, we have investigated the binding properties of nickel nanoparticles synthesized via a modified polyol method [11] for the purification of a His6-tagged recombinant protein, ToxA5.1, which is a single domain antibody that neutralizes *Clostridium difficile* toxin A [12]. Binding isotherm studies were performed under various imidazole concentrations and two models, a modified Langmuir and a modified Freundlich, are proposed.

8.3 Materials and Methods

8.3.1 Synthesis of the nickel nanoparticles

Nickel nanoparticles were synthesized using a modified polyol method [13, 14] by mixing 0.4 g $Ni(OH)_2$ (Acros Organics, Fisher Scientific, Pittsburgh, PA), 160 mL ethylene glycol (EG) (Fisher Scientific) and 0.1268 g of polyvinylpyrrolidone (PVP) (Fisher Scientific) to get a 1:0.5 w/w ratio of Ni:PVP, at room temperature in a 1 L three-neck boiling flask for 30 min after which the solution was heated to 190ºC. Once the $Ni(OH)_2$ and EG mixture reached 190ºC, a $PdCl_2$ solution was quickly added to the flask. The $PdCl_2$ catalyst solution (Sigma Aldrich, St. Louis, MO) was prepared by mixing 0.0076 g $PdCl_2$ in 40 mL EG in a beaker at room temperature for 45 min. Upon addition of the $PdCl_2$ solution, the initial mixture of $Ni(OH)_2$ in EG changed from a light green color to black within 15 min indicating the formation of metallic Ni. After 2 h of refluxing, the suspension was left to cool at room temperature and, then, the NNP were separated from the spent EG solvent using a magnet. The recovered NNP were thoroughly washed three times with 99% ethanol and

separated using a magnet. The washed particles were then suspended in 10 mL of 99% ethanol and stored at room temperature.

8.3.2 *E. coli* cell growth and protein expression

Escherichia coli TG1 bearing the plasmid for the ToxA5.1 expression gene [12] was grown from a starting patch, in modified LB media consisted in 20 g LB Lennox broth (Fisher Scientific), 6 g enzymatic tryptone (Fluka, St. Louis, MO) and 5 g yeast extract (Oxoid, Lenexa, KS) in 1000 mL of distilled water, overnight in a shaker at 37ºC and 200 rpm. The overnight culture served as inoculum for a fresh culture in the same medium that was induced for protein expression after reaching an OD_{600} of 0.6 using 2 mM isopropyl β-D-1-thiogalactopyranoside (IPTG, Promega, Madison, WI) at 37ºC for 18 h. Bacterial lysis was performed using the Promega Fastbreak lysis system (Promega) following the protocol provided by the manufacturer. Bacterial lysate was centrifuged at 1150 rcf for 10 min at 20°C. The clarified lysate was used for purification experiments.

8.3.3 Binding isotherms

For the binding isotherm experiments, four initial protein concentrations were tested for each of five different imidazole concentrations. The initial protein concentrations were 28, 56, 84 and 112 mg ToxA5.1/L while the final imidazole concentrations were 0, 0.01, 0.5, 1, and 1.5 M in the binding mixture, which was prepared by mixing appropriate volumes of cell lysate, wash bind buffer (100mM HEPES, 10 mM imidazole, pH 7.5) and 5 M imidazole solution to obtain a final volume of 400 μL.

To start the isotherm tests, 25 μL of NNP ethanol suspension was added into HPLC-type glass micro-vials. The micro-vials were then placed on a Promega magnetic stand for

approximately 1 min to attract the NNP to the vials wall. Ethanol was removed with a pipette and 300 μL of wash bind buffer was added to the micro-vials to remove all traces of ethanol. The NNP were re-suspended and hand shaken for 1 min. The micro-vials were then placed on the magnet stand and the buffer was removed with a pipette. The washing step was repeated a second time. After being washed, NNP were re-suspended in a combination of wash bind buffer and imidazole in accordance to a predetermined scheme of lysate-wash buffer-imidazole to satisfy the conditions described in the previous paragraph. Prior to lysate addition, the NNP and binding mixture was sonicated for 10-15 seconds in a Fisher Scientific ultrasonic cleaner (FS140, 135 w 42 kHz ± 6%) to better disperse NNP for effective binding of the protein. The clarified lysate was then added into the micro-vials. The micro-vials were incubated and hand shaken for 5 minutes after which they were placed on the magnetic stand for approximately 1 min. The supernatant fluid, which is referred to as unbounded fraction (UBF) from this point on, was removed from the micro-vials using a pipette and kept at 4°C for further analysis using SDS-PAGE gel electrophoresis.

8.3.4 Sample Analysis

Protein analysis was performed using SDS-PAGE gel electrophoresis and collected samples of UBF of appropriate dilutions along with samples of purified quantified ToxA5.1 serving as standards (500, 250, 100, 50 ng) were loaded on 4-15% discontinuous SDS-PAGE gels [15]. Gels were run at 190 V for 45 min. Proteins were stained using Fermentas PageBlue Protein Staining Solution (Glen Burnie, MD), fast procedure, as per manufacturer's recommendations. Quantification of scanned gels was achieved via densitometry using ImageJ software [16].

8.3.5 Binding capacity calculation

The quantity of ToxA5.1 adsorbed per unit amount of NNP (q_n in mg/g Ni) at the n^{th} separation cycle was calculated using Equation 2:

$$q_n = \frac{(V_{bm} \times C_{bm}) - (V_{UBF} \times C_{UBF})}{M_p} \qquad (2)$$

where V_{bm} is the volume of binding mixture (L), C_{bm} the concentration of ToxA5.1 in the initial binding mixture (mg/L), V_{UBF} the volume of the unbounded fraction (L), C_{UBF} the concentration of ToxA5.1 in the unbounded fraction (mg/L), M_p the mass of nickel nanoparticles (NNP) expressed as g of Ni.

8.3.6 Modeling

The modified Langmuir isotherm model was derived using Equations 1 and 3:

$$q = \frac{q_0 C}{K + C} \qquad (1)$$

$$q_0 = A + (B \times I) \qquad (3)$$

where q is the amount of adsorbed protein per unit mass of adsorbent (mg/g), q_0 is amount of protein adsorbed to form a monolayer (mg/g), C is the equilibrium concentration (mg/L) of proteins in solution, and K is the Langmuir constant (mg/L). To account for the effect of imidazole concentration (I) in the solution, q_0 was calculated using two parameters and a linear relationship, A (mg/g) and B ((mg/g) /(mol/L)) .

The modified Freundlich isotherm model was derived using Equations 4 and 5

$$q = K C^n \qquad (4)$$

$$K = A + (B \times I) \qquad (5)$$

where q is the amount of adsorbed protein per unit adsorbent (mg/g), K is the Freundlich constant ((mg/g)/(mg/L)^n) and, to account for the effect of imidazole concentration (I) in the solution, it was calculated using a straight line approximation with two parameters, A ((mg/g)/(mg/L)^n) and B (((mg/g)/(mg/L)^n)/mol/L), C is the equilibrium concentration (mg/L) of proteins in solution, and n is a coefficient.

8.4 Results

The specific binding capacity of the NNP under various imidazole concentrations can be seen on Figure 8-1. The amount of ToxA5.1 bounded to the NNP follows expected trends where higher q values are obtained when there is no imidazole present in the binding mixture as shown by the raw data in Figure 8-1. As the concentration of imidazole increased, less ToxA5.1 bounded to the NNP. The highest specific binding capacity of all of the tested conditions was achieved in the absence of imidazole, where 13.26 mg of ToxA5.1 were bounded to 1 g of Ni. As expected, in the presence of 1.5 M imidazole, the specific binding capacity was the lowest of the tested conditions with 8.53 mg ToxA5.1 bound per g of Ni. These results show that a low concentration of imidazole can have a significant impact on the specific binding capacity as seen for the 0.01 M imidazole concentration which follows very closely the trend of the solution with 0.5 M imidazole.

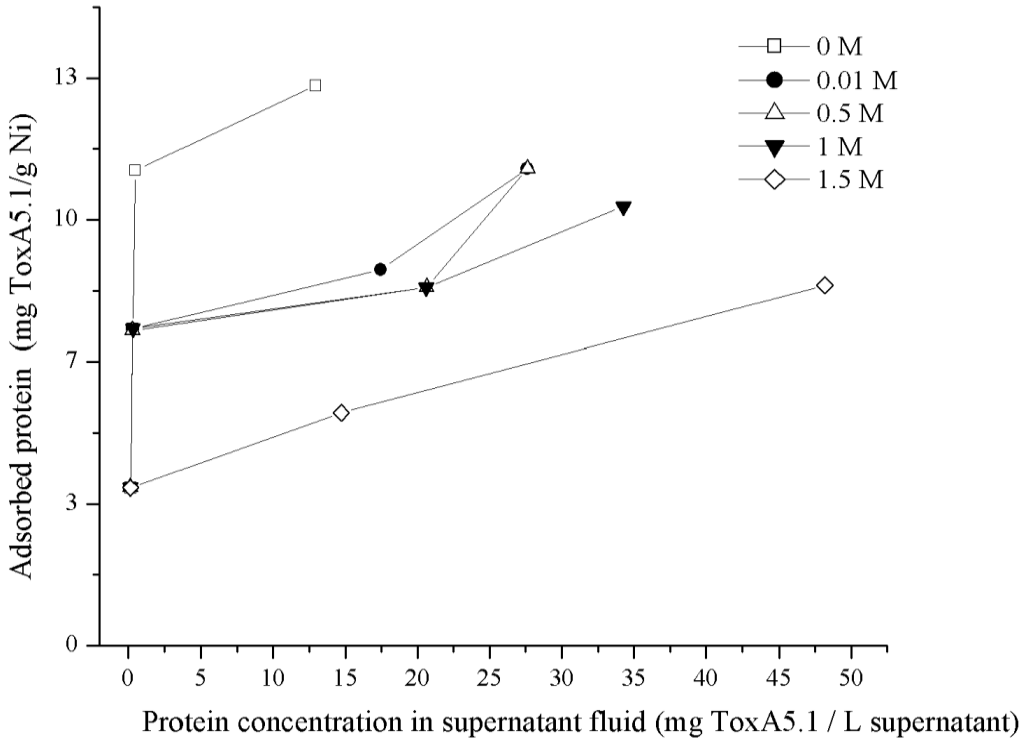

Figure 8-1: Specific binding capacities of nickel nanoparticles under various concentrations of imidazole.

Based on experimental data, a first model was derived using a Langmuir-type isotherm model that was modified to account for the effect of imidazole on the maximal binding capacity q_0. Parameters obtained for this modified model are reported in Table 8-1. A second model was also derived using a Freundlich-type isotherm model, which was also modified to account for the imidazole concentration present in the binding mixture. Parameters for the modified Freundlich model are also reported in Table 8-1.

Table 8-1: Modified Langmuir and Freundlich model parameters.

Modified Langmuir		Modified Freundlich	
A	11.48	A	7.720
B	-3.03	B	- 0.578
K	0.184	n	0.124

The two models were compared based on residual errors. The predictions and experimental data points as well as the sum of squares of the differences between the model predictions and the experimental data are presented in Table 8-2. It can be seen that the modified Langmuir model resulted in a model that better represents the experimental data. This can also be seen on Figure 8-2 where the derived models are plotted along with the experimental data. The values of q_0 for the modified Langmuir model, q_{exp} and the ratio q_0/K are presented in Table 8-3. As it was expected, the value of q_0 decreases when imidazole concentration increases. In the absence of imidazole, a q_0 of 11.5 mg/g was predicted while it was of 6.9 mg/g in the presence of 1.5 M imidazole. It can also be seen that the model generally under-predicted q_0 since q_{exp} was higher than q_0 for all of the imidazole concentrations tested except for the first prediction of 0, 0.01, 0.5, and 1 M imidazole. Values for the q_0/K ratio, which characterize the suitability of the adsorbent for the target protein, were 62.4 L/g in the absence of imidazole and decreased to 37.4 L/g when 1.5 M imidazole was present in the binding mixture.

Table 8-2: Values predicted by the modified Langmuir and Freundlich model compared to the experimental data.

Imidazole M	q_{exp} mg/g	Cs mg/L	Modified Langmuir		Modified Freundlich	
			$q_{predicted}$ mg/g	$(q_{exp}- q_{predicted})^2$	$q_{predicted}$ mg/g	$(q_{exp}- q_{predicted})^2$
0	3.75	0.16	5.41	2.75	7.72	15.76
0	7.50	0.33	7.35	0.02	7.72	0.05
0	11.25	0.49	8.35	8.39	7.72	12.46
0	13.26	12.95	11.32	3.76	7.72	30.68
0.01	3.75	0.16	5.39	2.70	7.72	15.73
0.01	7.50	0.33	7.33	0.03	7.71	0.05
0.01	8.90	17.45	11.33	5.89	7.71	1.42
0.01	11.29	27.60	11.37	0.01	7.71	12.81
0.5	3.75	0.16	4.69	0.89	7.49	13.98
0.5	7.46	0.31	6.25	1.45	7.47	0.00
0.5	8.48	20.63	9.88	1.96	7.30	1.39
0.5	11.29	27.61	9.90	1.93	7.28	16.04
1	3.75	0.16	3.98	0.05	7.26	12.31
1	7.50	0.33	5.41	4.36	7.22	0.08
1	8.48	20.62	8.38	0.01	6.88	2.57
1	10.39	34.28	8.40	3.95	6.82	12.75
1.5	3.75	0.16	3.27	0.23	7.03	10.75
1.5	5.52	14.71	6.85	1.76	6.51	0.97
1.5	8.53	48.16	6.91	2.62	6.31	4.90
			Sum	42.76		164.68

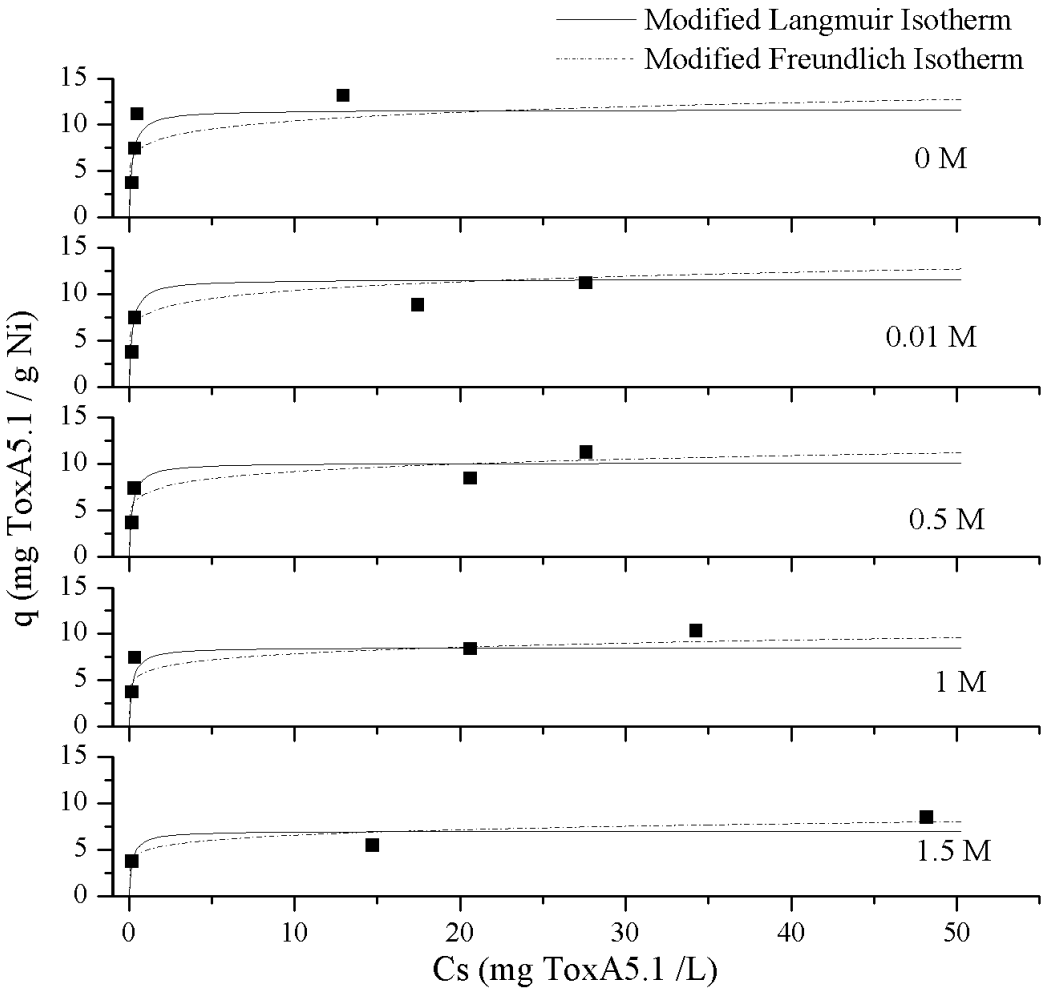

Figure 8-2: Binding isotherms of a modified Langmuir model and modified Freundlich model for nickel nanoparticles under various imidazole concentrations.

Table 8-3: Langmuir model parameters

Imidazole M	q_0 mg/g	q_{exp} mg/g	q_0/K L/g
0	11.5	13.3	62.4
0.01	11.5	11.3	62.4
0.5	10.0	11.1	54.3
1	8.5	10.3	46.1
1.5	6.9	8.5	37.4

8.5 Discussion

The trends observed in Figure 8-1 were expected since a higher imidazole concentration in the binding mixture results in more molecules competing with ToxA5.1 for binding sites. Surprisingly, a very low concentration of imidazole in the binding mixture can lead to a significant reduction in the specific binding capacity of the NNP. In practical applications, 0.01 M imidazole is used to prevent or, at least minimize, non-specific binding on the adsorbent. It can be seen from the isotherm models and experimental data (Figure 8-2) that the adsorption of ToxA5.1 was very favorable under the conditions used, which is a desired characteristic when valuable a protein is to be extracted from a medium. Unfortunately, a very favorable adsorption also implies that desorption of the desired protein will be harder. This behavior was reported in previous experiments [11, 17] where as high as 99% of the initially ToxA5.1 in the clarified cell lysate was bound to the NNP but recoveries as low as 4% were observed. Furthermore, looking at the initial slope of the binding isotherm (q_0/K), which gives a clear indication of the suitability of an adsorbate for a protein, we observe a ratio of 62.4 L/g, as seen in Table 8-3, when no imidazole or 0.01 M imidazole was used. The latter is closer to what would be used in day to day operation when purifying protein using affinity ligands. It is interesting to note that the value of the q_0/K ratio obtained for the NNP was closer to values observed in mono systems i.e., when no other proteins are present. In mono systems, the q_0/K ratio ranges from 0.58 to 99 L/g while for feedstock type systems, which are more realistic operation conditions, this ratio ranges from 2.5 to 13[10]. This also confirmed what was observed in previous studies where binding was fast and efficient but elution of the target protein was less efficient.

Binding isotherms were performed under conditions that would best represent practical application with feedstock and typical protein concentrations in cell lysates, and, therefore, the values of q_0 were lower that if no other proteins were present in the binding mixture. For feedstock systems akin to those used in this study, q_0 values of 8 to 180 mg/g[10] can be expected. The maximal specific binding capacity predicted by the model was of 11.5 mg/g but values of 13 mg/g were observed during experiments in the absence of imidazole. A lower predicted q_0 might be the result of considering imidazole in the calculation. If, as mentioned earlier, the ratio q_0/K was quite high, indicating suitability between adsorbate and adsorbent, the K value obtained from the model, which represents the stability of the complex, was 0.184. This value, which falls in the range of mono systems (0.001 to 0.43 g/L[10]) rather than the feedstock systems (0.00077 to 0.047 L/g[10]), is quite high, which indicate a less stable complex. This higher value of K, which represents the ratio of the of the adsorption rate constant over the desorption rate constant, also corroborates previous results where binding occurred but desorption of the bound protein was not efficient.

8.6 Conclusion

Using experimental data gathered under typical operation conditions i.e. using cell lysate and protein concentrations that would be encountered from actual cell expression systems, two models were derived to represent the binding of ToxA5.1 in the absence and presence of imidazole to NNP synthesized using a modified polyol method. Parameters obtained from the modified Langmuir model served to better understand the behavior of the NNP-ToxA5.1 system. Binding was quite favorable which meant that most of the target protein could be adsorbed to the NNP but also indicated that desorption was harder to

achieve. A modified Langmuir-type isotherm model best represented the system but slightly under predicted q_0, which was predicted to be 11.5 mg/g in the absence of imidazole but was actually 13.0 mg/g.

8.7 Acknowledgements

Financial support from the Natural Science and Engineering Council of Canada (NSERC) and The Canada Foundation of Innovation (CFI) is gratefully acknowledged.

8.8 References

1. Langer, E. and Ranck, J. Capacity bottleneck squeezed by downstream processes. *BioProcess Int* **4**, 14-18 (2006).

2. Low, D., O'Leary, R. and Pujar, N.S. Future of antibody purification. *Journal of Chromatography B: Analytical Technologies in the Biomedical and Life Sciences* **848**, 48-63 (2007).

3. Benelmekki, M., Montras, A., Martins, A.J., Coutinho, P.J.G. and Martinez, L.M. Magnetophoresis behaviour at low gradient magnetic field and size control of nickel single core nanobeads. *Journal of Magnetism and Magnetic Materials* **323**, 1945-1949 (2011).

4. Horák, D., Babič, M., Macková, H. and Beneš, M.J. Preparation and properties of magnetic nano- and microsized particles for biological and environmental separations. *Journal of Separation Science* **30**, 1751-1772 (2007).

5. Safarik, I. and Safarikova, M. Magnetic techniques for the isolation and purification of proteins and peptides. *BioMagnetic Research and Technology* **2** (2004).

6. Heebøll-Nielsen, A., Justesen, S.F.L., Hobley, T.J. and Thomas, O.R.T. Superparamagnetic cation-exchange adsorbents for bioproduct recovery from crude process liquors by high-gradient magnetic fishing. *Separation Science and Technology* **39**, 2891-2914 (2004).

7. Hoffmann, C., Franzreb, M. and Höll, W.H. A novel high-gradient magnetic separator (HGMS) design for biotech applications. *IEEE Transactions on Applied Superconductivity* **12**, 963-966 (2002).

8. Hubbuch, J.J., Matthiesen, D.B., Hobley, T.J. and Thomas, O.R.T. High gradient magnetic separation versus expanded bed adsorption: A first principle comparison. *Bioseparation* **10**, 99-112 (2001).

9. Meyer, A., Hansen, D.B., Gomes, C.S.G., Hobley, T.J., Thomas, O.R.T. and Franzreb, M. Demonstration of a strategy for product purification by high-gradient magnetic fishing: Recovery of superoxide dismutase from unconditioned whey. *Biotechnology Progress* **21**, 244-254 (2005).

10. Franzreb, M., Siemann-Herzberg, M., Hobley, T.J. and Thomas, O.R.T. Protein purification using magnetic adsorbent particles. *Applied Microbiology and Biotechnology* **70**, 505-516 (2006).

11. Parisien, A., Al-Zarka, F., Hussack, G., Baranova, E.A., Thibault, J. and Qingdao Lan, C. Nickel nanoparticles synthesized by a modified polyol method for the purification of histidine-tagged single-domain antibody ToxA5.1. *Journal of Materials Research* **27**, 2884-2890 (2012).

12. Hussack, G., Arbabi-Ghahroudi, M., Van Faassen, H., Songer, J.G., Ng, K.K.S., MacKenzie, R. and Tanha, J. Neutralization of *Clostridium difficile* toxin A with single-domain antibodies targeting the cell receptor binding domain. *Journal of Biological Chemistry* **286**, 8961-8976 (2011).

13. Ai, F., Yao, A., Huang, W., Wang, D. and Zhang, X. Synthesis of PVP-protected NiPd nanoalloys by modified polyol process and their magnetic properties. *Physica E: Low-Dimensional Systems and Nanostructures* **42**, 1281-1286 (2010).

14. Bai, L., Fan, J., Cao, Y., Yuan, F., Zuo, A. and Tang, Q. Shape-controlled synthesis of Ni particles via polyol reduction. *Journal of Crystal Growth* **311**, 2474-2479 (2009).

15. Laemmli, U.K. Cleavage of structural proteins during the assembly of the head of bacteriophage T4. *Nature* **227**, 680-685 (1970).

16. Abràmoff, M.D., Magalhães, P.J. and Ram, S.J. Image processing with imageJ. *Biophotonics International* **11**, 36-41 (2004).

17. Parisien, A., Ahmed, A., Thibault, J. and Lan, C. Q., Effect of polyvinylpyrrolidone:nickel ratio on properties and performance of nickel nanoparticles for purification of histidine-tagged recombinant protein (ToxA5.1) (in preparation).

Chapter 9: Conclusion and recommendations

In summary, this project proposed to study the production in *E. coli* TG1 of a novel therapeutic protein, ToxA5.1, a single domain antibody (sdAb), to neutralize toxin A of one of the deadliest nosocomial infection agent afflicting hospitals, *C. difficile*. We intentionally designed a project that would study the overall process providing a solution to the *C. difficile* problem from growing the bacteria expressing the sdAb to testing its activity once it was purified. This was achieved through high cell density cultures and protein expression optimization investigations. Recovery of functional ToxA5.1 was achieved using synergistic lysis as a selective cell disruption technology combining Triton X-100 and temperature while the synthesis of a novel adsorbent material enabled the purification of ToxA5.1. In the end, it was possible to produce 12 g/L of *E. coli* TG1 biomass that was able to express the recombinant ToxA5.1 sdAb at a concentration of 127 mg/L. The activity of ToxA5.1 purified using nickel nanoparticles after synergistic lysis at 60°C with Triton X-100 at 1% was tested against a control at NRC-IBS facilities. ToxA5.1 purified using synergistic lysis and NNP showed no significant difference in binding activity with the standard ToxA5.1 used in a binding assay against *C. difficile* toxin A. Furthermore, the interaction of ToxA5.1 and NNP was modeled using a modified Langmuir isotherm model. Therefore, it was possible to produce large quantities of active ToxA5.1 and the next step is to produce ToxA5.1 for animal studies.

The novel pH-stat strategy that we implemented enabled *E. coli* TG1 growth to relatively high cell densities. However, changing the mechanism that triggers the addition of the carbon source might prove to be more efficient. If, for instance, the change in pH value

was monitored, the carbon source could be added to the fermentation whenever the pH value remains constant for a certain period. This would serve two purposes 1) Ensure that acetate formed during the catabolism of glucose is fully depleted, thus, prevent accumulation of acetate to levels that are detrimental to cell growth and 2) Ensure that the fed-batch will start even if the pH does not reach the higher target setpoint. The latter can occur if initial carbon source concentration is too low which result in insufficient acetate production to enable a pH rise high enough to trigger the fed-batch. This strategy would ensure that the fed-batch would actually proceed in small systems that are not monitored on a 24 h period. It may not be as crucial for large scale industrial applications where monitoring is done around the clock but in small setting such as academia, this would prove to be an easy, efficient and affordable technique to achieve HCDC. Another aspect that would require monitoring is the concentration of macro-nutrients such as phosphorus and ammonia that are critical for biomass growth. This monitoring would ensure that the feeding solution could support even higher biomass during the growth phase.

The pH-stat strategy can also be used to express recombinant proteins. It was shown that the expression system that was studied needed to be induced early in the growth phase if a high titer of ToxA5.1 was desired. Furthermore, a pulse of concentrated yeast extract solution at the time of induction to obtain concentration higher than 10 g/L of yeast extract in the fermentation coupled with the increase in fermentation temperature to 37°C should be considered if a defined medium is used for the growth phase. As the induction phase lasts less than 8 h, changing the composition of the medium with yeast extract is less critical than when the growth rate needs to be controlled to avoid high acetate production. By adding a high concentration of yeast extract to the medium, it would not only ensure higher protein

titer but it could also lessen the concentration of the inducer needed since yeast extract acts as an inducer for certain types of recombinant strains like the one that was used in this study.

The synergistic selective cell lysis was found to be a suitable process to recover the thermostable protein from *E. coli* cells. A compromise exists between temperature and length of the synergistic lysis and with thermostable proteins, higher temperature can be used, which reduces cell lysis period. Using Triton X-100 at near critical micelle concentration of 1.5% w/w was optimal, and increasing the concentration does not improve lysis efficiency. The next step would be to test this strategy on HCDC as it is in these cases that the cell lysate becomes quite viscous due the release of genetic material in the lysate. It might be of interest to monitor the actual lysate viscosity in the hope of determining the optimal lysis time with respect to lysate viscosity and protein recovery.

The synthesis of nickel nanoparticles was not initially part of the experimental plan but proved to be an interesting addition. As it was seen, the binding of ToxA5.1 was quite favorable and being able to bind most of the protein of interest present in the lysate is desirable. However, further desorption studies would need to be performed on the bound protein. The elution scheme that was used might not have been appropriate for the protein-adsorbent system studied. We would suggest using a column type adsorption-desorption system as opposed to the batch system that was used. This might possibly increase the recovery of the target protein upon elution.

It is clear that PVP plays a role in controlling NNP size during the polyol method synthesis. However, the impact it has on the binding of protein is less obvious. There probably exists a balance between the small size of the nanoparticles, which increases surface area available for binding, and the availability of the NiO at the surface of the

particles. Further surface characterization experiments should be considered. These experiments might lead to understanding why desorption of ToxA5.1 was not efficient. If this type of adsorbent would need to be produced at large scale, hydrogen reduction of $NiCl_2$ might be a better route to investigate. Although the polyol method is a rapid, simple, and inexpensive method that uses less hazardous material than some other methods, it still produces large amounts of ethylene glycol wastes. It would be interesting to investigate if and how many times, the spent ethylene glycol could be re-used for synthesizing the NNP. Again, the polyol method is a good method for small scale production but hydrogen reduction, as mentioned earlier, would be a better alternative. It produces nanoparticles in minutes compared to hours with the polyol method and furthermore, it produces far less waste.

As mentioned earlier, this project was about looking into several aspects of the production of a single domain antibody, from cell growth and expression to accessing the target protein and purifying an active form of it. This project involved several aspects of research which all proved to be quite challenging. A lot has been learned throughout the project mainly due to the fact that small victories came late into the project giving me more than enough time to troubleshoot problems at every step of the project. Even though at times, when all experiments failed repeatedly I felt discouraged, I still enjoyed my experience as a graduate student. I cannot wait to put all that I have learnt during this project into practice.